Christian-Albrechts-Universität zu Kiel
Mathematisch-Naturwissenschaftliche Fakultät

The Logatchev Hydrothermal Field (MAR, 15°N): High- and Low-Temperature Alteration of Ultramafic Oceanic Crust – Geology, Geochemistry, Mineralogy

---

Dissertation
zur Erlangung des Doktorgrades
der Mathematisch-Naturwissenschaftlichen Fakultät
der Christian-Albrechts Universität zu Kiel

vorgelegt von
Nico Augustin

Kiel 2007

Referent:	Prof. Dr. Colin W. Devey
Koreferent / in:	Priv.-Doz. Dr. Thor Hansteen
Tag der mündlichen Prüfung:	05. Februar 2008
Zum Druck genemigt:	Kiel, …….

Der Dekan

Für Sophie.

Vorwort

Die vorliegende Arbeit stellt eine monographische Dissertation dar, deren Einzelkapiteln jeweils eine Einleitung voran gestellt ist und die bezüglich ihres Aufbaues derart konzipiert sind, dass sie unabhängig voneinander publizierfähig sind. Durch diesen Umstand besitzt jedes Kapitel eine eigene Einleitung, Diskussion und Literaturverzeichnis. Der Schreibstil sowie die Formatierung von Tabellen und Abbildungen wurden ebenfalls den Anforderungen moderner Fachzeitschriften angepasst. Der Leser möge dies berücksichtigen.

Kiel, November 2007
Nico Augustin

Table of Contents

Zusammenfassung

Detailierte bathymetrische Kartierungen vom Mittelatlantischen Rücken (MAR) bei 15°N sowie genaue geologische Beobachtungen ermöglichten eine sehr gute Beschreibung es Logatchev Hydrothermalfeldes (LHF) bei 15°45´N. Der größte Teil des LHF liegt in einer mit Sedimenten und Talus gefüllten Senke. Dieses Material ermöglicht eine erhöhte Porosität des Untergrundes und beeinflusst dadurch stark die Bewegungen hydrothermaler Lösungen. Die im LHF erstmals beschriebenen „rauchenden Krater" scheinen abhängig von der Beschaffenheit des Untergrundes zu sein und sind bisher nur noch von einer weiteren Lokalität im Nibelungen-Feld am südlichen MAR bekannt. Die Interpretation bathymetrischer Karten lässt darauf schließen, dass die Position des LHF an große Störungen gebunden ist. Im LHF kennt man bisher 5 rauchende Krater, 2 hydrothermale Hügel mit aktiven „schwarzen Rauchern" sowie einige diffuse hydrothermale Austrittsstellen. An den schwarzen Rauchern und den rauchenden Kratern wurden Temperaturen von bis zu 350°C gemessen. Die Umgebungsgesteine des LHF sind zu über 70% serpentinisierte Mantelperidotite sowie mehr als 20% Gabbros. Basalt spielt im LHF eine nur untergeordnete Rolle.

Mit TV-Greifer und ferngesteuerten, unbemannten Tauchrobotern konnten viele Serpentinite, Gabbros und alterierte Sedimente aus dem LHF und der näheren Umgebung geborgen werden. In dieser Arbeit werden neue Spurenelement-, sowie Strontium und Sauerstoffisotopendaten von Serpentiniten, Gabbros sowie deren <2μm Fraktion (Ton-Fraktion) vorgestellt. Mit Hilfe dieser Daten ist es möglich die Zusammenhänge von Alterationsprozessen, Wasser-Gesteins-Reaktionen und Spurenelementvariationen zu verstehen. Die gesammelten Mantelperidotite sind zu >95% serpentinisiert. Die meisten Gabbros sind relativ frisch und zeigen kaum Alterationsspuren. Die Variationen in den Spurenelementen der analysierten Gesteine zeigen eine sehr hohe Variation in den Alterationsbedingungen im LHF. Die leichten seltenen Erden zeigen eine starke Anreicherung in allen analysierten Serpentiniten, was auf starke Einflüsse der hydrothermalen Lösungen schließen lässt. Sauerstoffisotopendaten lassen auf Serpentinisierungstemperaturen von etwa 130-150°C schließen. Die Bildung von Chloriten in der Nähe von schwarzen Rauchern geschah bei etwa 150-200°C. Negative sowie positive Eu-anomalien in Serpentiniten zeugen weiterhin für unterschiedliche Alterationsbedingungen: (1) Hochtemperatur Alteration unter sauren, reduzierenden Bedingungen sowie (2) Tief-temperatur Alteration unter Seewasserbedingungen. Die Abwesenheit von Brucit sowie das Auftreten von Talk weist auf hohe Konzentrationen von SiO_2 in den Fluiden hin. Petrologische Beobachtungen, HFSE Daten (HFSE=Elemente mit hoher Feldstärke) sowie das Verhalten der seltenen Erden legen den Schluss nahe, dass eine Interaktion der Serpentinite mit mafischen Schmelzen wichtiger Prozess in der Umgebung des LHF ist.

Die Berechnung von relativen Anreicherungen und Verlusten von Haupt- und Spurenelementen ist ein weiterer Schritt um die verschiedenen Alterationsprozesse zu unterscheiden. Die Kombination von Serpentinisierung, hydrothermaler Alteration, Ozeanbodenverwitterung und Gesteins-Schmelze Wechselwirkungen ermöglichte deutliche Elementbewegungen. Die Serpentinisierung der Mantelgesteine war in erster Linie isochemisch. Nur der Verlust von CaO ist deutlich. Allerdings sind die meisten Spurenelemente stark in den Serpentiniten angereichert. Dabei sind die Elemente Cu, Ba, Eu, Th und U besonders in Proben direkt aus dem LHF angereichert, was auf die hohe hydrothermale Aktivität zurückzuführen ist. Mafische Intrusionen scheinen dagegen eine Senke für Mg darzustellen, welches für die Bildung von Mg-reichen Tonmineralen benötigt wird. Des Weiteren sind die mafischen Intrusionen wichtige Lieferanten für SiO_2, CaO und Na_2O sowie viele Spurenelemente.

Abstract

Detailed bathymetric mapping of the area of 15°N (MAR) as well as geological mapping of the Logatchev hydrothermal field at 14°45´N (MAR) leads to a very well description of the Logatchev hydrothermal field and adjacent areas. Main parts of the Logatchev hydrothermal field are located in a depression filled with talus material and pelagic sediment this causes an increase in porosity and permeability in the subseafloor influencing fluid pathways importantly and provide aquifers wherein fluids can spread out laterally in layers of mafic/ultramafic talus. The "smoking craters" of the Logatchev hydrothermal field are rare structures which have only been identified at Logatchev and the, in 2005 newly discovered, Nibelungen-Field at the southern MAR (Koschinsky at al., 2006). Bathymetric maping of the seafloor reveal that the hydrothermal activity at Logatchev mainly is fault controlled. The Logatchev hydrothermal field is characterized by five smoking craters, two hydrothermal mounds with black smokers and a couple of diffuse vent sites. The smoking craters emanate fluids with temperatures up to ~350°C. Host Rocks of the field are mainly serpentinites (>70%) and gabbroic rocks (>20%) with subordinately basalt.

Serpentinites, gabbroic rocks, and altered sediments were sampled from the active ultramafic hosted Logatchev hydrothermal field (LHF) by ROV deployments and TV-guided grab. In this study we present new data of clay-size separates and whole rock chemistry as well as strontium and oxygen isotopic compositions in order to investigate the alteration processes, water-rock reactions and associated elemental exchanges.

The samples of mantle peridotites are mostly serpentinized (>95 vol%) whereas some gabbroic samples are moderately to completely altered. Changes in geochemical compositions, especially trace element compositions, of the altered rocks indicate a highly heterogeneous distribution of alteration styles. Light rare earth elements are enriched in all serpentinites and suggest a strong influence of Logatchev vent fluids during some stages of serpentinization. Oxygen isotopic data of lizardites reveal formation temperatures of 130-150°C whereas chlorite formation in altered gabbroic samples occurred between 150° and 200°C in the LHF. Negative as well as positive Eu anomalies in serpentinites suggest varying alteration processes: (1) high temperature alteration in acidic, reducing conditions as well as (2) low temperature alteration in neutral, oxidizing environments. The absence of brucite and the formation of talc indicate high concentrations of aquatic silica in the Logatchev area. Petrographic investigations, high field strength element data and elevated rare earth elements indicate that melt–rock interaction is also an important factor affecting mantle peridotite prior to serpentinization processes at LHF. Therefore gabbroic intrusions are the most probable source for aquatic silica. Strontium isotopic data suggest high water/rock ratios in the range of 2.6-27 and alteration fluids which are characterized by high contents of heated seawater.

Calculations of relative gains and losses of major and trace elements as well as mineralogical observations reveal that a large variety of alteration styles take place at the Logatchev hydrothermal field. A combination of serpentinization, hydrothermal fluids, melt-rock interaction and low-temperature seafloor weathering lead to significant gains and losses of major and trace elements. We found that serpentinization at Logatchev was isochemical for the most major elements (excepting a loss of TiO_2 and CaO). However, the concentration of trace elements e.g., Cu, Nb, Ba, La, Sm, Eu, Th or U increases strongly in the serpentinites. In addition, gabbroic intrusions are a sink for MgO during the formation of chlorite and serpentine after clinopyroxene and play a major role as distributors of SiO_2, TiO_2, CaO, and Na_2O as well as numerous trace elements in the circulating fluids.

Chapter 1:
The geology and structure of the Logatchev hydrothermal field

Abstract

Detailed bathymetric mapping of the area of 15°N (MAR) as well as geological mapping of the Logatchev hydrothermal field at 14°45´N (MAR) leads to a very well description of the Logatchev hydrothermal field and adjacent areas. Main parts of the Logatchev hydrothermal field are located in a depression filled with talus material and pelagic sediment this causes an increase in porosity and permeability in the subseafloor influencing fluid pathways importantly and provide aquifers wherein fluids can spread out laterally in layers of mafic/ultramafic talus. The "smoking craters" of the Logatchev hydrothermal field are rare structures which have only been identified at Logatchev and the Nibelungen-Field at the southern MAR (Koschinsky at al., 2006). Bathymetric mapping of the seafloor reveal that the hydrothermal activity at Logatchev mainly is fault controlled. The Logatchev hydrothermal field is characterized by five smoking craters, two hydrothermal mounds with black smokers and a couple of diffuse vent sites. The smoking craters emanate fluids with temperatures up to ~350°C. Host Rocks of the field are mainly serpentinites (>70%) and gabbroic rocks (>20%) with subordinately basalt.

1. Introduction

The Mid-Atlantic Ridge at 15°N is characterized by slow spreading rates and magma starved short ridge Segments (Cannat et al., 1997). Tectonic extension occurs along large scale faults leading to a significant cooling of the crust (Alt and Bach, 2003). In case of low magmatic production and low spreading rates, mantle peridotites may be transported to the seafloor due to the tectonically extension. Consequently, ultramafic rocks are a major and an important part of the oceanic lithosphere especially along slow- and ultra-slow spreading ridge systems comprising more than 20% of the lithosphere (Humphris et al., 2003). At the MAR, between 14°30´N and 15°50´N, , extensive exposures of lower crust and upper mantle rocks were found suggesting a highly reduced magma supply along the MAR in this area (Cannat et al., 1992; Rona et al., 1987).

At least two hydrothermal systems between 14° and 17°N are characterized by high-temperature circulating fluids. The northernmost one is an inactive field, discovered in 2002 at 16°38´N (Bel´tenev et al., 2004). The second is the active ultramafic hosted Logatchev hydrothermal field at 14°45´N which was first described by Cherkashev et al. (2000).

In the framework of the German Priority Program SPP-1144: "From Mantle to Ocean", funded by the Deutsche Forschungsgemeinschaft (DFG) three cruises (M60/3 and M64/2) to the Logatchev hydrothermal field were carried out in 2004 and 2005 by the German RV Meteor. In Addition two more expeditions to the Logatchev area with the RV Maria S. Merian were carried out in 2006 and 2007 (MSM03-2 and MSM04-3). The main scientific aim of these cruises were to investigate the interrelationship of geological, geochemical, and biological processes in the active Logatchev hydrothermal field at 14°45′N on the MAR (Kuhn et al., 2004a; Kuhn et al., 2004b; Kuhn et al., 2005; Lackschewitz et al., 2005).

This paper uses a combination of bathymetric mapping and video observations to characterize the geological characteristics of the MAR at 15°N with a very strong focus to the detailed description of the so-called Logatchev-1 hydrothermal field. In addition we give discuss some evidences for possible heat sources and compare the attributes of the Logatchev field with other known vent-fields.

2. **Methods**

Bathymetric data between 14°26'N and 15°02'N were gathered during the HYDROMAR I-III cruises with R/V Meteor and R/V Maria S. Merian (Kuhn et al., 2004a; Lackschewitz et al., 2005, Petersen et al., in prep.). The bathymetric coverage was acquired with Hydrosweep multibeam echosounding system which was installed on the hull of R/V Meteor (Atlas-Elektronik GmbH, Bremen) as well as with Simrad EM 120 installed on the hull of R/V Maria S. Merian (Kongsberg Simrad). The footprint of each beam of the Hydrosweep system was approximately 100 m, the footprint of the Simrad system was approximately 30 m.

After data acquisition depth offsets were removed and the raw data were transformed into XYZ data based on Mercator projection and regular gridding. The analysis of the bathymetric data and the creation of bathymetric maps were carried out with the software package Generic Mapping Tool (GMT) and Surfer™.

Small- (some hundreds of metres) and medium-scale (few kilometres) video mapping was carried out with the Remotely Operated Vehicles (ROV) Quest and Jason II as well as a TV-sled (OFOS = Ocean Floor Observation System). Geological mapping within the Logatchev-1 field was carried out using the ROV Quest (MARUM, University of Bremen) and Jason II (Woods Hole Oceanographic Institute). Both systems are remotely operated vehicles (ROV) with electric propulsion equipped with a set of online color cameras, sensor tools, two manipulators and a fluid sampling system. Data produced during ROV dives was organized in the Geo Information System Adelie GIS.

The navigation of ROV Quest was realized by two systems: a Doppler-Velocity-Log navigation and an USBL navigation (ultra short base line). The position of the ROV was calculated relative to a calibrated reference station. Navigational purposes were supported

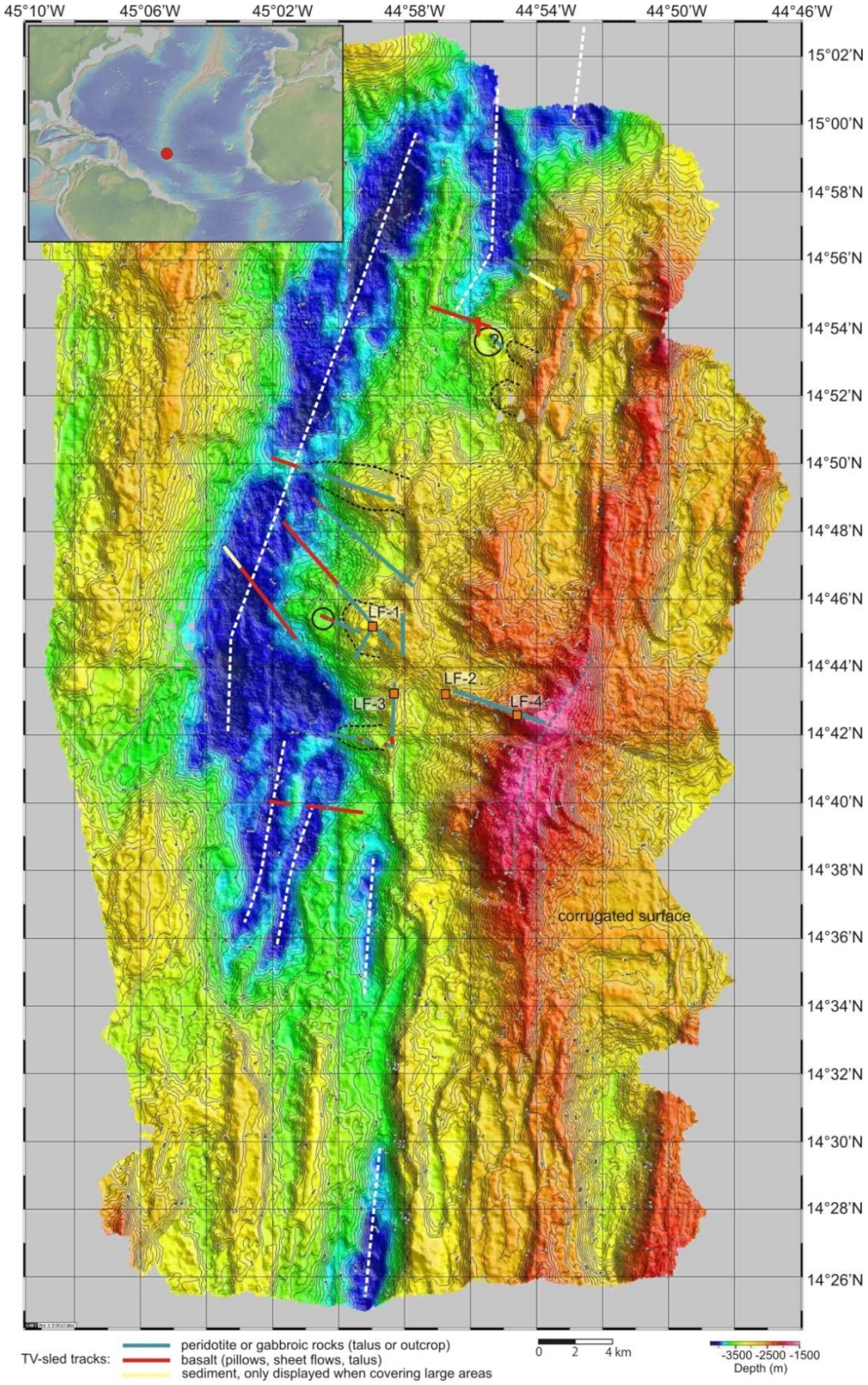

Fig. 1.1: Bathymetric map of the studied area produced with *GMT* during M60/3. Orange squares: Logatchev hydrothermal fields-1 to -4. White lines: striking of the axial vally deeps (at 15°00'N after Fujiwara et al., 2003). Grey, stippled lines: flexure-like shape of the rift mountain crest and a N108° striking "structure" (fault) cross cutting it. Black circles: off-axis basalt volcanoes. Black, dotted lines: suggested slumping structures. ?: marks an area of ultramafic rocks in a basalt volcano which probably is the result of a navigational error.

by an array of Sonardyne HF beacons set in the vent field connected with a ROV Homer System mounted on the ROV. The Doppler-Velocity-Log navigation under the given conditions is characterized by a gradually increasing offset which becomes obvious at calibrated markers like homer beacons, temperature loggers, markers from other cruises or certain structures. If the offset was realized during a ROV station the position was reset. Accuracy of the USBL navigation is about ±15 m (in each direction). The recorded positional data of several ROV tracks during Hydromar I cruise in 2004 showed offsets up to 38 m. In order to minimize the navigational errors of prominent seafloor structures the mean value of all positions for one structure mapped during different dives was taken in the final geological map. The more dives visited one and the same structure the better the result and the smaller the positional error.

ROV Jason II used a LBL navigation during cruise MSM 04/2 in the Logatchev-1 field (Borowski et al., in prep.). Navigational data from this cruise was used to correct navigational errors from the previous dives in order to create a comprehensive geological map of the Logatchev-1 hydrothermal field. This geological map was prepared using the video data from the ROV dives as well as by rock and sulfide samples which were recovered using the ROV as well as a TV-grab (Kuhn et al., 2004a; Lackschewitz et al., 2005; Borowski et al., in prep.).

3. Geological setting

The Logatchev hydrothermal field is situated on the eastern flank of the MAR rift valley south of the "Fifteen-Twenty fracture zone" near 14°45'N (Fig. 1; Batuyev et al., 1994). Full spreading rates of that area are estimated to be about 2.6 cm/yr (DeMets et al., 1990; Escartín and Cannat, 1999; Fujiwara et al., 2003).

Between 12°N and 16°N the Mid-Atlantic Ridge is characterized by magma-starved, short ridge segments interrupted by non-transform discontinuities as well as closely spaced major fracture zones (Cannat et al., 1997). The segments show a discontinuous and irregularly shaped structure with a deep central rift valley (>3000 m) due to slow spreading.

In this area tectonic spreading dominates over basaltic magma supply resulting in a tectonic uplift of mantle and lower crust rocks (peridotites, gabbros) to the seafloor (Cannat et al., 1997). Especially between 14°30'N and 15°50'N outcropping of these lower crustal and mantle rocks on both flanks of the axial valley is widespread and the most extensive yet reported for the MAR (Cannat et al., 1997).

Between the Fifteen-Twenty fracture zone and 14°30'N, axial deeps form a series of 8 to 18 km long basins that are offset to the west between the Fifteen-Twenty fracture zone and 14°50'N, then to the east between 14°50'N and 14°30'N (Fig. 1.1; Cannat et al., 1997). The axial deep south of 14°30'N is continuous and trends N 07°, perpendicular to the fracture zone trend.

In the area south of the Fifteen-Twenty fracture zone hydrothermal mineralization were detected at 14°55'N (Eberhardt et al., 1988; Rona et al., 1987) and in the Logatchev field at 14°45'N (Batuyev et al., 1994). This sites are hosted by ultramafic rocks. Subordinate outcrops of gabbros and basalts also occur (Franz et al., submitt.; Krasnov et al., 1995).

The Logatchev hydrothermal field (at least 800 m NW-SE, 500 m SW-NE) is situated on the eastern rift flank at 14°45'N / 44°58'W on a plateau right below a 350 m high cliff between 3060 m and 2900 m water depth (Fig. 1.1). Serpentinized peridotites and subordinately basalts as well as gabbronorites form the host rocks. Coarse- to large-grained gabbronoritic cumulates, norites and Plg-websterites which are interpreted as magmatic cumulates from the crust/mantle transition zone also occur (Kuhn et al., 2004a; Franz et al., submitt.).

4. Seafloor morphology of the MAR at 14°45'N

Rift Valley

The Rift valley floor at 3900-4200 m depths consists of a moderately (< 30%) sedimented area with isolated volcanic constructions forming small mounds and elongated ridges often with step faulted outcrops (Fig. 1.1, 1. 2). The previous sampling of the rift valley (Simonov et al., 1999), mainly in the northern part (north of 14º50'N), showed the presence of both ultramafics and basaltic rocks. The present study confirms this finding and shows that basaltic outcrops are prominent in the Rift Valley deeper than 3900 m depths (Fig. 1.2).

It was also found that the spreading is taking place in a narrow zone (< 1 km) with active fault scarps and recent, N-S oriented fissures. The younger flows observed are tubular and bulbous lava with preserved small "yam-like" protrusions extruded from the larger pillows. Sheet flows in the form of lobated, flat and ropy surfaces were observed during deep towed bottom camera stations. The sheet flows often show collapsed features of drained lava.

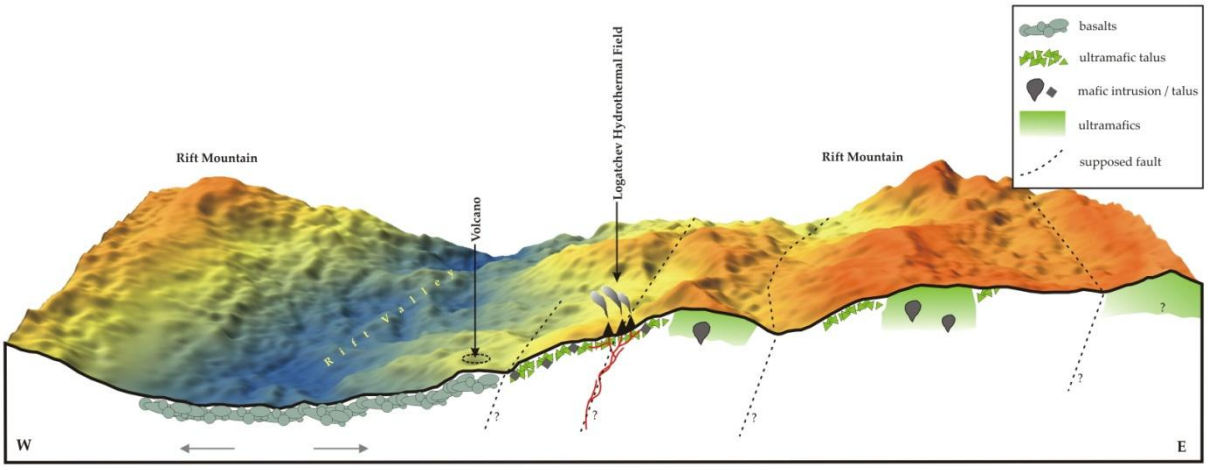

Fig. 1.2: Schematic cross-section through the Mid-Atlantic Ridge rift segment at 14°45'N including the Logatchev-1 hydrothermal field. Batymetric data from cruise M60/3.

Rift Mountains (RM)

The eastern and the western wall of the Rift Valley axis, also called the "Rift Mountains", are asymmetrical with respect to the axis of the MAR near 14°45'N (Figs. 1.1, 1.2). In the explored area, the summits of the east and west walls culminate at 1600 m and 2900 m respectively, at about 10 km and 4 km away from the MAR axis. Also the east Rift Mountain is characterized by several cross-cutting faults (Fig. 1.1). The main orientation of the fault scarps are to the N010° direction which also corresponds to the general spreading direction. The other direction of faulting is to N270°-280° which is transverse to the other main faulted structures (Fig. 1.1).

The RM region located to the east of the Rift Valley at 14°45'N and along longitudes 44°57'W and 44°52'W constitute the prominent features of ridge crest marginal highs oriented to N013° as the MAR axis. The summit of the first discontinuous set of the rift mountain consists of a plateau culminating at about 2900 m depths that is about 1000 meters above the rift valley floor (4100 m depths; Fig. 1.2). The first structural break of the RM on the east wall at 3050 m contour line shows a narrow (<300 m wide) "sliver-like" linear structure with a small east facing depression (<300 depth), which is oriented to N013º. A bottom video camera station along this plateau near 2970 m depths showed abundant sediment cover and horizontal ledges of ultramafics outcrops associated with patches of inactive hydrothermal fields made up of dead clam shells. The west facing flank of this east Rift Mountain wall between 2950 m and 3600 m depths consists of several small staircase scarps representing normal faults also oriented to N013°. Several of these scarps are covered with large landslides forming poorly sorted talus made up of large mafic and ultramafic rocks (Fig. 1.2). Another TV-sled station (84OFOS on M60/3; Kuhn et al., 2004a) carried out along a N-S track on top of the plateau near 14°43'N / 44°58.50'W at about 3020 m depths shows in situ massif ultramafic outcrops (Fig. 1.1). These outcrops extend few hundreds of meters along faulted scarps. Further to the south near 14°41.70'N / 44°58'W a volcanic construction made up pillow lava was seen at about 3000 m depths.

The rift mountain becomes shallower (1600-2400 m depths) further to the east with steep faulted scarp culminating with a plateau along longitude 44°52'W (Fig. 1.2). As observed from a TV-sled station (27OFOS) and sampling (TV-grab), several of these scarps, near 14°42'N / 44°52'W at 2700 m and at about 2500 m depth show in situ outcrops of serpentinized peridotite alternating with basaltic flows. Altered debris of basalts and serpentinized peridotites were recovered at 1608 m and 1950 m depths near 14°42.3'N / 44°51.87'W (Kuhn et al., 2004a).

Thus, the RM walls going from the summit plateau at 1600m depth down to the intersection with the rift valley at 3850 m depths consists of several step-faulted structures with small relief which are often buried by slumped material. However, during two video camera stations large ultramafic blocks were observed and it is not clear weather these large blocks are in place or they represent down-slope transported debris.

The contact between peridotites, gabbronorites and the basalts is mainly situated at the lower part of the inner flank close to the morphological transition from the slope to the rift valley floor. This contact is often burried by talus material (Fig. 1.2; Kuhn et al., 2004a).

Between 14°38'N and 14°46'N the top of the eastern rift mountains are characterized by a NNE-SSW striking flexure-like shape (Fig. 1.1). Also the smaller and younger ridges to the west of the main chain and the axial rift valley show a change of striking direction to NNE-SSW. However, there is a gradual offset to the south of this flexure-like structure starting from the rift valley to the top of the eastern rift flank (Fig. 1.1). This could be interpreted by a propagating of the rift segment (spreading) to the north implying a magmatically dominated rift segment. The magmatic activity could also be proven by basalts found in the central valley and the basalt volcanoes at the lower rift flank.

In the east of the rift mountain crest lineations, sub-parallel to the spreding direction, are present at about 14°38.5'N – 14°35'N / 44°50'W – 44°56.3'W (Fig. 1.1, marked "corrugated surfaces"; Schreiber, 2006). These could be interpreted as a megamullion which is a large (up to 10's of km on a side), domed seafloor edifice that has surfaces corrugated by distinctive mullion structures (Tucholke et al., 2003). These lineations are interpreted as the exposed surfaces of long-living (~1 – 2 m.y.) normal, "detachment" faults that tectonically uplift ultramafic rocks (Fig. 1; Cann et al., 1997; Tucholke et al., 1998, 2003; Escartín & Cannat, 1999). The striations or corrugations have been interpreted variously as abrasion marks (Cann et al., 1997), compressional structures (Tucholke et al., 1998, 2003), and ridge-perpendicular extensional faults (Karson, 1999).

While oceanic detachments elsewhere seem to occur in crust formed at the inside corner of ridge discontinuities, in the 15°N region they occur on both sides of the axis and away from the main transform fault (here the Fifteen-Twenty fracture zone), and cannot be associated with any non-transform discontinuity (Escartín & Cannat, 1999). Although the western border cannot be determined precisely the proposed megamullion at ~14°36'N is at least 13 km across-axis and 6 km along-axis, and has a wavelength of ~1 km. To the east and the south of the megamullion there are two other regions which might show corrugated surfaces (Schreiber, 2006). If this is the case the megamullion has an extension of 18 x 10 km. The megamullion is not well developed in terms of the dome shape that is normally exhibited and it is uncertain whether the detachment fault that formed this feature is still active or has been replaced by a younger fault closer to the rift axis (Fujiwara et al., 2003).

The formation of oceanic crust detachment faults is hypothesized to be promoted by tectonic extension due to low magma supply to the ridge axis (Cannat et al., 1995; Karson and Lawrence, 1997; Fujiwara et al., 2003; Tucholke et al., 2003). However, Tucholke et al. (2003) suggest that there is a distinct melt supply, otherwise more frequent and shorter-lived faults may become dominant. The basalts forming the central valley and the off-axis volcanoes are a reference to this melt supply.

About 60 km off-axis near 15°00'N / 44°28'W there is a second, domed and corrugated surface discribed from the eastern flank (about 4 Ma; Fujiwara et al., 2003).

Slumped structures (land-slide)

The presence of irregularly bulged features bounded by E-W oriented transverse faults near the base of the rift mountain at the intersection with the rift valley floor are believed to represent large slumped structures. They are defined by their concentric oval shaped contour lines observed from bathymetry (Fig. 1.1). These features are bounded by "en echelon" faults and form several "step like" terraces bounded by west facing small and semi-circular scarps (<100 m relief) covered with talus material (Fig. 1.3). The terrace and fault steps extend down to the western slope at the intersection with the rift valley floor (Figs. 1.1, 1.2).

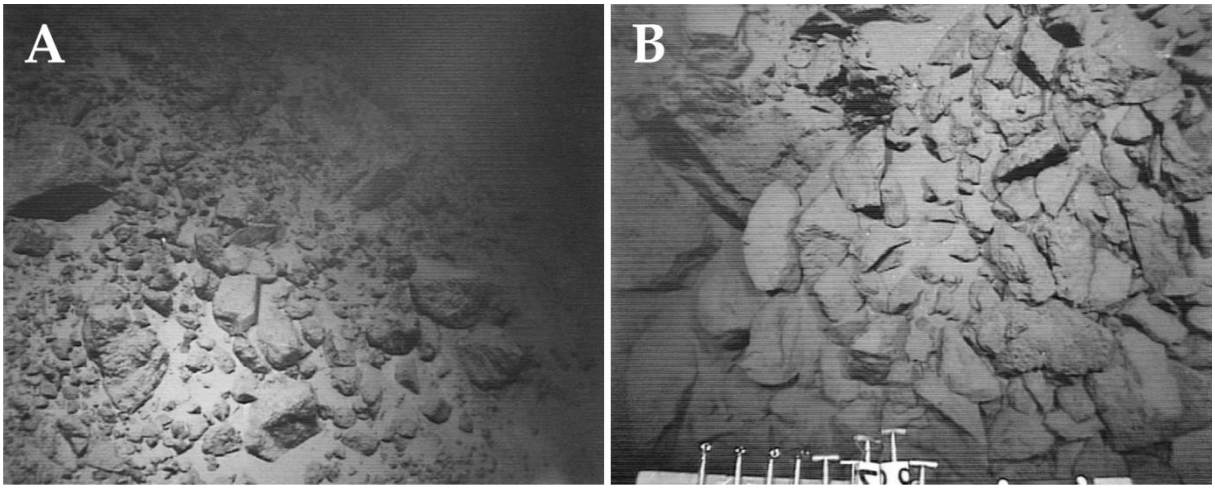

Fig. 1.3: A+B typical appearance of ultramafic or mafic talus.

The sizes of these slumped structures vary from about 1 km to 4 km in length and 1 km to 2 km in width. The mass-waste forming these structures extends over more than 4 km down slope of the eastern wall between 3100 and 3400 m depth. They are covered by pelagic and hydrothermal sediment, with some isolated patches of loose tabular and irregularly shaped blocks of ultramafics (Fig. 1.3). The irregular distribution of the sediment and the avalanches of debris indicate that the slumping is still an on-going process, probably as the result of major tectonic events that must have taken place during the uplift of the rift mountain structures forming the rift valley walls.

Hydrothermal fields

Based on the detection of hydrothermal plumes in the water column and diverse seafloor observations up to four hydrothermal fields (Logatchev 1-4) were observed or suggested in the northern region between 14°45'N and 14°42.38'N (Fig. 1.1; Cherkashev et al., 2000; Lein et al., 2003, Kuhn et al., 2004a). This work is primarily concerned with the description of the well observed, so-called Logatchev-1 field.

There seems to be three factors which control the location of: (1) cross-cutting faults, (2) young basaltic volcanism, and (3) slumped structures (Kuhn et al., 2004a). The Logatchev hydrothermal field occur at the intersection of a large WNW-ESE structure with N-S faults Apart from the obvious N-S and WNW-ESE orientation of bathymetric structures, there is another prominent orientation of NW-SE (N330° – N340°). This orientation is present both in large-scale structures (Fig. 1.1) as well as in small-scale structures like the orientation of the vent sites in the Logatchev hydrothermal field along a N330°-striking line (Fig. 1.4; Schreiber, 2006).

A possible heat source for the hydrothermal fields could be a magmatic one since relatively fresh basaltic lava flows were discovered in the rift valley just west of the Logatchev fields. Moreover, a young off-axis volcano was mapped at the intersection of the rift valley with the eastern valley wall at 14°45.3'N and 45°02'W (Fig. 1.1 and 1.2). The interpretation of the bathymetric structures of the rift valley as a propagating rift which means that the segment is in a volcanically active phase, also supports a magmatic heat source for the hydrothermal system. A third factor in favour of the site of formation of the Logatchev hydrothermal fields could be the presence of a porous medium like rock talus. The presence of such slump structures were detected from bathymetry and ocean floor observations (Kuhn et al., 2004a).

5. Geology of the Logatchev hydrothermal field

The Logatchev hydrothermal field is situated on the eastern rift mountain of the MAR below a 350 m high cliff at water depths between 3060 and 2900 m. The hydrothermal field extends at least 800 m in NW-SE and 500 m in SW-NE direction (Fig. 1.4).

About 550 – 600 m SW of the field and 320 m WNW of the field atacamite group minerals (a copper chloride) were sampled and hydrothermal precipitates have been observed suggesting an even larger field than yet explored (samples: 14°44.109'N / 44°58.97'W; 14°45.23'N / 44°58.58'W; TV-sled observation: 14°44.86'N / 44°59.12'W; Lackschewitz et al., 2005; Kuhn et al., 2004a).

Most of the main vent sites (except QUEST) follow a "line" with an orientation of about N333°. Nevertheless some inactive smoker and numerous hydrothermal precipitates are located outside of this zone (Fig. 1.4).

The Logatchev area is largely covered by pelagic sediment along with ultramafic or mafic rock talus. The edges of the hydrothermal field are characterized by pelagic sediment with some talus. Rippled sediments indicate strong bottom currents (Schreiber, 2006). Outcropping ultramafic or mafic material is scarce. There are only a few large blocks which might be outcrops.

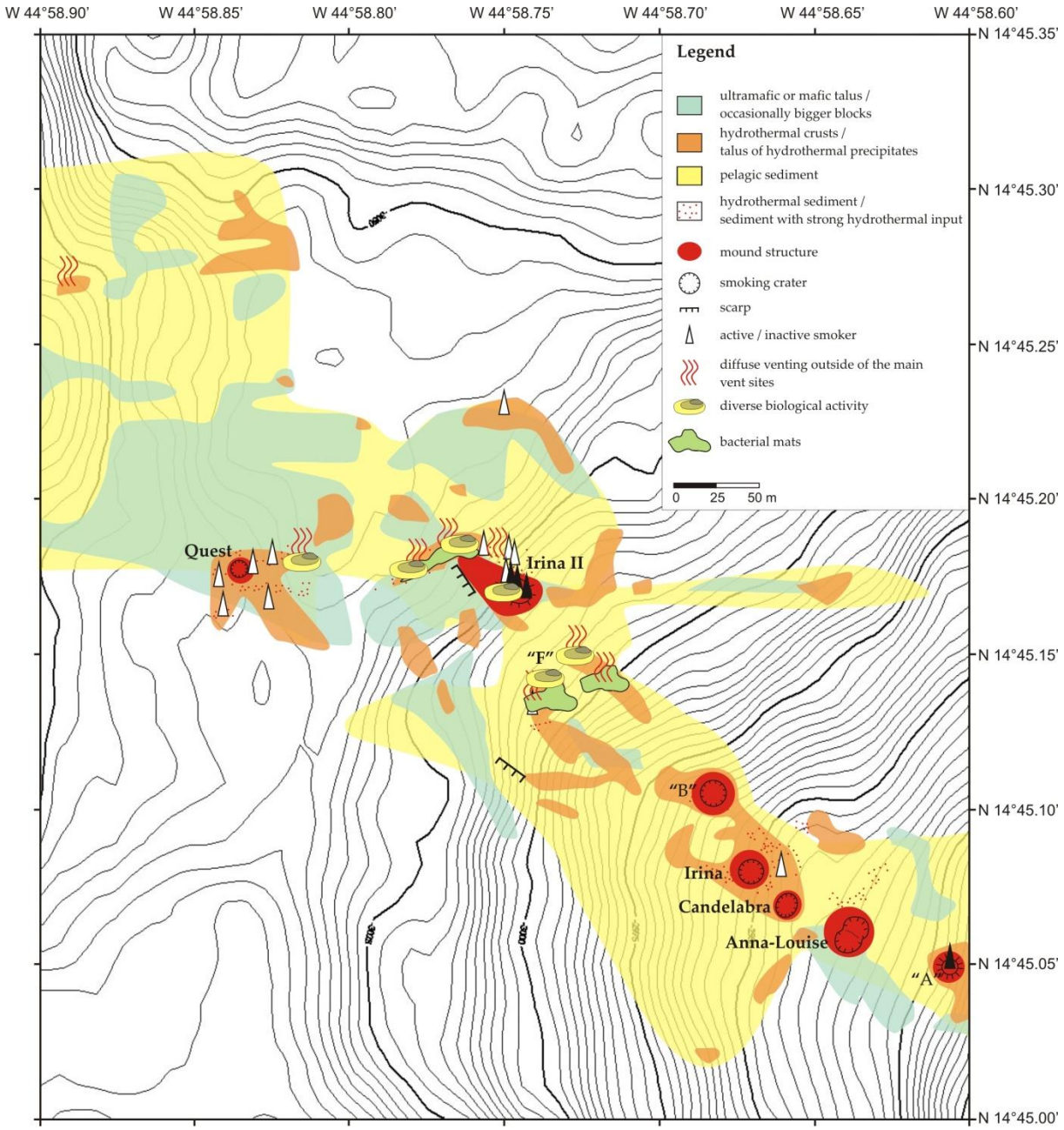

Fig. 1.4: General geological map of the Logatchev (-1) hydrothermal field (based on Schreiber, 2006). Bathymetric and geological data from cruises M60/3, M64/2 and MSM04-3. The displayed high- and low-temperature vent sites are situated in a narrow NW-SE striking zone.

Host rocks of the Logatchev field are mainly serpentinized peridotites (>70%) while basalt and gabbro occur subordinately (>20 %; Kuhn et al., 2004b). The dominating ultramafics are medium- to coarse-grained serpentinized peridotites (harzburgites and dunites; Fig. 1.5; Kuhn et al., 2004a).

The suite of mafic rocks comprises mafic intrusives like medium-grained gabbronorites and coarse- to large-grained gabbronoritic cumulates, norites and Plg-websterites (Fig. 1.5). Whereas the latter are interpreted as dykes, cumulates or cristallysates of polyphase magma intrusions (at the crust/mantle transition zone), the gabbronorites are typical MOR-intrusives

(Franz et al., 2005; 2006). The intrusives often show magmatic contacts with or xenoliths of serpentinites indicating their intrusion into the ultramafics (Kuhn et al., 2004a; Franz et al., 2007). Since these contacts were formed after the serpentinization, the mafic intrusions could also be a heat source for the Logatchev field (Franz et al., 2005).

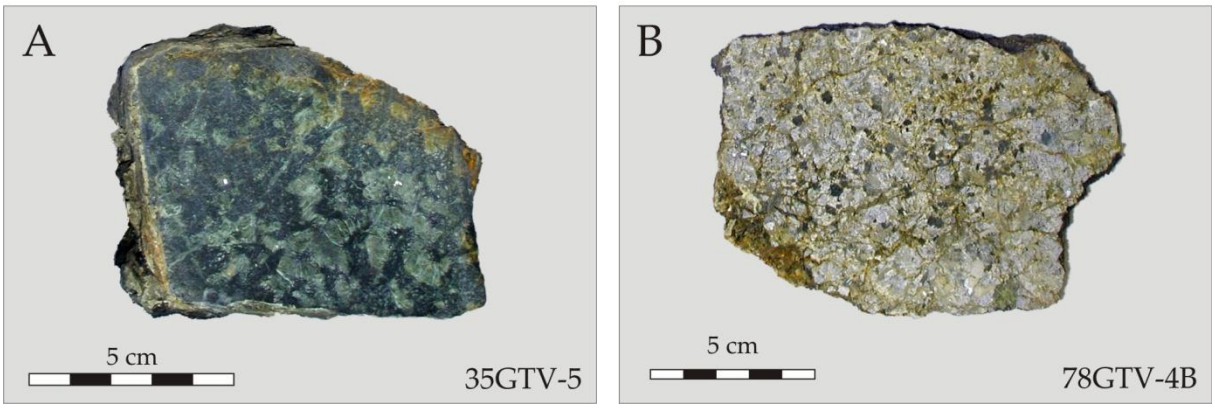

Fig. 1.5: Host rocks of the Logatchev hydrothermal field: (A) Serpentinized Harzburgite; (B) slightly altered, coarse grained gabbro.

Basalts subordinately occur as mafic extrusives of the MOR-volcanism, mainly on the rift valley floor (Fig. 1.1). The occurrence of pillow basalts in the surroundings of the Logatchev field also point to a possible magmatic heat source.

The large variety of hydrothermal precipitates include active and inactive massive chalcopyrite chimneys, massive sulphides, silicified breccias and crusts, soft and indurated hydrothermal sediment, abundant secondary Cu-sulphides, abundant Fe-Mn-oxyhydroxides as well as atacamite (Fig. 1.6; Kuhn et al., 2004a, b; Petersen et al., 2005).

The Logatchev-1 field consists of seven known high-temperature sites with different morphologies (Fig. 1.4). Whereas IRINA II and Site "A" are build up of a mound with 1 to 5 m high black smoker chimneys on top, the other five sites QUEST, "B", IRINA, CANDELABRA and ANNA-LOUISE are so-called "smoking craters".

Smoking craters are not sitting on top of a large mound structure but they rather form single low-lying mounds on the seafloor causing a terrace-like appearance of an otherwise steep slope. The craters show a rim that is 1 to >5 m high and a 2 – 5 m deep central depression. They consist mainly of partly oxidized sulphide talus. Furthermore, red stained serpentinites and altered rock talus can occur. Numerous small but sometimes up to 1 m high, delicate chimneys and small smoking pipes are situated on the crater rims and inside the crater. Black smoke is intensely emanating either from the chimneys or from holes in the ground within the craters.

In-between or northwest of the main sites there are also numerous small active and inactive sites (e.g. site "F", see Fig. 1.4). Due to diffuse venting there are mussel beds, biomats and hydrothermal precipitates as crusts or talus. The inactive sites consist of inactive

smokers and/or mussel shells as well as hydrothermal crusts or talus indicating shifting localities of hydrothermal activity in the past. These changes may be the expression of subsurface processes such as repeated dissolution and precipitation as well as repeated periods of hydrothermal activity.

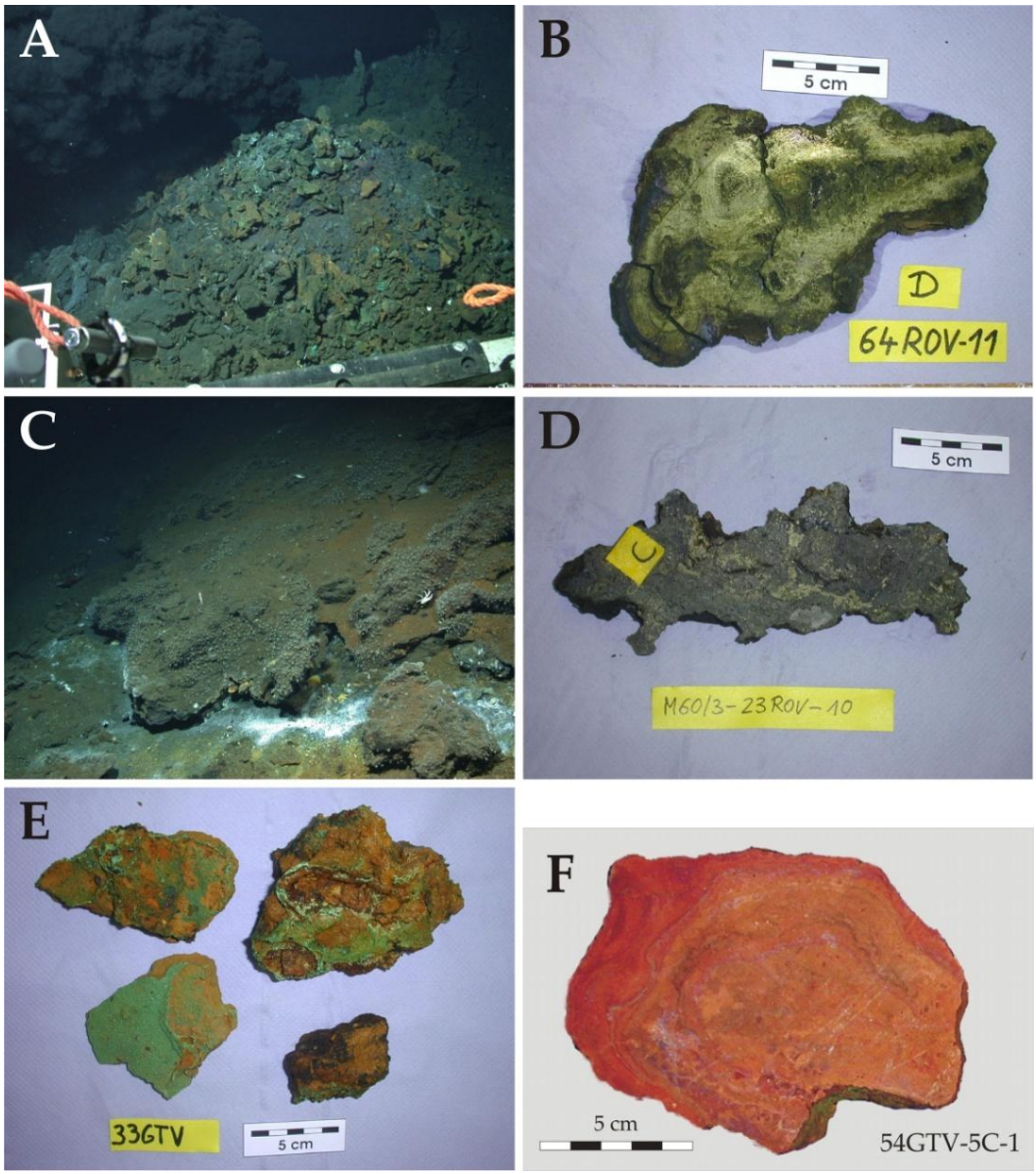

Fig. 1.6: Hydrothermal precipitates of the Logatchev hydrothermal field (photographs from cruise M60/3 and M64/2). **A:** Partly oxidized sulphide talus. Black smoke is emanating on top (IRINA). **B:** Cross-section of an inactive smoker consisting of chalcopyrite and isocubanite (ANNA LOUISE). **C:** Silica-rich cap consisting of rock fragments cemented by silica and pyrite / marcasite. (south of QUEST. **D:** Cross section of C. Sometimes the silica-rich cap is cut by hot fluids forming conduits of sulphides like chalcopyrite. **E:** Atacamite on Fe-oxihydroxides. **F:** Red hematite impregnated strongly altered serpentinite.

The **IRINA II** mound is located at 14°45.19'N / 44°58.75'W (± 30 m) and consists of an elongate mound structure rising over 15 m above the surrounding seafloor (Fig. 1.4). It has a basal diameter of about 50 m in NW-SE direction and 25m in NE-SW direction and is characterized by a steep NW and W-slope and a flat NE-slope of only a few meters. The basement consists of altered rock talus. Silicified crusts from the surroundings of IRINA II contain abundant basalt glas and plagioclase, indicating the presence of mafic extrusive material in the vicinity. At higher levels of the mound only hydrothermal precipitates occur, mainly sulphides, Fe-oxides and -hydroxides as well as hydrothermal sediment. A complex of black smoker chimneys marks the top of the mound (Fig. 1.7). Apart from some small chimneys in the west and northwest of the complex the smokers are active. Black smoke is emanating only from a few smokers but diffuse flow is evident through the chimney walls. Temperature measurements showed values up to 300 °C at a beehive structure (Borowski et al., in prep). Some of the chimneys or parts of them are densely overgrown by mussels (*Bathymodiolus cf. puteoserpentis*). Clusters of gastropods occur subordinately. The other chimneys are devoid of fauna or densily populated by shrimps (mainly: *Rimicaris cf. exoculatus*; Lackschewitz et al., 2005).

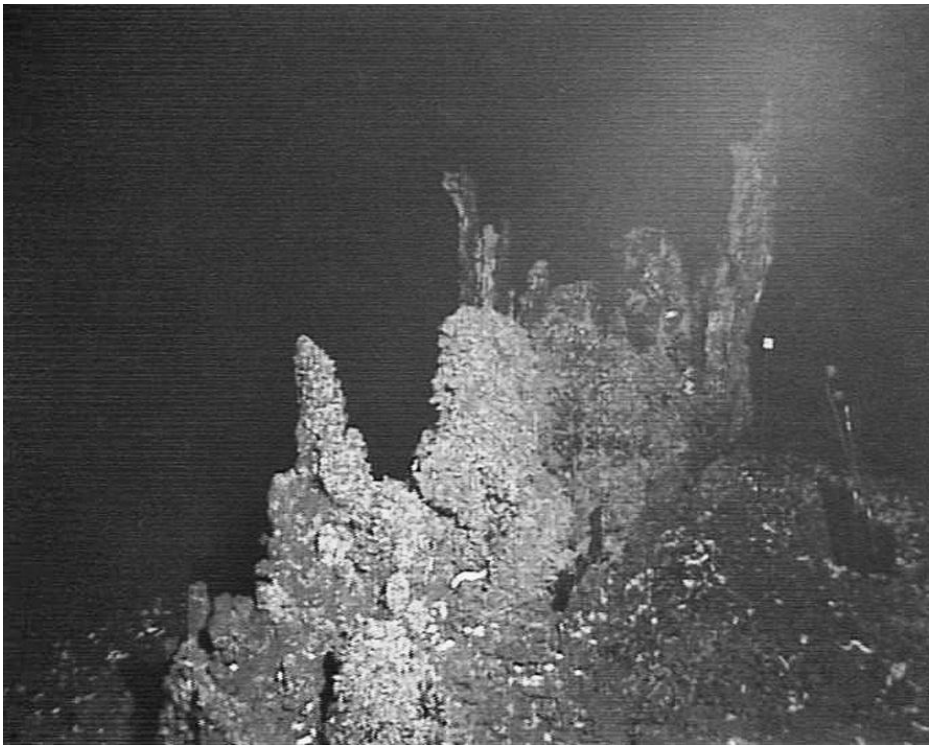

Fig. 1.7: IRINA II-complex. View to southeast and onto to the north-western side of the smoker complex. The chimneys follow a NW-SE striking line (photograph taken during cruise M60/3 in 2004).

At the southeastern end of the smoker complex about two meter away, there is a separate, small but very active black smoker. The smoker differs from the other smokers in the main complex since it has only a small chimney and smoke is emanating mainly through sulphide

talus. Fluid measurements revealed temperatures of 353°C (Gebruk et al., 2000) and 340 °C (Borowski et al., in prep.). The small and separate black smoker is characterized by few shrimps, but is otherwise uninhabited.

The whole IRINA II chimney complex is surrounded by densely populated mussel beds with a *Bathymodiolus cf. puteoserpentis* association. The mussel beds are characterized by diffusely venting fluids. The temperature of these fluids range between 2.6 and 8 °C (Lackschewitz et al., 2005).

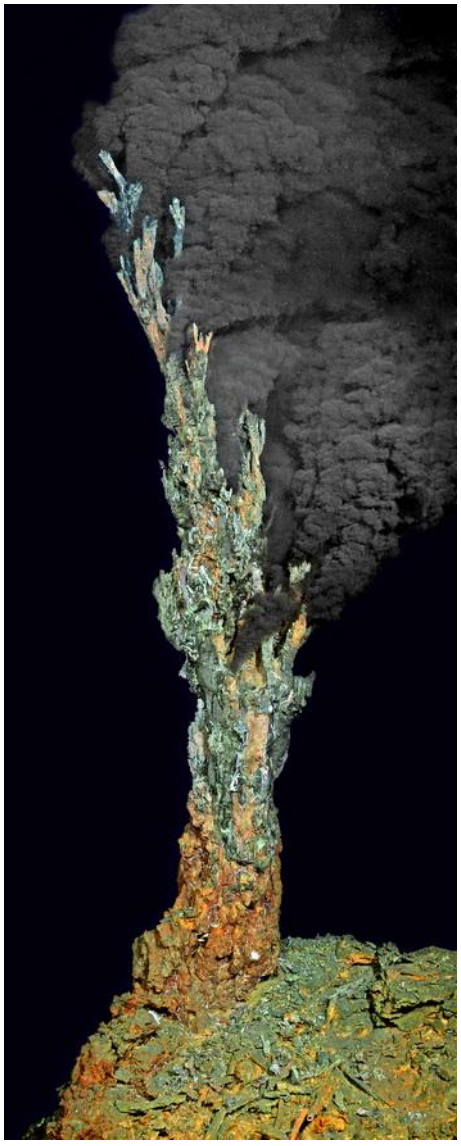

Fig. 1.8: The 5m high black smoker Barad-Dûr at SITE A marks the known south-eastern end of the Logatchev hydrothermal field. This view of the chimney was realized by post-processing of five single pictures which were taken by ROV Jason II during the cruise MSM 04/3 (2007).

Site A is situated at the southeastern end of the Logatchev hydrothermal field (14°45.043'N / 44°58.677'W) about 55 m southeast of CANDELABRA and 290 m southeast of IRINA II (± 30 m; Fig. 1.4). It consists of a mound with about 5 m high, steep slopes and the black smoker "Barad-Dûr" (approx. 5 m tall) at its top (Fig. 1.8). The mound is made up of talus of hydrothermal precipitates, probably sulphides. "Barad-Dûr" consists of a single chimney with black fluids emerging in the top region (Temperatures up to 330°C, Borowski et al., in prep.). Hydrothermal fauna is restricted to few shrimps, see-anemones (*actinaria*) and some gastropodes (*Peltospira smaragdina*) on the upper part of the chimney (Lackschewitz et al. 2005). In contrast to IRINA II and similar to most of the smoking craters there are no mussel fields but only shrimps and several actinians around the smoker or at the smoker base. The biomass density is considerably smaller than at the IRINA II mound.

The smoking crater **QUEST** is a high-temperature, black smoke venting site about 140 m westnorthwest of IRINA II (14°45.221'N / 44°58.815'W ± 30 m; Fig. 1.4). The crater rim itself has a basal diameter of about 11 m and is made up of hydrothermal sediment as well as talus of hydrothermal precipitates. The steep central depression is about 2 m deep and consists mainly of sulphide talus and its oxidation products (Fig 1.9). At the eastern rim some small inactive smokers occur. At active black smoke venting sites fluid temperatures up to 347 °C were measured (Borowski et al., in prep.). Compared to the other smoking craters in the south of the Logatchev-1 hydrothermal field, QUEST shows a higher biodiversity. Next to shrimps, a few crabs, actinarias and ophiuridaes, there are sporadic clusters of mussels (*Bathymodiolus cf.*

puteoserpentis) at the northern and eastern rim. Additionally some bacterial mats occur at the SE-rim and close to it. The surroundings of QUEST are also characterized by hydrothermal activity. Mussel beds, bacterial mats, an hydrothermal crusts assuming diffuse venting (Fig. 1.4).

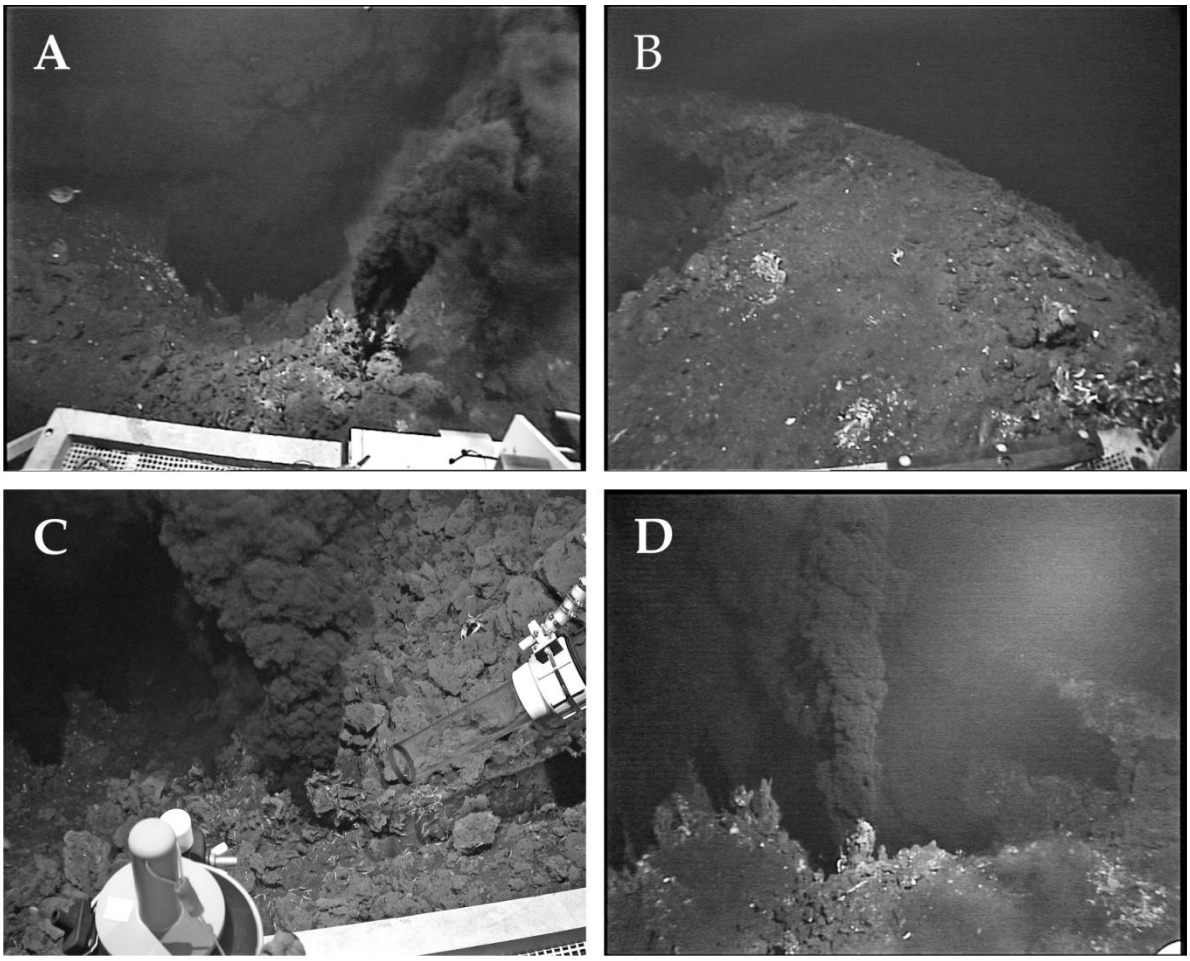

Fig. 1.9: (A) View from crater rim of Site "B" with active black smoker into the central depression where black smoke is emanating from holes in the ground. The depression is about 4 to 5 m deep and is made up of partly oxidized sulphide talus and hydrothermal sediment. (B) Northern crater rim of the smoking crater QUEST with some clusters of mussels. Left side with central depression and emanating black smoke; right side with steep slope. (C) Inner crater wall and central depression of smoking crater CANDELABRA. Both at the crater wall and in the depression black smoke is emanating from holes in the ground.(D) Crater rim of smoking crater QUEST with some small black smokers. In the back black smoke is emanating from from holes in the crater wall and in the central depression (All pictures taken during cruise M60/3 in 2004).

The smoking crater **B** is situated at 14°45.11'N / 44°58.71'W around 160 m southeast of IRINA II and 280 m southeast of QUEST (± 30 m; Fig. 1.4). With a crater rim of about 17 m in diameter it is the biggest smoking crater in the hydrothermal field. Since Gebruk et al. (2000) describes B with 1 – 3 m in diameter the smoking crater has been grown enormously in the

last years. The central depression is about 4 to 5 m deep with a gentle to steep slope (Fig. 1.9). It is made up of partly oxidized sulphide debris and hydrothermal sediment. Black smoke is emanating from holes in the ground at the deepest part of the V-shaped depression. Talus of partly oxidized sulphides as well as rock talus build up the crater rim. Several black smokers (up to 60 cm) are standing at the crater rim. Measured fluid temperatures are up to 343°C (Borowski et al., in prep.). The smoking crater B is characterized by the typical scarce fauna without any mussels.

IRINA, also called **IRINA I**, is situated at 14°45.08'N / 44°58.70'W about 200 m SE from IRINA II smoker complex, about 50 m SSE of site B and 30 m NW of the smoking crater CANDELABRA (± 30 m; Fig. 1.4). The estimated size of the crater rim lies between 10 to 15 m in diameter. Due to the partly large-sized debris the crater rim is characterized by a rough morphology with a small mound of talus at one location. The crater rim consits of partly oxidized sulphide talus, red serpentinites and probably rock debris. According to the position of the smoking craters to the ridge slope the western slope of the crater is over 5 m high whereas the outside slope in the southeast is almost missing. There are numerous small black smokers on the crater rim as well as in the central depression. Gebruk et al. (2000) published fluid temperatures of 348°C for IRINA and during cruise M64/2 temperatures of 177°C were measured (Lackschewitz et al., 2005). Apart from the typical smoking crater fauna, there are small bacterial mats growing on at the western part of the rim.

CANDELABRA is situated around 30 m SE of the smoking crater IRINA, 82 m SSE of site B and 55 m NW of site A (14°45.07'N / 44°58.69'W ± 30 m; Fig. 1.4). The smoking crater is characterized by an oval shape and a diameter of about 15 m in NE-SW direction and 12 m in NW-SE direction, i.e. it is elongated perpendicular to the preferred orientation in the Logatchev field (Fig. 1.4). The crater rim as well as the central depression are made up of partly oxidized sulphide talus (Fig 1.9). There are only a few active and inactive smokers on the rim and in the depression. Nevertheless the smokers can reach a hight of approximately 1 m. According to the terrace like location this smoking crater also shows a flat outside slope at the south and an over 2 m high slope at the north of the crater (Fig. 1.10). In the central depression, which is about 3 – 4 m deep, most of the black smoke is emanating from holes in the ground. Fluid temperature measurements revealed minimum temperatures of up to 335 °C (Borowski et al., in prep.).

The smoking crater **ANNA-LOUISE** is located around 30 m ESE of the crater CANDELABRA. Although there is a marker (round and weathered plate) it has not been described before its detection during MERIAN cruise MSM 04/3 (Borowski et al., in prep.). It is made up of one big crater which is devided by a steep wall into a bigger and a smaller subcrater. With a diameter of about 25 m this smoking crater is the biggest one in the field.

Both crater rim and the depressions are partly made up of oxidized sulphide talus and hydrothermal sediment occurs in parts of the little depression. There are only very few active and inactive smokers up to about 30 cm height on the rim but none of them in the depressions. Whereas the smaller depression is characterized by black smoke emanating only from holes in the ground, the bigger depression is characterized by smoke emanating

from holes in the depressions floor, from the inner side of the crater wall and from a little chimney on the top of the exterior crater wall. Like the other smoking craters this one also has a higher and a smaller crater wall (Fig. 1.10). ANNA-LOUISE is characterized by the scarce fauna typical of smoking craters with a few shrimps, crabs, as well as some actinaria.

Between the high-temperature venting sites IRINA II and B several mussel beds, bacterial mats and an inactive smoker occur named as **Site F** (Fig. 1.4). The area is situated approximately 80 m S to SSE of IRINA II and 80 – 100 m NW of B. Despite most of the mussels being dead, there are still some living *Bathymodiolus* mussels which together with the bacterial mats suggest diffuse venting. An inactive smoker is surrounded by empty mussel shells indicating an extinct high-temperature venting accompanied by diffuse venting nearby similar to IRINA II.

About 200 m NW of QUEST and 330 m NW of IRINA II there is a hydrothermal active zone characterized by **diffuse venting** (14°45.31'N / 44°58.88'W ± 30 m; Fig. 1.4). It has a diameter of about 15 m and consists of hydrothermal crusts, probably Fe-crusts, partly covered by sediment. Shimmering water could be observed at little holes in unsedimented parts of the crusts. There are also a few ophiuridaes.

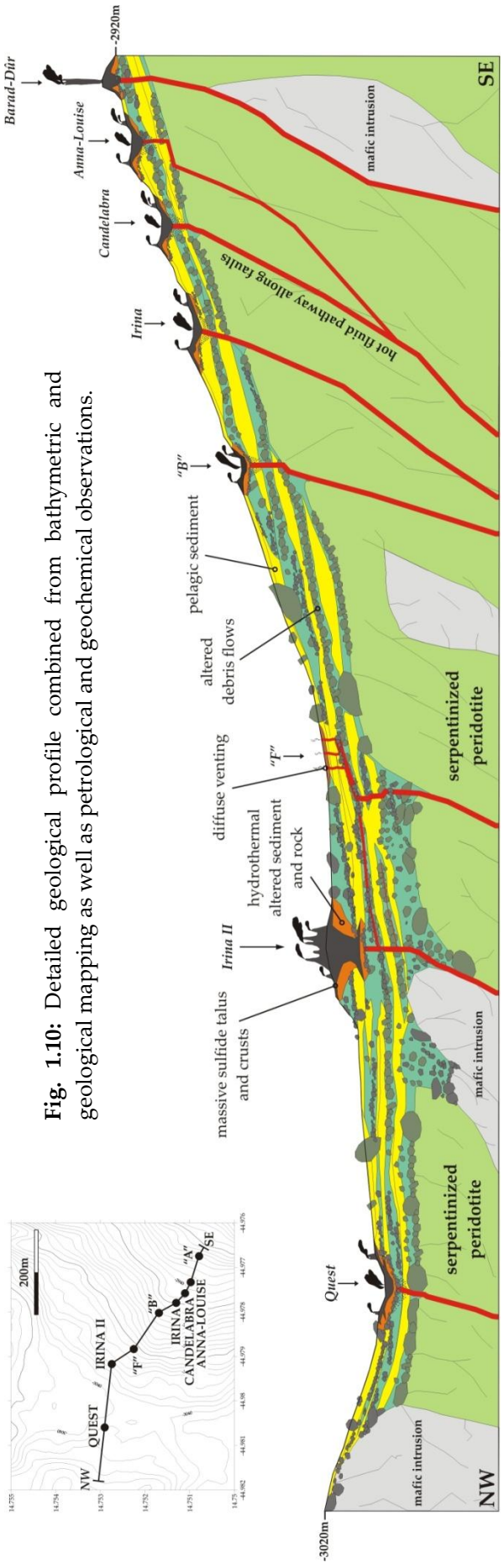

Fig. 1.10: Detailed geological profile combined from bathymetric and geological mapping as well as petrological and geochemical observations.

6. Discussion and Conclusions

The MAR at the Logatchev area displays a rugged morphology that is atypical for most parts of the MAR (Cannat et al., 1997). This morphology is caused by tectonic spreading

dominating over magmatic spreading which has lead to the emplacement of mantle rocks on both flanks of the rift valley (Cannat et al., 1997). However, the formation of a detachment fault close to the hydrothermal fields at the MAR at 14°45'N indicates a certain, stable ratio between tectonics and magmatism (Tucholke et al., 2003). The overlapping ends in the north and south of the Logatchev MAR segment suggests propagation of this segment which is also indicative for magmatic activity. Moreover, the chemistry of the mafic rocks also indicates a rather robust magmatic activity in this MAR area. Therefore, we suggest that the hydrothermal system at Logatchev is driven by a magmatic heat source (Augustin et al., submitt.). This suggestion is further supported by the chemistry of the hydrothermal fluids e.g., high concentrations of aquatic silica (Schmidt et al. 2007).

Characteristics which make Logatchev a special hydrothermal system can be summarized as follows (Murphy & Meier, 1998; Gablina et al., 2000; Lein et al., 2003; Kuhn et al., 2004a; Petersen et al., 2005):

- it is situated rather high (approx. 1000 m) above the middle valley floor,
- it appears in avalanches consisting of rock talus from cm- to house-sizes,
- so-called smoking craters occur which are not known from any other seafloor hydrothermal system
- its hydrothermal fluids have equilibrated with both mafic and ultramafic rocks
- sulphide chimneys are rather small and generally very fragile,
- there is almost no anhydrite at or within the first meters of the seafloor,
- the system is characterized by an extreme copper and gold enrichment,

Sulfide chimneys-dominated seafloor hydrothermal systems on sediment-starved mid-ocean ridges are generally divided into a TAG- (Tivey, 2007) respectively a Galapagos-type (Hannington et al., 1995), an Endeavour-type (Tivey, 2007), an East-Pacific-Rise-type and "Lost City"-type (Tivey, 2007). However, the Logatchev hydrothermal system does not fit into this classification, i.e., it may represent another type of hydrothermal system on sediment-starved mid-ocean ridges.

The **TAG-type** deposits (Tivey, 2007; Hannington et al., 1995) are characterized by large mounds where smoker fluids are extremely well focused and exit vigorously from a central black smoker complex (Rona et al., 1986; Tivey, 2007). The large size results in part from significant seawater entrainment into the mound, which triggers precipitation of anhydrite, chalcopyrite, and pyrite within the mound, and remobilization of metals (Tivey et al., 1995, Tivey, 2007). In the Logatchev-1 field there is only a small mound at IRINA II the basement of which consists of altered rock talus and only on the higher levels of the mound hydrothermal precipitates occur. The whole mound is approximately 15 m high and is probably made up of talus material rather than sulphides (Fig. 1.10). This suggestion is supported by TV-grabs and ROV observations which revealed a 5 - 10 cm thick crust covering at least parts of the Logatchev field including the IRINA II mound. This crust mainly consists of rock talus of different sizes cemented by silica. Underneath this crust Cu-

rich sulphide precipitates occur with a thickness of a few decimeter followed by completely hydrothermally altered rocks (Kuhn et al., 2004a).

In contrast to the TAG-type the **Endeavour-Type** deposits is characterized by single high and steep-sided chimney structures which rise nearly vertically from the seafloor to heights greater than 10 or 20 meters (Hannington et al., 1995; Tivey, 2007). The intense silification reduces mixing with seawater and stabilizes the structures that form dominantly by flange growth (Tivey et al., 1999). There are no such tall sulphide structures in the Logatchev field. The highest structure is an approx. 5 meters high tower (Barad-Dûr at site A, Lackschewitz et al., 2005) whereas Logatchev is mainly characterized by small and delicate chimneys. Venting high-temperature fluids generally lack the high silica content typical for Endeavour-type fluids (Schmidt et al., 2007).

The East-Pacific-Rise-Type Vent Deposits are build up of combinations of small (<10m diameter), low-lying mounds with individual 1 – 2 m diameter structures that stand < 15 m high, formed by the coalescence of smaller chimneys (Haymon and Kastner, 1981; Tivey, 2007). At EPR fields lower-temperature, diffuse flow is also observerd exiting from cracks and crevices in the basaltic seafloor (Haymon and Kastner, 1981). Overall, the deposits at most East Pacific Rise vent fields are small because much of the fluid and precipitate is carried upward into plumes above the vent fields, and spreading rates are high and eruptions frequent so that deposits do not have time to attain a large size (Tivey, 2007). Logatchev is also characterized by small low-lying mounds and small chimneys. However, it is not situated at the middle valley floor. The Age of the Logatchev field is unclear, but a large amount of strongly altered sulphidic material indicates that Logatchev is a hydrothermal system that has been active for a considerable amount of time. Apart from the active high- and low-T vent sites there are numerous inactive sites indicating shifting localities of hydrothermal activity in the past.

The **"Lost City"-Type** deposits consisting mainly of aragonite, brucite and secondary calcite and were formed by vent fluids with an alkaline pH (~ 10-11), low metal and sulphide content and with maximum observed temperatures of 91 °C (Kelley, 2005; Proskurowski et al., 2006). Nevertheless, efficient mineral deposition occurs because of seawater entrainment into the subsurface, and from mixing of warm, very-high-pH, reduced vent-fluid with seawater (Tivey, 2007). These factors together with the longevity of Lost City which has been active for about 30,000 years (based on ^{14}C dating; Früh-Green et al., 2003) leading to the large size of the structures like TAG. Logatchev is situated in ultramafic rocks similar to Lost City. However, there are a number of arguments indicating that the driving force for the hydrothermal system at Logatchev indeed is a magmatic heat source, whereas the serpentinization of ultramafic rocks at Lost City it is supposed to drive the hydrothermal system. The chemistry of fluids and precipitates at Logatchev-1 is also typical for a magmatically driven system. One more difference between the Logatchev site and Lost City is the topographical situation. Lost City is localized at an elevated position were sedimentation is limited, whereas main parts of the Logatchev hydrothermal field are located in a depression filled with talus material and pelagic sediment.

Above, a number of characteristics of the Logatchev hydrothermal field were outlined which makes it special compared to other hydrothermal systems on sediment-starved mid-ocean ridges. The most typical structure in this context are the smoking craters (Fig. 1.10). These structures form small hills maybe 10 – 15 m in diameter and 2 – 5 m high. The central part of which is a depression a few meters deep and conically shaped. The formation of these craters was related to anhydrite dissolution at depth (Cherkashev and other Russian colleagues, pers. comm.). However, plenty of anhydrite must have been dissolved at depth to form such depressions and there should be a lot of anhydrite generally available in the Logatchev field if this hypothesis is true. In contrast, there is almost no anhydrite.

In 2006, a German-lead expedition drilled at Logatchev using the British Geological Survey Rockdrill 2 (Petersen et al., in prep.). During drilling at Logatchev a complete loss of the drill fluid in the borehole was observed. Seawater is used as drill fluid. It is pumped into the borehole at the central part of the drill string during the drill process and it emanates from the drill hole between the inner and outer steel tube of the drill string. The fluid carries the cuttings and precipitates them close to the borehole. However, during drilling this bore fluid was lost, i.e., it didn't emanate from the borehole. Looking around with the video camera it was observed that this fluid re-appeared a couple of tens of meters away from the borehole forming a small crater with a low surrounding wall. It was suggested that an aquifer was hit during drilling guiding the fluids away from the borehole. The aquifer contained a number of fine-grained material which was washed out by the fluid. The wash-out process formed the small depression and the material being washed out was then precipitated around the emanation site.

The same process may have lead to the formation of the smoking craters. Slumping processes which are typical for the site of Logatchev-1 may have caused the formation of layers or pockets of material with different grain sizes (gravitationally driven movements downhill always cause some sort of sorting according to grain size). Hydrothermal fluids may use such layers as aquifers and may have washed out fine grained materials leading to the formation of the smoking craters (Fig. 1.10).

7. References

Alt, J.C. and Bach, W., 2003. Alteration of Oceanic Crust - Subsurface Rock-Water Interactions. In: P.E. Halbach, V. Tunnicliffe and J.R. Hein (Editors), Dahlem Workshop Reports 89 - Energy and Mass Transfer in Marine Hydrothermal Systems. Dahlem University Press, pp. 7-27.

Augustin, N., Lackschewitz, K.S., Botz, R., Eisenhauer, A., Garbe-Schönberg, D., Kuhn, T., Schmidt, M. (submitt.): Alteration Processes at the Ultramafic-Hosted Logatchev Hydrothermal Field, MAR 14°45´ N: Trace Elements and Isotope Signatures as Tracers for Water/Rock and Melt/Rock interaction. Submitted to Chemical Geology.

Batuyev, B.N., Kratov, A.G., Markov V.F., Cherkashev G.A., Krasnov S.G., and Lisitsyn Y.D, 1994. Massive sulfide deposits discovered at 14º45'N Mid-Atlantic Ridge. Bridge Newsletter, 6: 6-10.

Borowski C. and shipboard scientific party (in prep.) RV Maria S. Merian Cruise MSM 04-1, Logatchev Hydrothermal Field, MAR 15°N. In preparation for Merian Berichte.

Cann, J.R., Blackman, D.K., Smith, D.K., McAllister, E., Janssen, B., Mello, S., Avgerinos, E., Pascoe, A.R., and Escartin, J., 1997. Corrugated slip surfaces formed at North Atlantic ridge-transform intersections, Nature 385: 329-332.

Cannat, M., Bideau, D. and Bougault, H., 1992. Serpentinized peridotites and gabbros in the Mid-Atlantic Ridge axial valley at 15°37´N and 16°52´N. Earth and Planetary Science Letters, 109: 87-106.

Cannat, M. and Casey, J.F., 1995. An ultramafic lift at the Mid-Atlantic Ridge: Successive stages of magmatism in serpentinzed peridoties from the 15°N region. In: R.L.M. Vissers and A. Nicolas (Editors), Mantle and lower crust exposed in oceanic ridges and in ophiolites. Kluwer Academic Press, Dordrecht/Boston/London, pp. 5-34.

Cannat, M., Lagabrielle, Y., Bougalt, H., Casey, J., de Coutures, N., Dmitriev, L., and Fouquet, Y., 1997. Ultramafic and gabbroic exposures at the Mid-Atlantic Ridge: geological mapping in the 15°N region. Tectonophysics, 279: 193-213.

Cherkashev, G.A., Ashadze, A.M., and Gebruk, A.V., 2000. New fields with manifestations of hydrothermal activity in the Logatchev area (14°N, Mid-Atlantic Ridge). InterRidge News, 9(2): 26-27.

DeMets, C., Gordon, R.G., Argus, D.F., and Stein, S. (1990). Current plate motions, Geophysical Journal International, 101: 425-478.

Eberhardt, G.L., Rona, P.A., and Honnorez, J., 1988. Geologic Controls of Hydrothermal Activity in the Mid-Atlantic Ridge Rift Valley: Tectonics and Volcanism. Marine Geophysical Research, 10: 233-259.

Edmonds, H.N., Michael, P.J., Baker, E.T., Connelly, D.P., Snow, J.E., Langmuir, C.H., Dick, H.J.B., Mühe, R., German, C.R., and Graham, D.W., 2003. Discovery of abundant hydrothermal venting on the ultraslow-spreading Gakkel ridge in the Arctic Ocean. Nature, 421: 252-256.

Escartín, J. and Cannat, M. 1999. Ultramafic exposures and the gravity signature of the lithosphere near the Fifteen-Twenty Fracture Zone (Mid-Atlantic Ridge, 14°-16.5°N). Earth and Planetary Science Letters, 171: 411-424.

Fouquet, Y., Murphy, P., Bougalt, H., Prieur, D., Meyer, G., Henry, K., Poroshima, I., and Krasnov, S., 1997a. Massive Sulfides and Stockwork Mineralization in Ultramafic Environments. Mid Atlantic Ridge near 15°N, SEG Neves Corvo Field Conference, Lisbon, pp. 34.

Fouquet, Y., Charlou, J.L., Ondreas, H., Radford-Knoery, J., Donval, J.P., Douville, E., Apprioual, R., Cambon, P., Pellé, H., Landuré, J.Y., Normand, A., Ponzevera, E., German, C., Parson, L., Barriga, F., Costa, I., Relvas, J., and Ribeiro, A., 1997b. Discovery and first submersible investigations on the Rainbow hydrothermal field on the MAR (36°14'N). Eos Trans., 78, 832 (abstract).

Franz, L., Kuhn, T., and Fretzdorff, S., 2005. Petrology and geochemistry of ultramafic and mafic rocks from the Logatchev field, 14°45'N MAR. Beih. z. European Journal of Mineralogy, 17(1): 40.

Franz, L., Kuhn, T., Fretzdorff, S., and Hekinian, R., 2006. Syn- and post-magmatic evolution of oceanic lithosphere at an slow spreading ridge: the Logatchev hydrothermal field, 14°45'N. In prep. Franz et al., subm.,

Franz L.; Kuhn, T.; Petersen, S.; Augustin, N.; Fretzdorff, S. & Hékinian,R. (2007): Syn- and post-magmatic evolution of the oceanic lithosphere underneath the Logatchev hydrothermal field (MAR 14°45`N). 5th Swiss Geoscience Meeting Bern, Abstract Volume, 89-91.

Früh-Green, G.L. et al., 2003. 30,000 Years of Hydrothermal Activity at the Lost City Vent Field. Science, 301: 495-498.

Fujiwara, T., Lin, J., Matsumoto, T., Kelemen, P.B., Tucholke, B.E., and Casey, J.F., 2003. Crustal Evolution of the Mid-Atlantic Ridge near the Fifteen-Twenty Fracture Zone in the last 5 Ma. Geochemistry Geophysics Geosystems, 4(3): doi:10.1029/2002GC000364.

Gablina, I.F., Mozgova, N.N., Borodaev, Y.S., Stepanova, T.V., Cherkashev, G.A., and Il'in, M.I., 2000. Copper Sulfide Associations in Recent Oceanic Ores of the Logatchev Hydrothermal Field (Mid-Atlantic Ridge, 14°45'N). Geology of Ore Deposits, 42(4): 296-316.

Gebruk, A.V., Chevaldonné, P., Shank, T., Lutz, R.A., and Vrijenhoek, R.C., 2000. Deep-sea hydrothermal vent communities of the Logatchev area (14°45'N, Mid-Atlantic Ridge): diverse biotopes and high biomass. Journal of the Marine Biological Association of the UK, 80: 383-393.

Gebruk, A., Galkin, S., Krylova, E., Vereschaka, A., Vinogradov, G., Borowski, C., and the Mir submersibles team, 2002. Hydrothermal fauna discovered et Lost City (30°N, Mid-Atlantic Ridge). InterRidge News, 11(2): 18-19.

Humphris, S.E., Halbach, M. and Juniper, K., 2003. Low-temperature Alteration - Fluxes and Mineralization. In: P.E. Halbach, V. Tunnicliffe and J.R. Hein (Editors), Dahlem Workshop Report 89 - Energie and Mass Transfer in Marine Hydrothermal Systems. Dahlem University Press, pp. 163-181.

Hannington, M.D., Jonasson I.R.; Herzig, P.M.; Petersen S. (1995): Physical and chemical processes of seafloor mineralization at mid-ocean ridges. In: Seafloor hydrothermal systems; physical, chemical, biological, and geological interactions. Geophysical Monograph. 91; 115-157

Haymon, R.M., Kastner, M. (1981): Hot spring deposits on the East Pacific Rise at 21 degrees N; preliminary description of mineralogy and genesis. Earth and Planetary Science Letters. 53; 3, 363-381

Karson, J.A. and Lawrence, R.M., 1997. Tectonic window into gabbroic rocks of the middle oceanic crust in the MARK area near Sites 921-924. Proceedings of the Ocean Drilling Program Science Results, 153: 61-76.

Karson, J.A., 1999. Geological investigation of a lineated massif at the Kane transform: Implications for oceanic core complexes: Royal Society of London Philosophical Transactions, 357: 713-740.

Kelley D.S. (2005): From the mantle to microbes; the Lost City hydrothermal field. Oceanography 18; 3: 32-45

Koschinsky, A. et al., 2006. Discovery of new hydrothermal vents on the southern Mid-Atlantic Ridge (4°S-10°S) during cruise M68/1. InterRidge News, 15: 9-15.

Krasnov, S.G., Cherkashev, G.A., Stepanova, T.V., Batuyev, B.N., Krotov, A.G., Malin, B.V., Maslov, M.N., Markov, V.F., Poroshina, I.M., Samovarov, M.S., Ashadze, A.M., Lazareva, L.I., and Ermolayev, I.K., 1995. Detailed geological studies of hydrothermal fields in the north atlantic. Geological Society Special Publication, 87: 43-64.

Kuhn, T. and Shipboard Scientific Party, 2004a: Mineralogical, geochemical, and biological investigations of hydrothermal systems on the Mid-Atlantic Ridge between 14°45'N and 15°05'N (HYDROMAR I). In: Christiansen, B., Morgan, J.P., Kuhn, T., Send, U. and Wallace, D.W.R., 2004. Mid-Atlantic Expedition 2003/2004, Cruise No. 60, 11 November 2003 - 15 April 2004. METEOR-Berichte. Universität Hamburg., in prep.

Kuhn, T. and Shipboard Scientific Party, 2004b. The Logatchev hydrothermal field - revisited: Preliminary results of theR/V Meteor cruise HYDROMAR I (M60/3). InterRidge News, 13: 1-4.

Lackschewitz, K.S. and Shipboard Scientific Party, 2005. Longterm study of hydrothermalism and biology at the Logatchev field, Mid-Atlantic Ridge at 14°45′N (revisit 2005) (HYDROMAR II), Meteor Berichte 05. Universität Hamburg.

Lein, A.Y., Cherkashev, G.A., Ul'yanov, A.A., Ul'yanov, N.V., Stepanova, T.V., Sagalevich, A.M., Bogdanov, Y.A., Gurvich, E.G., and Torokhov, M.P, 2003. Mineralogy and Geochemistry of Sulfide Ores from the Logatchev-2 and Rainbow Fields: Similar and Distinctive Features. Geochemistry International, 41(3): 271-294.

Lilley M.D., Butterfield D.A., Olson E.J., Lupton S.A., Macko S.A., and McDuff R.E. (1993) Anomalous CH4 and NH4 concentrations at an unsedimented midocean-ridge hydrothermal system. Nature 364, 45-47.Murphy, P.J. and Meyer, G., 1998. A Gold-Copper Association in Ultramafic-Hosted Hydrothermal Sulfides from the Mid-Atlantic Ridge. Economic Geology, 93: 1076-1083.

Murphy, P.J. and Meyer, G., 1998. A Gold-Copper Association in Ultramafic-Hosted Hydrothermal Sulfides from the Mid-Atlantic Ridge. Economic Geology, 93: 1076-1083.

Petersen, Sven ; Herzig, Peter ; Kuhn, Thomas ; Monecke, T. ; Franz, L. ; Hannington, M.D. ; Gemmel, J.B.: Shallow Drilling of Seafloor Hydrothermal Systems Using the BGS Rockdrill: Conical Seamount (New Ireland Fore-Arc) and PACMANUS (Eastern Manus Basin), Papua New Guinea. Marine Georesources and Geotechnology 23 (2005), Nr. 3, S. 175-193

Petersen, S., Augustin, N., Cherkashov, G., Fischer, S., Franz, L., Han, X., Klein, F., Maggiulli, M., Ockert, C., Perner, M., Peters, M., Rahders, E., Rudzitis, E., Smith, D., Stepanova, T., Storm, S., Strauss, H., Zhou N. (in prep.): Detailed geological, geochemical, and biological investigations of the Logatchev-1 hydrothermal field with shallow drill cores. In preparation for Merian Berichte.

Proskurowski, G., Lilley, M.D., Kelley, D.S. Olson, E.J., 2006. Low temperature volatile production at the Lost City Hydrothermal Field, evidence from a hydrogene stable isotope geothermometer. Chemical Geology, 229: 331-343.

Rona, P.A., Widenfalk, L. and Boström, K., 1987. Serpentinized ultramafics and hydrothermal activity at the Mid-Atlantic Ridge crest near 15°N. Journal of Geophysical Research, 92: 1417-1427.

Schmidt, K., Koschinsky, A., Garbe-Schönberg, D., De Carvalho, L.M. and Seifert, R., 2007. Geochemistry of hydrothermal fluids from the ultramafic-hosted Logatchev hydrothermal field, 15°N on the Mid-Atlantic Ridge: temporal and spartial investigation. Chemical Geology, 242: 1-21.

Schreiber, K., 2006. Geology and bathymetry of the Mid-Atlantic Ridge between 14°26N and 15°00´N with special emphasis on the Logatchev-1 hydrothermal field at 14°45´N / 44°58´W. Diplomkartierung, TU Bergakademie Freiberg

Simonov, V.A., Kolobov, V.Yu., and Peive, A.A., (1999): Petrologiya i geokhimiya geodinamicheskikh protsessov v Tsentral'noi Atlantike (Petrology and Geochemistry of Geodynamic Processes in the Central Atlantic), Novosibirsk: Sib. Otd., Ross. Akad. Nauk

Smith, W.H.F. and Sandwell, D.T., 1997. Global seafloor topography from satellite altimetry and ship depth soundings. Science, 277: 1956-1962.

Tivey, M.K., (1995) Modeling chimney growth and associated fluid flow at seafloor hydrothermal vent sites. In: Seafloor hydrothermal systems; physical, chemical, biological, and geological interactions. Geophysical Monograph. 91; 158-177.

Tivey, M.K., D.S. Stakes, T.L. Cook, M.D. Hannington, and S. Petersen (1999). A model for growth of steep-sided vent structures on the Endeavour Segment of the Juan de Fuca Ridge: results of a petrologic and geochemical study. J. Geophys. Res., 104: 22,859-22,883.

Tivey, M.K. (2007) Generation of Seafloor Hydrothermal Vent Fluids and Associated Mineral Deposits, Oceanography, 20, 1: 50-65

Tucholke, B.E., Lin, J., and Kleinrock, M.C., 1998. Megamullions and mullion structure defining oceanic metamorphic core complexes on the Mid-Atlantic Ridge. Journal of Geophysical Research, 103: 9857-9866.

Tucholke, B.E., Buck, W.R., Lavier, L., and Lin, J., 2003. Investigation of Megamullion Formation in Relation to Magma Supply. Geophysical Research Abstracts, Vol.5, 07925.

Chapter 2:

Trace elements and isotope signatures as tracers for water/rock and melt/rock interaction

---

Abstract

Serpentinites, gabbroic rocks, and altered sediments were sampled from the active ultramafic hosted Logatchev hydrothermal field (LHF) by ROV deployments and TV-guided grab. In this study we present new data of clay-size separates and whole rock chemistry as well as strontium and oxygen isotopic compositions in order to investigate the alteration processes, water-rock reactions and associated elemental exchanges.

The samples of mantle peridotites are mostly serpentinized (>95vol%) whereas some gabbroic samples are moderately to completely altered. Changes in geochemical compositions, especially trace element compositions, of the altered rocks indicate a highly heterogeneous distribution of alteration styles. Light rare earth elements are enriched in all serpentinites and suggest a strong influence of Logatchev vent fluids during some stages of serpentinization. Oxygen isotopic data of lizardites reveal formation temperatures of 130-150°C whereas chlorite formation in altered gabbroic samples occurred between 150° and 200°C in the LHF. Negative as well as positive Eu anomalies in serpentinites suggest varying alteration processes: (1) high temperature alteration in acidic, reducing conditions as well as (2) low temperature alteration in neutral, oxidizing environments. The absence of brucite and the formation of talc indicate high concentrations of aquatic silica in the Logatchev area. Petrographic investigations, high field strength element data and elevated rare earth elements indicate that melt–rock interaction is also an important factor affecting mantle peridotite prior to serpentinization processes at LHF. Therefore gabbroic intrusions are the most probable source for aquatic silica. Strontium isotopic data suggest high water/rock ratios in the range of 2.6-27 and alteration fluids which are characterized by high contents of heated seawater.

1. Introduction

The production of new oceanic crust at mid-ocean ridges drives hydrothermal circulation, which is important for Earth's heat budget and the chemical composition of the oceans. Slow-spreading ridges, like the Mid Atlantic Ridge (MAR) are characterized by a disrupted and thinned crust due to variations in the magmatic processes. Tectonic extension occurs along large scale faults leading to a significant cooling of the crust (Alt and Bach, 2003). In case of low magmatic production and low spreading rates, mantle peridotites may be transported to the seafloor due to the tectonically extension. Consequently, ultramafic rocks

are a major and an important part of the oceanic lithosphere especially along slow- and ultra-slow spreading ridge systems (e.g., MAR, Gakkel Ridge, southwest Indian Ridge) comprising more than 20% of the lithosphere (Humphris et al., 2003). Mantle peridotites are often completely serpentinized in these areas (Humphris et al., 2003). At the MAR, between 14°30′N and 15°50′N, , extensive exposures of lower crust and upper mantle rocks were found suggesting a highly reduced magma supply along the MAR in this area (Cannat et al., 1992; Rona et al., 1987). A geochemical, and isotopic anomaly in volcanic rocks from 14°N to 17°N across the Fifteen-Twenty Fracture Zone is interpreted to be related to a mantle "hot spot", with strongly localized large amounts of melting of a high temperature, fertile mantle source producing a large thickness of igneous rocks (Dosso et al., 1993; Hémond et al., 2006). Additional geochemical characteristics of serpentinized peridotites reflect high degrees of mantle melting (Fujiwara et al., 2003). These observations are in contrast to a reduced magma supply derived from the extensively exposures of ultramafic rocks and point to a strongly localized magma supply system.

At least two hydrothermal systems between 14° and 17°N are characterized by high-temperature circulating fluids. The northernmost one is an inactive field, discovered in 2002 at 16°38′N (Bel′tenev et al., 2004). The second is the active ultramafic hosted Logatchev hydrothermal field at 14°45′N which was first described by Cherkashev et al. (2000).

In the framework of the German Priority Program SPP-1144: "From Mantle to Ocean", funded by the Deutsche Forschungsgemeinschaft (DFG) two cruises (M60/3 and M64/2) to the Logatchev hydrothermal field were carried out in 2004 and 2005 by the German RV Meteor. The main scientific aim of these cruises were to investigate the interrelationship of geological, geochemical, and biological processes in the active Logatchev hydrothermal field at 14°45′N on the MAR (Kuhn et al., 2004a; Kuhn et al., 2004b; Kuhn et al., 2005; Lackschewitz et al., 2005).

This paper uses a combination of petrological, mineral chemistry and isotope (Sr and O) analyses of whole rock and mineral separates to examine the extent, style and sequence of low- to high-temperature alteration in the area of the active, high-temperature Logatchev hydrothermal field. This field has become one of the key sites for an ultramafic-hosted hydrothermal system. The effects of a varying surface lithology and changes in the physico-chemical conditions on the evolution of the hydrothermal system are also examined.

The data show variations in the behavior of the high field strength elements and rare-earth elements of ultramafic and mafic rocks and secondary minerals indicating rock-seawater reactions under changing conditions. We report also evidence for melt impregnations as recorded in several serpentinized peridotites from the Logatchev hydrothermal field.

2. Geological Setting

The Mid-Atlantic Ridge (MAR) segment around the Fifteen-Twenty Fracture Zone has an irregular, morpho-structural setting characterized by abundant faulting (Escartin and Cannat, 1999; Fujiwara et al., 2003) including the tectonic exposure of upper mantle rocks, massively tectonic drift, low rates of magmatism and resulting slow spreading rates in this region. The abundant faulting allows deep penetration of fluids into the crust causing alteration at variable P-T conditions.

The samples were obtained from 2 locations (Fig. 2.1a). One is the active Logatchev Hydrothermal Field and surrounding seafloor. The other site is located approximately 20 km north of the Logatchev Hydrothermal Field, where hydrothermal activity was previously postulated by other workers (Eberhardt et al., 1988). The most important characteristics of the study area between 14°26′N and 15°02′N is the presence of abundant serpentinite outcrops on both walls of the ridge axis as well as on parts of the rift valley floor. N-S and WNW-ESE striking faults cause segmentation of the eastern wall into a blocky and irregular, terrace-like structure. Relatively fresh pillow basalts as well as some off-axis volcanoes are present in the deeper parts of the rift valley and also on the valley floor (Kuhn et al., 2004b).

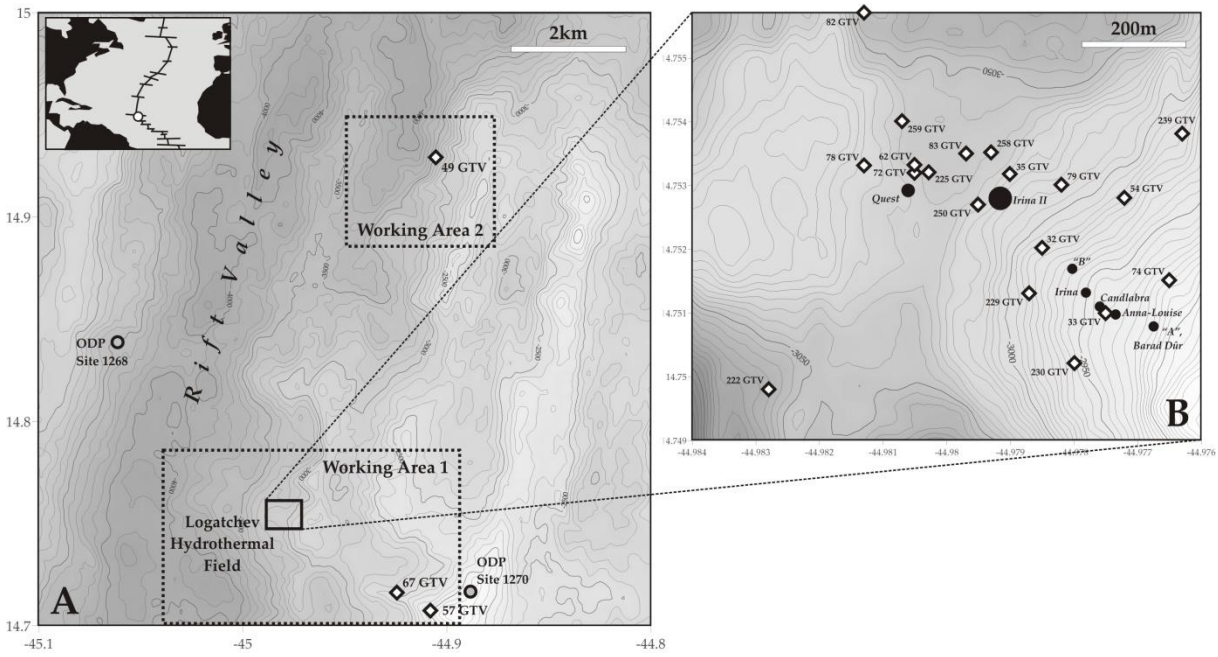

Fig. 2.1: (A) Map is showing the working areas 1 (Logatchev hydrothermal field) and 2 at the Mid-Atlantic ridge at 14°45′N, squares indicate TV-Grab sample stations during Meteor cruises M60/3 and M64/2. (B) Detailed Map with sampling stations during Meteor cruises M60/3 and M64/2 within the active Logatchev hydrothermal field. The positions of known active vent sites are marked with black circles.

The Logatchev Hydrothermal Field was first discovered in 1993 by Russian scientists (Batuyev et al., 1994; Cherkashev et al., 2000) and is part of a ultramafic-hosted hydrothermal system situated at 14°45′N, 44°59′W. It is located at the lower, eastern ridge-flank between two terrace-like structures at about 3000 m water depth close to the axial valley (Fig. 2.1). The results of Meteor cruises M60/3 (Kuhn et al., 2004a; Kuhn et al., 2004b) and M64/2 (Lackschewitz et al., in press) show that the field is larger than previously described (Bogdanov et al., 2004; Gablina et al., 2000; Gebruk et al., 2000). The Logatchev Hydrothermal Field extends at least 800 m in a NW-SE direction and 200 m in the SW-NE direction. Two main areas of high-temperature hydrothermal activity make up the central part of the Logatchev field: (i) an area of at least four "smoking craters" (CANDELABRA, IRINA and SITE "B", QUEST) and (ii) the mound of IRINA II with black smoker chimneys at its top as well as the diffuse venting at SITE "F" (Fig. 2.1b). The "smoking craters" of the Logatchev hydrothermal field are rare structures which have only been identified at Logatchev and the, in 2005 newly discovered, Nibelungen-Field at the southern MAR (Koschinsky et al., 2006).

A small diffuse venting site discovered during cruise M64/2 marks the known NW-end of the field whereas a single, isolated 5m high black smoker named BARAD-DÛR at Site "A" marks the preliminary SE-end of the Logatchev Hydrothermal Field. The highest fluid-temperature measured in the Logatchev Hydrothermal Field was 353°C (Douville et al., 2002). Evidences for at least three more hydrothermal sites south and south-east of Logatchev Hydrothermal Field (Kuhn et al., 2004b) show that the hydrothermal activity in the Working Area 1 is or was possibly much wide-ranging than recognized so far.

The host rocks of the Logatchev Hydrothermal Field are mainly serpentinized harzburgites and lherzolites with significant amounts of gabbroic rocks (>20%; (Kuhn et al., 2004b). The seafloor of the surrounding area of the vent sites is mainly characterized by sediment-covered talus of ultramafic and mafic rocks (Kuhn et al., 2004b). The sediments are locally more than 1m thick. Close to the vent sites the sediments are generally hydrothermally altered, covered by hydrothermal crusts and contain highly altered rocks, rock-forming minerals, sulfides and secondary clay minerals. These sediments are often covered by a silicified hydrothermal crust.

Working Area 2 is situated about 20 km north of the active Logatchev field around 14°54′N, 44°54′W (Fig. 2.1a) and is hosted by ultramafic rocks and subordinate outcrops of gabbros and basalts (Krasnov et al., 1995; Kuhn et al., 2004b). Hydrothermal activity postulated by other workers, like hydrothermal precipitates observed in OFOS pictures (Eberhardt et al., 1988) was not found during cruise M60/3. Bathymetric and photographic mapping of the seafloor has shown that rather young basalts, pillow mounds with larger scarps and faults are characteristic for the rift valley and the lower part of the rift mountains in Working Area 2. A hydrocast station in Working Area 2 during M60/3 detected strong methane and hydrogen anomalies in the water column (Kuhn et al., 2004b) which suggests strong serpentinization in this area. This is supported by serpentinite samples taken during cruise M60/3.

3. Material and Methods

During this study we analyzed 9 sediment samples and 43 rock samples from the active Logatchev hydrothermal field (Working area I) and 10 rock samples from Working Area 2 (Figs. 2.1b, 2.2). The TV-grab samples commonly consist of brownish to grey pelagic sediments with large amounts of foraminifer shells and rock samples of harzburgites, lherzolites and dunites which were mostly totally serpentinized with a sample size up to 25 cm in diameter (Table 2.1). In addition, significant amounts of gabbros (>20%) were also sampled. A large variety of hydrothermal samples were recovered, including silicified breccias and crusts, soft and indurate hydrothermal sediments, Fe-Mn-oxyhydroxides as well as atacamite (copper-chloride), single fragments of quartz and talc. After drying, the sediment samples were divided into fine (<63 μm) and coarse fractions (>63 μm) by wet sieving. The rock samples were crushed gently by hand before separating the fine fraction. Grain size separation into silt (2-63 μm) and clay fraction (<2 μm) was performed according to Stokes´ law by settling the particles in water filled cylinders (Atterberg, 1912; Moore and Reynolds, 1989).

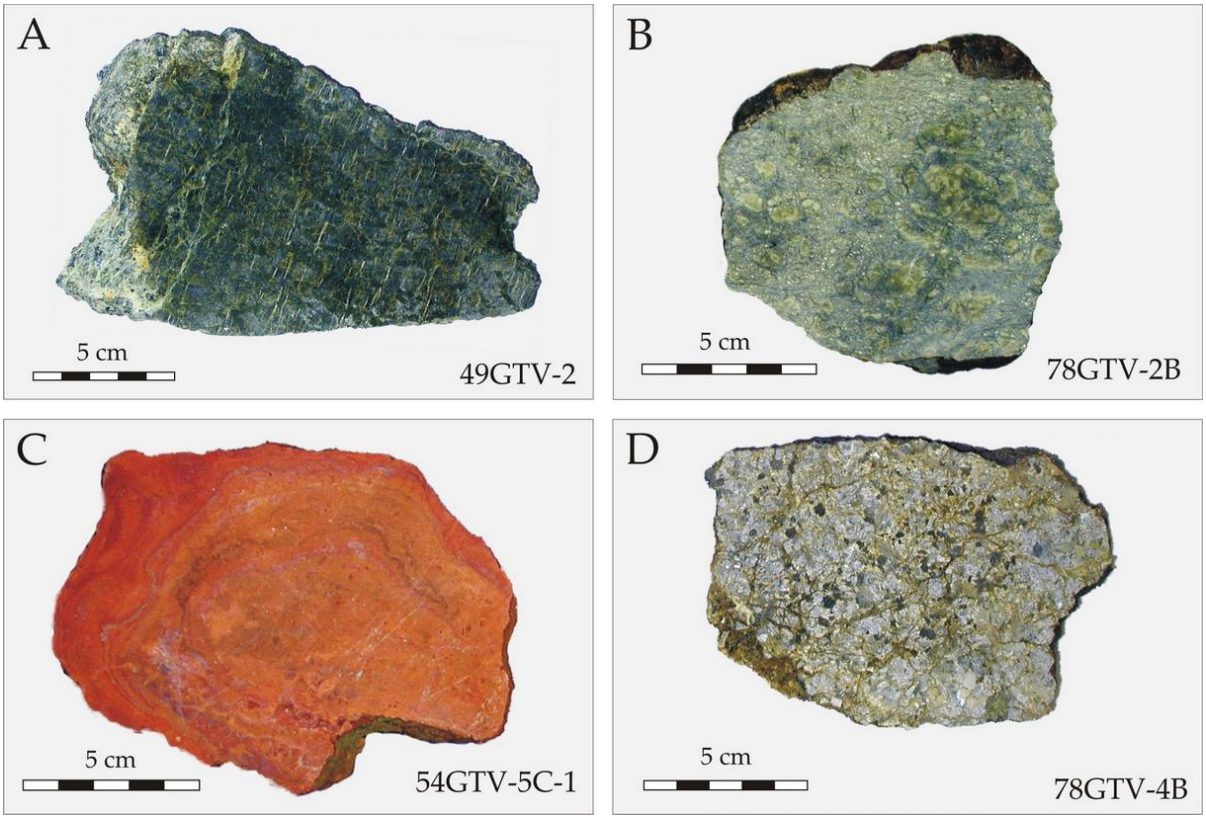

Fig. 2.2: Sample photographs of rocks from the Logatchev hydrothermal field: (A) serpentinized foliated peridotite from working area 2. (B) Serpentinized peridotite west of site IRINA II. (C) Serpentinized and hematite impregnated rock northeast of Site "B". (D) Moderately altered gabbro east of site IRINA II. Note that all samples are talus material up to a depth of approximately 1m.

Trace elements were determined on 14 bulk samples and 24 clay (<2μm size fraction) separates by ICP-MS using a VG Plasma-Quad PQ1 at the Institute of Geosciences of the University of Kiel and a Finnigan MAT Element 2 double-focusing, single collector ICP-MS at the Department of Geosciences of the University of Bremen, Germany. All samples were dissolved by performing a pressurized HF-HCl-HNO_3-aqua regia attack (Garbe-Schönberg, 1993). The bulk rock samples had to be high-pressure cooked with HF, HCl and HNO_3 for 48 hours at 200°C in a "steel bomb" to dissolve refractory phases (e.g., spinel). The accuracy of the analyses was monitored using international rock standards AGV-1 (andesite), BHVO-1, BHVO-2 and BIR-1 (basalts), JR-1 (rhyolite) and UB-N (serpentinite) (Govindaraju, 1994; Jochum et al., 2005; Wilson, 1997). Our values are generally within <5% of the recommended values for most elements. However, larger discrepancies from the given standard values can be observed for the elements Cr (16-25%; AVG-1, JR-1), Rb (14-18%; BHVO-1, JR-1), Eu (16%; AGV-1) in analyzes of some of the standard reference materials. The standard analyses are listed in Table 2.2. The precision of duplicates as well as repeated analyses is better than 5% for most elements (Tab. 2.2).

Radiogenic Sr isotope ratios were measured on 9 bulk rock and 22 clay-sized samples by MC-ICP-MS (VG Elemental Axiom) and thermal ionization mass spectrometry (ThermoFinnigan TRITON) at the mass-spectrometer facilities of the IFM-GEOMAR in Kiel, Germany, following standard chemical separation (Sr-Spec; 50-100 mesh; 0.6 ml) and measurement procedures (White and Patchett, 1983). Blanks were less than 1‰ of the total sample amount and therefore negligible. During the course of the project 7 NBS 987 standards were measured yielding a Sr-isotopic ratio of 0.71024(3) (2sd). In addition 6 measurements of the IAPSO seawater standard yielded a Sr-isotopic ratio 0.70918(2) (2sd). All standards measured throughout the course of this project are in agreement with the certified standard values.

For oxygen isotope analysis, 10 clay-size concentrates were analyzed (9 lizardites; 1 chlorite). Before isotope analysis, free Fe- and Mn-oxides were removed using the method of Mehra and Jackson (1960). Oxygen was extracted from silicates using the ClF_3 method. The samples were transferred to nickel reaction vessels and heated for 2 h at 150°C. All samples were then reacted with ClF_3 at 600°C for 12 h. Oxygen was quantitatively converted to CO_2 which then was analyzed isotopically in a Finnigan MAT 251 stable isotope mass spectrometer. Oxygen isotope ratios are expressed in the conventional δ-notation as deviation in per mil from SMOW (Standard Mean Ocean Water):

$$\Delta^{18}O_{A-B} = \delta^{18}O_A - \delta^{18}O_B = 1000\ln\left(a[A-B]\right)$$

4. Results

Petrography & X-ray diffraction

The proportions of serpentinized olivine and pyroxene in the ultramafic rocks suggest that dunites (>90% olivine) and harzburgites (≤50 vol% pyroxene + ≥50 vol% olivine) are the precursor rocks of the Logatchev serpentinites. Serpentinization ranges from 80-90 vol% in the harzburgites whereas the dunites are nearly completely serpentinized (90-100 vol%). Often relicts of partial serpentinized coarse orthopyroxene can be found. Relicts of olivine are rare. X-ray diffraction and microscope studies show that lizardite is the dominating serpentine mineral often together with magnetite (Fig. 2.3a). Mostly the whole groundmass of the serpentinites is composed by mesh-cell structured lizardite which is very well shown in SEM pictures (Fig. 2.3b).

Chrysotile is in general a minor serpentine phase in some samples (Fig. 2.3c + d) and occurs mainly in fractures and fissures (Augustin et al., submitt.). Chrysotile occurs mostly in form of chrysotile-asbestos in very small mm-sized veins which are not longer than 3-4cm. Talc is rare in most of the serpentinite samples. However, a few samples show significant talc formation after serpentine (Fig 2.3c + e). Magnetite is the opaque phase in the serpentinites. Mostly magnetite occurs fine grained in the matrix or at grain boundaries. Some magnetite grains show cores of magnesiochromite.

The serpentinization of orthopyroxenes (Fig. 2.3e) is forming pseudomorphs after pyroxene and are generally named bastites (Wicks and Whittaker, 1977). Serpentinization of pyroxenes begins at the grain boundaries and fractures, follows the cleavages and commonly forms lizardite fibers parallel to the original pyroxene cleavage (Wicks and Whittaker, 1977). Lizardite-filled veins and fractures cutting the earlier mesh-texture, bastites as well as earlier veins can be observed in all serpentine samples. These veins typically consist of fibrous or pillar-like to platy lizardite.

Some thin-sections show sharp contacts between gabbroic rocks and serpentinites where the serpentine minerals are completely metamorphosed to talc.

Based on microscopic analyses gabbroic rocks are classified as coarse to medium-grained gabbronorites (Streckeisen, 1974). Most of them are rather fresh and were only slightly affected by hydrothermal and/or seawater alteration. However, a few samples are highly altered indicated by chlorite-formation, serpentinization and hematitization. Fresh gabbros display varying mostly coarse-grained textures, with hypidiomorphic pyroxene crystals in a matrix of xenomorph, granular plagioclase. Altered gabbros show pseudomorph bastite-serpentinization after pyroxenes and additional chlorite-formation (with bluish interference colors, Fig. 2.3f). In general, clay minerals were identified by XRD (Augustin et al., submitt.). A common chlorite phase is clinochlore which is a typical hydrothermal alteration product of pyroxenes which is often associated with serpentine (Bideaux et al., 1995). Additional some altered samples comprise minor corrensite, a 1:1 regular interstratification of trioctahedral chlorite and trioctahedral smectite (Augustin et al., submitt.). Some highly altered gabbro

samples (54GTV-5A, B, C) show late stage hematite impregnation, and fine to coarse grained, columnar hematite grains. Ilmenite occurs as the only opaque phase.

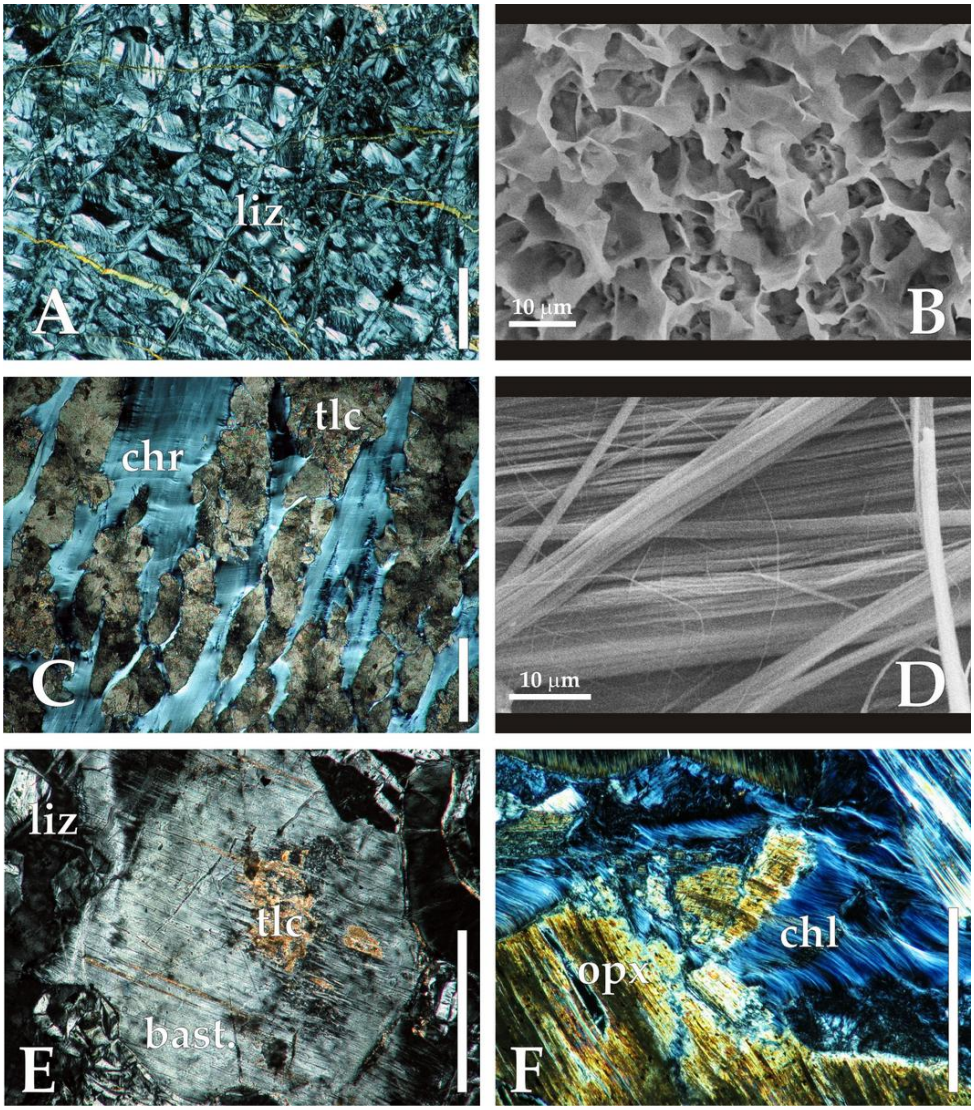

Fig. 2.3: (A) Thin section image of lizardite (liz) matrix with thin chrysotile (chr) veines (mesh texture, sample 67 GTV-2C). (B) Scanning Electron Microscope (SEM) picture of lizardite mesh cell texture (sample 222 GTV-2A). (C) Thin section image of talc (tlc) replacing fibrous chrysotile (chr) (sample 49GTV-1A-3). (D) SEM image of fibrous chrysotile (sample 49GTV-1A-3). (E) Lizardite bastite (bast.) after orthopyroxene with center of talc in matrix of mesh-textured lizardite (sample 33GTV-12). (F) Thin section image of chlorite replacing fractured pyroxene (sample 78GTV-3A). All thin section images under crossed nickols. Scale bar represents 0.5mm.

Trace element concentration of gabbro, serpentinite and sediment

Trace elements compositions of the analyzed rock samples and mineral-concentrates are presented in Table 2.3. Trace element compositions of the analyzed sediments are

distinctively diverse (Tab. 2.3). Chondrite-normalized trace-element pattern show a major increase in the concentration of Cu, Sr, Ba, Pb, Th, and U (Fig. 2.4a) whereas Cr, Co, and Ni are depleted. The chondrite-normalized patterns of the rare earth elements (REE) show a general increase of the REE concentrations with a major enrichment in the LREE and a distinct positive Eu anomaly in nearly all samples (Fig. 2.4b).

Gabbroic samples are characterized by strong variations of the elements Li, Cr, Ni, Cu, Zn, Sr, and Ba as well as Tl, Pb, Th and U (Tab. 2.3). Primitive mantle normalized trace elements of the gabbros show a strong enrichment of Li, Cr and U as well as a significant loss of Co and Ni (Fig. 2.4c). In addition, two samples reveal also a significant increase in U. All other trace elements indicate a slight enrichment and/or depletion in their concentration compared to a primitive mantle. The chondrite normalized REE-pattern of the gabbroic rocks is characterized by a significant positive Eu anomaly (Fig. 2.4d). Sample 53 ROV-2 reveals a minor negative Ce anomaly. All REE are slightly enriched compared to the chondrite concentration (McDonough and Sun, 1995). Sample 49 GTV-4A from Working Area 2 is characterized by a REE pattern showing a distinctive enrichment in the light REE but lacks an Eu anomaly.

The trace element composition of serpentinites is highly variable for many elements such as Cr, Ni, Cu, Zn, Sr, Ba, as well as Tl and Pb (Tab. 2.3). Nearly all analyzed serpentinite samples show high concentrations in Cr, Cu, Zn. Depleted mantle normalized patterns of trace elements in serpentinites show that Li, Cu, Zn, Rb, Sr, Cs, Ba, Tl, Pb and U are in some places highly enriched (Fig. 2.4e). The high field strength elements (HFSE) Zr and Hf as well as Nb are characterized by low values. V, Cr, Co, and Ni concentrations are similar to a depleted mantle. The chondrite normalized REE patterns (McDonough and Sun, 1995) of the serpentinites show a slight enrichment in the light REE with significant positive as well as negative Eu anomalies in most of the analyzed samples (Fig. 2.4f).

Trace element concentration of clay mineral concentrates

Trace element compositions of the clay mineral concentrates are presented in Table 2.3. In contrast to the high variability of trace element concentrations in whole rock serpentinites the trace element concentration in lizardites displays only minor compositional variation. In general, the elements Cr, Ni, Cu, Zn, Sr, Nb, and Ba show the highest concentration in the lizardites (Tab. 2.3). Depleted mantle normalized concentrations show a clear enrichment in Cu, Zn, Sr, Cs, Ba, Tl, Pb, Th, and U (Fig. 2.4g). Even the HFSE Zr and Hf are significant enriched in the lizardites compared to a depleted mantle. Chondrite normalized REE concentrations of the lizardites reveal a light U-shaped pattern with an increase of the light and heavy REEs (L-REE, H-REE) as well as distinctively positive or negative Eu anomalies (Fig. 2.4h).

Primitive mantle normalized trace element concentrations of three chlorite concentrates show an increase of Li, Cr, Cu, Pb, and U and a decrease of Ni (Tab. 2.3). All other trace

elements mostly show similar concentrations compared to a primitive mantle (Fig. 2.4k). Chondrite normalized REE pattern of chlorite concentrates in general show a slight to

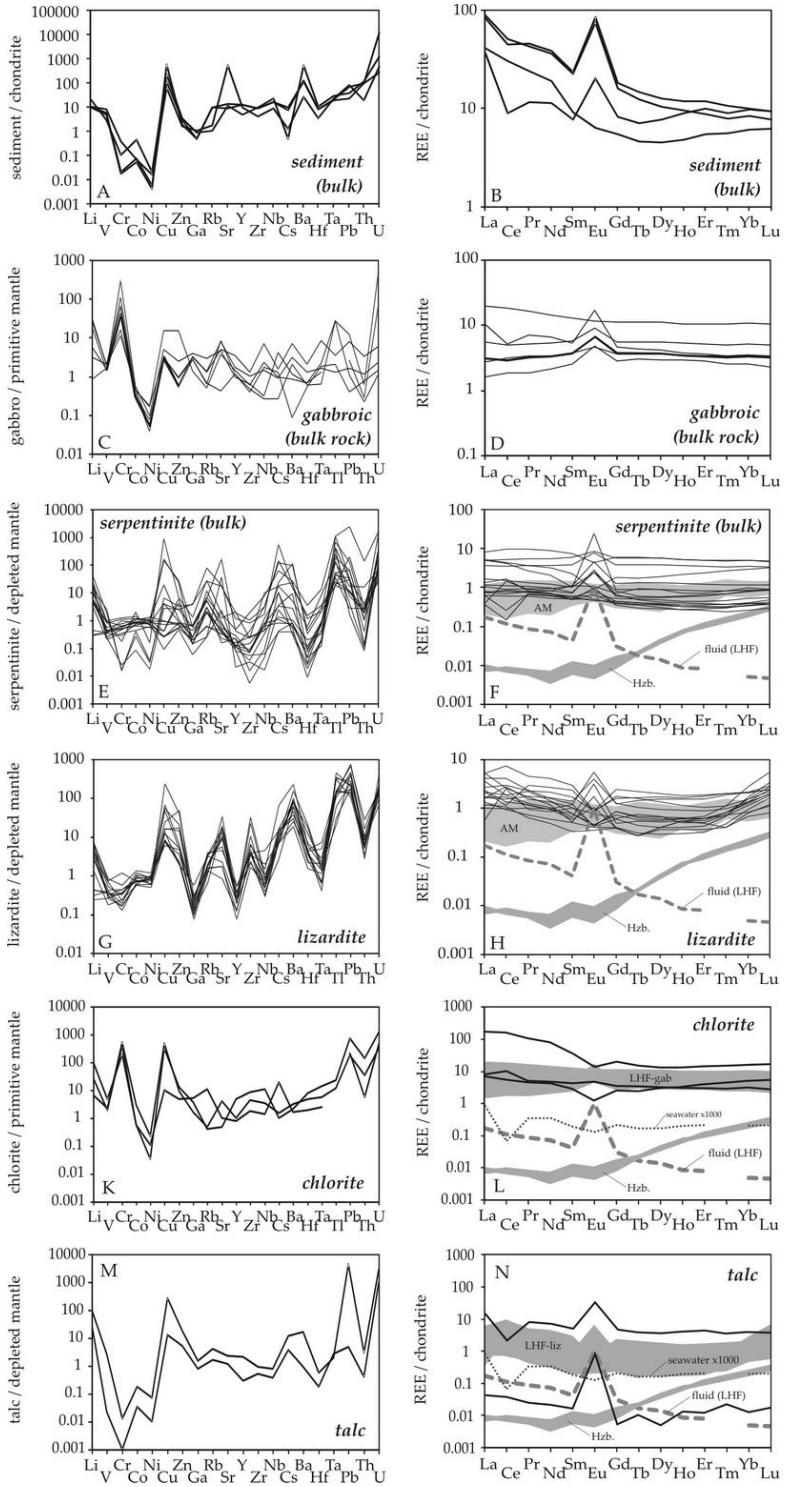

Fig. 2.4: (A) Chondrite normalized pattern of sediment samples. (B) Chondrite normalized REE patterns of sediments. (C) Primitive mantle normalized trace element pattern of bulk rock gabbroic rocks. (D) Chondrite normalized REE pattern of gabbroic rocks. Significant is the positive Eu anomaly in most of the samples. (E) Depleted mantle normalized trace element pattern of bulk rock serpentinites (Salters and Stracke, 2004). (F) Chondrite normalized REE pattern of the serpentinites, fresh harzburgite (ODP Leg 209, Site 1274; thick grey lines); Atlantis Massif serpentinites (AM) and hydrothermal fluids (Schmidt et al., 2007; dashed line). (G) Depleted mantle normalized pattern of trace element concentration in monomineralic lizardite concentrates (Salters and Stracke, 2004). (H) Chondrite normalized REE pattern of lizardites showing a more U-shaped pattern compared to bulk rock analyses. (K) Primitiv mantle normalized pattern of trace element concentration in chlorite. (L) Chondrite normalized REE pattern of chlorite concentrates compared to gabbroic rocks (grey), Logatchev vent fluid (dashed gray; (Schmidt et al., 2007)) and Seawater (dotted gray, (Douville et al., 2002)) (M) Depleted mantle normalized trace element concentration in talc samples from the LHF. (N) REE pattern of talc samples from the LHF (black) compared to fresh harzburgites (ODP Leg 209, site 1274; gray), Logatchev vent fluid ((Schmidt et al., 2007); dashed grey), seawater (Douville et al., 2002), gray-white) and an average serpentinite from Logatchev.

medium increase in the L-REE with a small negative Eu anomaly. Sample 35 GTV-11A shows a slight positive Ce anomaly together with a positive Eu anomaly (Fig. 2.4l).

Two talc samples have been analyzed for their trace element concentration. One bulk rock talc sample (239 GTV-4A) as well as one talc concentrate (239 GTV-4B). Compared to the bulk talc sample the talc concentrate shows significant higher concentrations in V, Cr, Co, Ni, Cu, Zn, Y, Ba, and Pb as well as in all REE (Tab. 2.3). Normalized to a depleted mantle in both talc samples the concentration of Li, Cu, Pb, and U are clearly increased. The concentration of Cr, Co, and Ni is significant decreased compared to a depleted mantle (Fig. 2.4m).

Chondrite normalized REE pattern of talc show a relatively flat shape with light increase in L-REE and clear positive Eu anomalies in both samples. Additionally, the talc concentrate shows a negative Ce anomaly (Fig. 2.4n).

Isotopic composition

Strontium and oxygen isotopic composition of bulk rock samples and clay mineral separates are shown in Table 2.4.

Both, bulk rock serpentinites (n=6) as well as lizardite (n=13) and talc (n=2) separates show $^{87}Sr/^{86}Sr$ ratios of 0.7086 to 0.7096 which is very close to the seawater ratio of 0.7092 (IAPSO). In contrast to the high variability of the Sr concentration in these samples the $^{87}Sr/^{86}Sr$ ratios are relatively constant. The chlorite concentrates from IRINA II show $^{87}Sr/^{86}Sr$ ratios of 0.7083 and 0.7092. $^{87}Sr/^{86}Sr$ ratios in the analyzed gabbroic rocks (n=3) vary from 0.7029 to 0.7037.

The lizardite separates from the Logatchev field (n=7) have homogenous $\delta^{18}O$ composition of 6.1‰ (± 0.6‰) whereas the lizardite separates from Working Area 2 (n=2) show a $\delta^{18}O$ composition of 4.6 and 5.6‰. Analysis of one chlorite separate, from the mound of IRINA II, yields a $\delta^{18}O$ value of 5.6‰.

5. **Discussion**

Secondary mineral formation under varying temperatures

Lizardite after olivine and pyroxene (associated with magnetite) is the most common serpentine phase observed in thin sections of serpentinite samples from the Logatchev hydrothermal field area. In contrast, Bach et al., (2004) also reported brucite as a common phase in serpentinite samples obtained during ODP Leg 209 from the 15°20´N area. The formation of brucite depends on the availability of silica in the fluid. If there is enough $SiO_2(aq)$ in the fluid phase, serpentine can form directly from olivine. Hence the absence of brucite in the samples from the Logatchev field may suggest a high SiO_2 activity in this area. A likely source of $SiO_2(aq)$ might be represented by gabbroic rocks intrusions (Wetzel and

Shock, 2000) that theoretically produce silica rich fluids with low in pH during the interaction with seawater. These seems to be a major source for SiO_2 in the fluid and is supported by the high amount of gabbroic rock samples from the Logatchev area (>20%) and confirmed by the model of massive emplacement of mafic rocks in the oceanic lithosphere at magma-poor slow spreading ridges by Cannat (1993).

An alternative or additional source for aqueous silica is given by the breakdown of pyroxenes in peridotite during peridotite-seawater/fluid reactions at elevated temperatures >270°C (Bach et al., 2006) after the reaction:

$$3\ Mg_{0.9}Fe_{0.1}SiO_3 + H_2O = Mg_{2.7}Fe_{0.3}Si_2O_5(OH)_4 + SiO_2(aq)$$

The hydrothermal vent fluids at Logatchev contain relatively high Si concentrations of about 24 ppm (Schmidt et al., 2007) supporting the conclusion that release of SiO_2(aq) during hydrothermal reactions at depth is on-going.

Alternatively, lizardite and magnetite may have formed from olivine by an sequence of reactions involving brucite as an transitional phase. The following sequence of serpentinization is possible (Bach et al., 2006).

1. Reaction of olivine to serpentine and brucite:

$$2\ Mg_{1.8}Fe_{0.2}SiO_4 + 3\ H_2O = 1\ Mg_{2.85}Fe_{0.15}Si_2O_5(OH)_4 + 1\ Mg_{0.75}Fe_{0.25}(OH)_2$$

2. Reaction of brucite with aqueous silica and formation of serpentine and magnetite:

$$57\ Mg_{0.75}Fe_{0.25}(OH)_2 + 30\ SiO_2(aq) = 15\ Mg_{2.85}Fe_{0.15}Si_2O_5(OH)_4 + 23\ H_2O + 4\ Fe_3O_4 + 4\ H_2$$

The observed formation of talc from serpentine minerals in serpentinite samples from the LHF is a metasomatic process. Bach et al. (2004) presented the following reaction between serpentine and fluid to form talc:

$$Mg_3Si_2O_5(OH)_4 + 2\ SiO_2(aq) = Mg_3Si_4O_{10}(OH)_2 + H_2O$$

This reaction clearly also requires an increased amount of SiO_2 in the fluid.

Formation temperatures of lizardites from the Logatchev hydrothermal field were calculated for 9 mineral separates (Tab. 2.4). However, a variety of different fractionation factors have been proposed and consequently we may obtain variable formation temperatures for the same sample. For example, a calculation after Früh-Green et al. (1996) for the Logatchev lizardites gives the lowest formation temperatures in the order of 115°C (±14°C), whereas a calculation after Harper et al. (1988) yields formation temperatures of about 179°C (±19°C). O´Hanley (1996) combined the fractionation factors of quartz-water and serpentine-water to a modified serpentine-water fractionation factor:

$$\Delta^{18}O_{Srp-H_2O} \approx 1.69 \times 10^6 T^2 - 4.23$$

We prefer the modified fractionation factor for serpentines after O´Hanley (1996) because it is based on natural samples and considers the quartz-water fractionation which could be important during the serpentinization of pyroxenes.

Calculations using this modified fractionation factor gives formation temperatures of about 140-150°C for lizardites at the Logatchev hydrothermal field, using a $\delta^{18}O$ value of 0.3‰ for the background seawater at Logatchev (pers. com. H. Strauß, 2007). The $\delta^{18}O$ value of the high temperature hydrothermal fluid at Logatchev is 1.5‰ (pers. com. H. Strauß, 2007). Considering a involvement of hydrothermal fluid between 0% and 100% during the serpentinization process we infer formation temperatures of the lizardites of 150 - 170°C.

In addition we have analyzed the $\delta^{18}O$ composition of a chlorite-separate taken close to the black smoker complex of IRINA II. Electron microprobe analyses reveal that the chlorites are mainly Mg-Fe-chlorites. Savin and Lee (1988) have published fractionation factors that consider different bond-type approaches as well as the chemical compositions of the chlorites. Using the bond-type calculation for Mg-Fe-chlorites:

$$\Delta^{18}O_{(\text{chlorite-water})} \approx 3.72 \times 10^3 T^{-1} + 2.5 \times 10^6 T^{-2} - 0.321 \times 10^9 T^{-3} + 0.028 \times 10^{12} T^{-4} - 12.62$$

we calculated formation temperatures of about 150 - 200°C considering an involvement of hydrothermal fluid between 0% and 100% respectively.

Trace element variations and fluid/rock interaction

Fluid/rock interactions in the Logatchev hydrothermal field caused an variable addition of many trace- and rare earth elements (REE) to the rocks. Several elements (e.g., Cu, Zn, Rb, Sr, Ba, Pb and U as well as most REE) are increased in their concentration in various proportions. It is important to distinguish the different processes that have influenced the high variability in the multi-element pattern.

The vent fluids at Logatchev are highly enriched in the trace metals Cu (2800 ppb) and Zn (2350 ppb) compared to seawater (0.2 ppb and 18.3ppb; (Schmidt et al., 2007)). Cu and Zn are highly elevated (up to ~2.7 wt% and ~0.2 wt% respectively) in most of the ultramafic bulk rocks and sediment samples compared to a depleted mantle (Cu ≈ 30 ppm, Zn ≈ 56 ppm). However, no significant increase in the Cu concentration of the gabbroic rocks is visible which is probably related to the low degree of alteration. In addition most of the lizardite and chlorite concentrates also show high Cu and Zn concentrations even up to 0.7 wt% and 0.28 wt% respectively. However, electron microprobe analyses of single lizardite grains of serpentinized peridotites revealed even lower CuO and ZnO concentrations of 0.02 wt% and 0.08 wt% in maximum respectively (Augustin et al., submitt.). Therefore the very high

copper concentration in the analyzed ultramafic samples may depend on the presence of trace impurities of sulfides in the rocks as well as in the clay concentrates.

The increase of Rb and Sr in the serpentinites, gabbros and lizardite concentrates are most likely due to seawater alteration. Hart et al. (1974) showed that Rb and Sr are readily supplied by seawater and easily incorporated into, or absorbed on, secondary clay minerals. The strontium isotope composition of whole-rock samples and clay concentrates, combined with petrographic observations provide important constrains on the nature of fluid rock interactions, and the composition of the fluids during hydrothermal alteration (Bickle and Teagle, 1992; Kimbal and Gerlach, 1886; Lackschewitz et al., 2004; Teagle et al., 1998). Figure 2.5 illustrates the $^{87}Sr/^{86}Sr$ ratios in clay mineral concentrates and rocks from the area of the Logatchev hydrothermal field. The $^{87}Sr/^{86}Sr$ ratios of all clay minerals and serpentinites are close to seawater ($^{87}Sr/^{86}Sr = 0.7092$) with mostly enriched Sr concentrations. Gabbroic rocks reveal much lower $^{87}Sr/^{86}Sr$ ratios than the ultramafics. No correlation between Sr-isotopic ratios and Sr concentration in the samples could be observed.

Several previous studies have used Sr-isotopes to calculate water/rock ratios (Bickle and Teagle, 1992; Hart et al., 1974). We calculated water/rock (w/r) ratios under the assumption that the alteration fluid and the host rocks are in equilibrium after the proposed equation of Albarède (1981) for a closed system:

$$\frac{W}{R} = \left(\frac{\varphi_r^a - \varphi_r^o}{\varphi_w - \varphi_r^a}\right) \times \frac{C_r^o}{C_w}$$

W is the mass of the alteration fluid, R is the mass of rock being altered, φ_w is the $^{87}Sr/^{86}Sr$ ratio of the fluid, φ_r^o is the $^{87}Sr/^{86}Sr$ ratio of the unaltered rock and φ_r^a is the $^{87}Sr/^{86}Sr$ ratio of the altered rock. C_w is the elemental Sr-concentration of the fluid and C_r^o is the Sr-concentration of the unaltered rock. The calculated w/r ratios for serpentinites at the Logatchev hydrothermal field vary from 2.6 to 27 for a precursor Sr concentration of about 1 ppm for unaltered peridotites (Decitre et al., 2002; Takazawa et al., 2000) and a $^{87}Sr/^{86}Sr$ ratio of 0.7022 (Decitre et al., 2002). Paulick et al. (2006) reported much lower Sr concentrations of fresh peridotites from the ODP Leg 209 of about 0.18 ppm. Because of the relatively low Sr concentration in peridotites from ODP Leg 209 an average strontium concentration of about 0.58 ppm is a reasonable assumption for the precursor peridotites at Logatchev and we calculated a w/r ratio of 0.7 to 15.7 with an average w/r ratio of 4.3 (Tab. 2.4) for samples of this study. These w/r ratios in the sub-seafloor system of the Logatchev area are comparable to calculated w/r ratios for hydrothermal circulation in the Oman Ophiolite (Bosch et al., 2004). In addition, our calculated w/r ratios fit in the range of computed w/r ratios of Palandri and Reed (2004) were serpentinization simulations with seawater yield alteration assemblages dominated by serpentine similar to serpentinites commonly observed in submarine systems. The absence of brucite could substantiate our calculated w/r ratios because continued fluid-rock interaction leads to changes in fluid pH and silica activity and

causing reaction of brucite to serpentine or brucite dissolves in seawater (Bach et al., 2004; Palandri and Reed, 2004).

Sr is a useful tracer for fluid-crustal interactions because $^{87}Sr/^{86}Sr$ ratio of seawater (0.7091) and mafic rocks (≤ 0.7040) are significantly different and there is no temperature- or mineral-depend isotopic fractionation of Sr. Thus, Sr isotope ratios of altered rocks/minerals, and fluids can provide a measure of the degree of interaction of seawater with the crust (Alt et al., 1996). Sr isotopic data of the Logatchev vent fluid are characterized by $^{87}Sr/^{86}Sr$ ratios of 0.7037 (Amini, 2007) which is comparable with the $^{87}Sr/^{86}Sr$ ratios of gabbroic rocks and basaltic glasses in the area (Fig. 2.5). The similarity of the $^{87}Sr/^{86}Sr$ ratios of the vent fluids to unaffected gabbros and basalt-glasses suggests a strong influence of magmatic intrusions to the composition of the vent fluids.

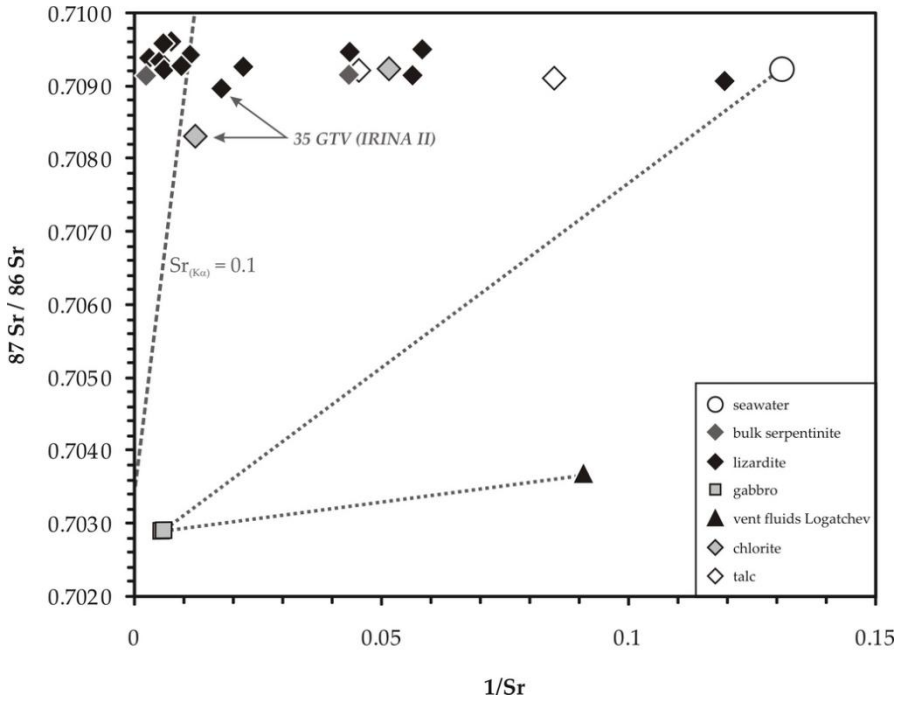

Fig. 2.5: $^{87}Sr/^{86}Sr$ ratio of serpentinites, lizardites, chlorites and talc compared to gabbroic rocks, seawater (IPSAO) and Logatchev vent fluids (Amini, 2007).

Similarities of the $^{87}Sr/^{86}Sr$ data to seawater values as well as the significant increase of Sr concentrations of the serpentinites and secondary minerals compared to fresh peridotites suggest a formation/alteration under seawater-dominated conditions. However, samples very close to the black smoker complex of IRINA II show values just below the $^{87}Sr/^{86}Sr$ ratio of seawater indicating only minor contributions of vent fluids below IRINA II.

However, the elevated $^{87}Sr/^{86}Sr$ ratios in the bulk rock samples and mineral separates of ultramafic rocks could be due to late-stage re-equilibration in the near seafloor environment and may be of little significance regarding the initial conditions of serpentinization. In contrast, the high mobility of LREE and Eu may be much better indicators for fluid-rock interactions during hydrothermal processes suited for the calculation of water/rock ratios. Figure 2.6 indicates that secondary mineral formation was controlled by mixed fluids derived from seawater and hydrothermal fluids in variable proportions. The REE systematic may reflect the particular conditions of secondary mineral formation. The mobility of REE,

especially the LREE and the significance of Eu-anomalies may provide evidence regarding the proportions of the fluid end-members (Allen and Jr., 2005; Bau, 1991). Chondrite normalized REE pattern of all analyzed serpentinite and lizardite samples show flat to U-shaped REE pattern with strong increases in the light rare earth elements (LREE; Fig. 2.4f+h) and variable positive and negative Eu anomalies. In addition, the REE pattern of the hydrothermal vent fluid shows strongly increased LREE (La_N/Lu_N ratio ~39.0) with a strong positive Eu anomaly (Eu_N/Eu^*_N ~35.0, Fig. 2.3f+h; 2.7; Schmidt et al. (2007)). LREE are mobile under hydrothermal, aqueous conditions at high water/rock ratios (Niu, 2004; Paulick et al., 2006). Therefore elevated LREE as well as high w/r ratios suggest a strong influence of hydrothermal fluids during the alteration of the peridotites. Bau (1991) explained positive Eu anomalies by the presence of Eu^{3+} in hot alteration fluids at acidic and reducing conditions associated with positive La_N/Lu_N ratios whereas negative Eu anomalies with $(La/Lu)_N$ <1 are indicators for low temperatures, neutral and oxidizing conditions.

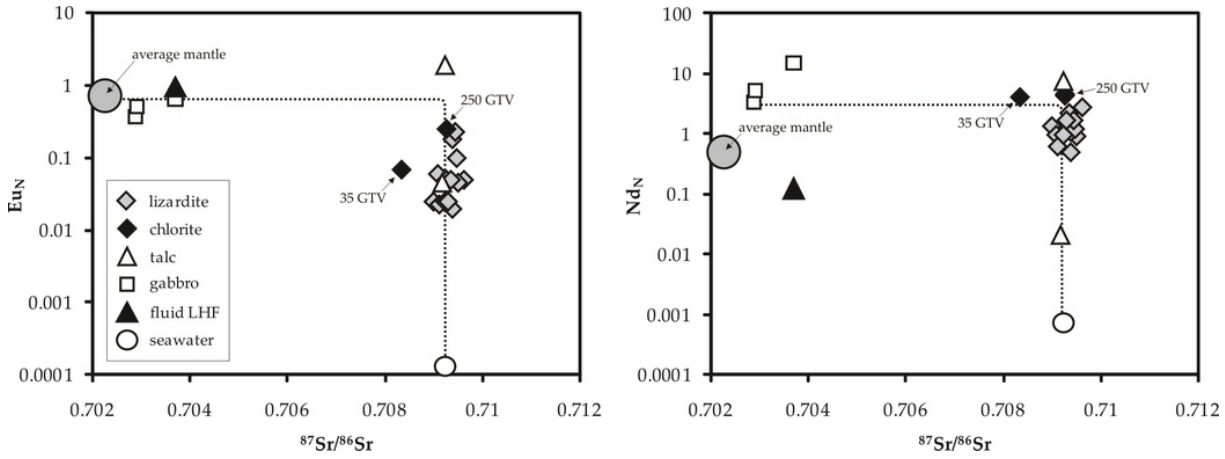

Fig. 2.6: Eu_N and Nd_N versus $^{87}Sr/^{86}Sr$ diagrams showing the compositions of lizardite, chlorites, talc and gabbros compared to the LHF hydrothermal fluid, seawater and peridotitic mantle. The $^{87}Sr/^{86}Sr$ isotopic composition of secondary minerals is very homogeneus whereas the REE show a broad range of their values. The indicated samples from 35 GTV and 250 GTV revealed on-board temperatures of >100°C and >50°C respectively (average mantle data: Takazawa et al. (2000) and Decitre et al. (2002).

Figure 2.7 illustrate the $(La/Lu)_N$ versus Eu_N/Eu^*_N ratios (strength and character of Eu-anomalies) of analyzed serpentinites and lizardites. The relatively variable $(La/Lu)_N$ ratios (range 0.2-5.9, average 1.4) in all samples, show no comparable correlation to the Eu-anomalies and can not be explained by only hydrothermal processes. Therefore an additional process must be responsible for the enrichment in LREE. For example melt-rock interactions could be possible processes to change concentrations of REE and is discussed below.

However, the Eu_N/Eu^*_N ratios vary between seawater and hydrothermal conditions and possibly indicate influences of hydrothermal fluids to the samples. Therefore, samples that

were affected by higher temperatures under acidic and reducing hydrothermal conditions show significant positive Eu anomalies. Figure 2.7 reveals that most of the samples were only poor or no influenced by hydrothermal fluids, whereas the sample 35 GTV close to the black smoker complex of IRINA II reveal the highest Eu_N/Eu^*_N ratio of 25.8 close to the hydrothermal fluid what suggest a strong hydrothermal impact. The observed high variability of Eu anomalies may reflect the varying physico-chemical conditions in the Logatchev field. Fluid-cooling processes and intermixing with seawater in various proportions are most likely the main processes in the shallow sub-seafloor (e.g. beneath hydrothermal crusts or in horizontal sediment covered aquifers) and control the nature of Eu anomalies.

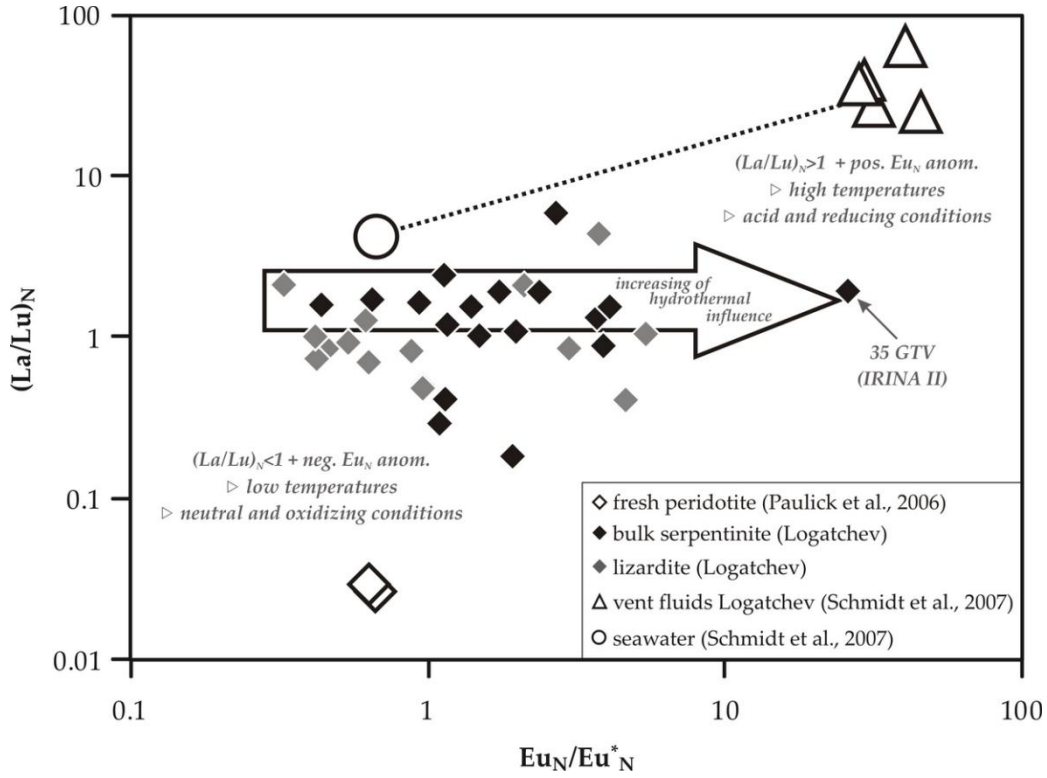

Fig. 2.7: The relationship between the increasing/dec-reasing of L-REE and a positive or negative Eu anomalie in rocks and fluids (Logatchev vent fluid: Schmidt et al., (2007) seawater: Douville et al. (2002)) show that samples from the Logatchev hydrothermal field represent at least two main geochemical environments which lead to different behavior of Eu. After Bau (1991) neutral, oxidizing conditions with low temperatures and $(La/Lu)_N<1$ negative Eu anomalies will occure, whereas positive Eu anomalies develop under acidic and reducing conditions at high temperatures and $(La/Lu)_N>1$. (N = chondrite normalized value; Eu^*_N is the Eu_N value interpolated from Sn_N and Gd_N; $(Eu_N/Eu^*_N) >1$ = positive Eu anomaly; $(Eu_N/Eu^*_N) <1$ = negative Eu anomaly)

Talc alteration

In contrast to the negative Eu anomalies in talc-altered samples from Site 1268 (Paulick et al., 2006) we found strong positive Eu anomalies in pure talc samples from the Logatchev field (Fig. 2.4n). Paulick et al. (2006) have concluded that negative Eu anomalies in talc developed through a destruction of an Eu bearing phase while other REE phases are stable during serpentinization or alternative a release of Eu during the talc recrystallization because Eu does not fit into the crystal lattice of talc. This suggests an influence of a hydrothermal, SiO_2 rich fluid enhancing the dehydration of serpentine to form talc. Alternatively the talc could keep the principal REE pattern of their precursor. In thin sections, we found 2-3cm thick contact-zones between gabbro and serpentinites that consists of pure talc together with magnetite. This suggests that hot, SiO_2-rich fluids originating from the gabbroic intrusions (Bach et al., 2004) may have entered the already serpentinized peridotite host-rock causing talc formation from serpentine. In addition, gabbroic intrusions can produce silica rich and acidic fluids during mafic rock-seawater reactions (Wetzel and Shock, 2000).

Two analyzed talc samples reveal significant different REE patterns and suggest different types of formation: (1) One talc samples shows very similar REE pattern as the Logatchev fluids and indicating a vent fluid controlled talc alteration after Wetzel and Shock (2000). (2) The second talc sample reveals a REE enriched pattern like the serpentinites (except the negative Ce anomaly) and suggest a formation during a contact metamorphosis of the serpentine minerals without significant influences of a hydrothermal fluid.

Implications for melt/rock interaction

More than 20% of the sampled rocks in the area of the Logatchev hydrothermal vent field are gabbroic rocks and cumulates, intruded into serpentinized mantle peridotite. These mafic intrusions are evidence for the transgression of melt through this mantle section to interact with the surrounding ultramafic rocks at various scales.

When mafic melts intrude into the serpentinites, REEs (preferred LREEs) and HFSEs becomes mobile and readily for transport during the melt/rock interactions, e.g. melt extraction or post-melting processes and increase in the host-rock in about equal proportions (Niu, 2004; Paulick et al., 2006). Figure 2.8 shows the positive correlations of LREE (e.g., La, Sm) with HFSE (e.g., Nb, Ta, Zr and Hf) which suggest that both were added to the peridotite during interaction with percolating melts. However, some samples show elevated Zr and Hf concentrations without a corresponding effect in LREE. This could be due to variations in the composition of percolating melts and/or processes during melt rock interaction. Additionally LREE could be mobilized during serpentinization as well as hydrothermal alteration processes (Niu, 2004). However, HFSE are immobile under normal seafloor conditions (Salvi et al., 2000; Salvi and Williams-Jones, 1996). Therefore any other processes e.g., melt/rock interaction causes the addition of HFSE. We suggest that both

processes played a role. Melt/rock interactions, i.e. reported by Niu (2004) can explain the addition of HFSE as well as LREE in samples without significant Eu-anomalies.

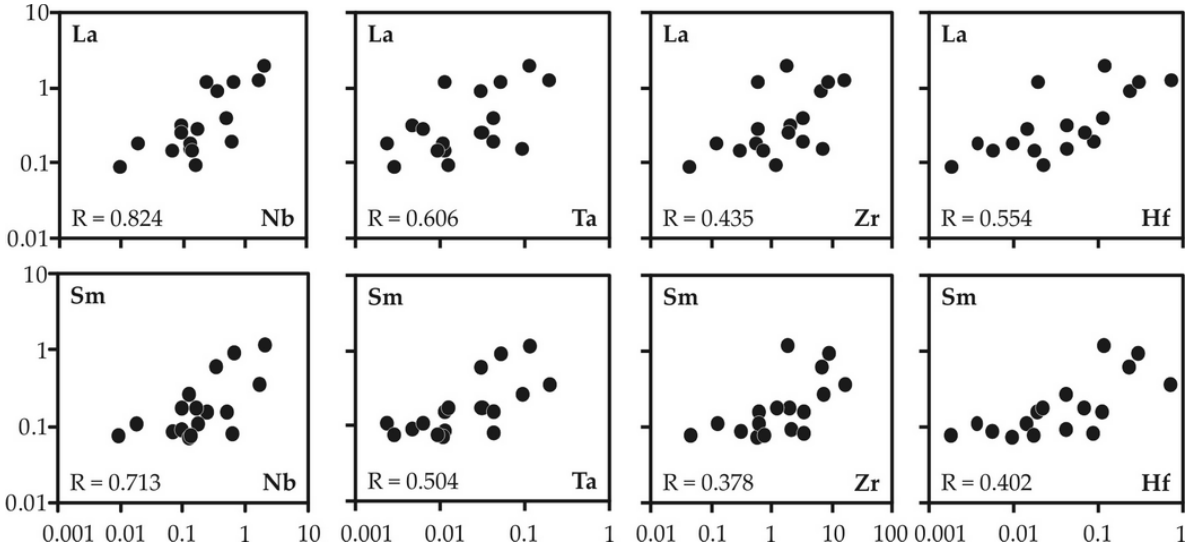

Fig. 2.8: The positive correlations of LREE (e.g. La, Ce and Pr) with HFSE (e.g. Nb, Ta, Zr and Hf) could indicate that the same process/processes lead to the increase of REE and HFSE (R = value of Pearson correlation, n=17).

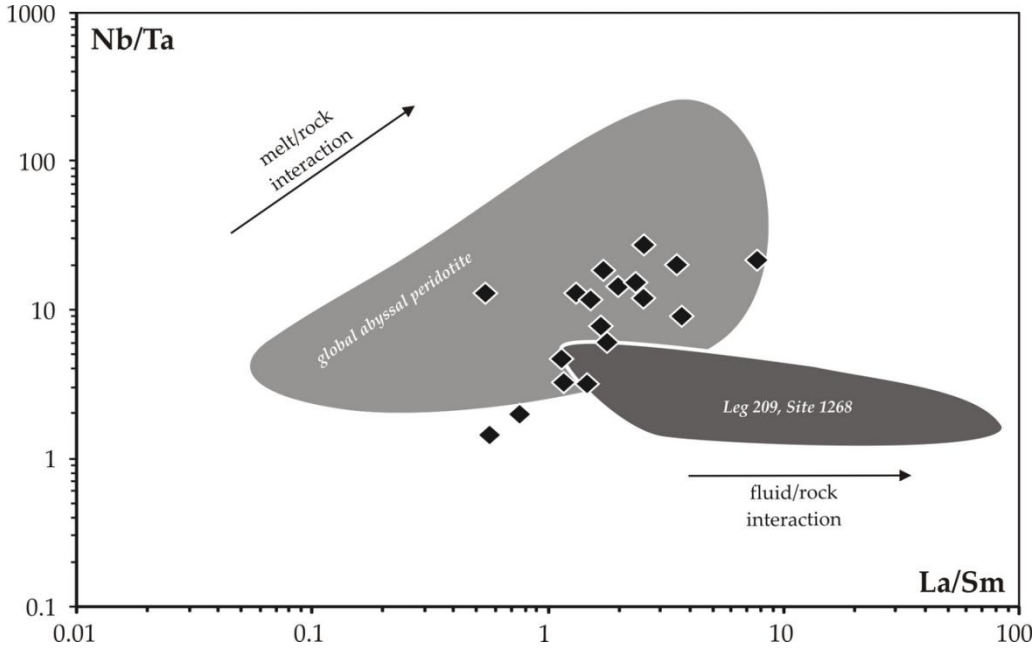

Fig. 2.9: Diagram showing the variations of HFSE and REE during melt-rock interaction as well as fluid-rock interaction compared to data of Niu (2004) and Paulick (2006). (A) Nb/Ta ratios follow the trend of global abyssal serpentinites which is interpreted as melt/rock interaction.

Samples with strong positive Eu anomalies were subsequently affected by stronger hydrothermal influence (high temperatures, high w/r-ratios).
The HFSE and LREE concentrations of Logatchev-serpentinites follow the trend of global abyssal peridotite samples (Fig. 2.9) which were defined as melt/rock interaction (Niu, 2004). Paulick et al. (2006) clearly illustrate that fluid/peridotite interaction can produce larger LREE enrichment that lacks a current increase of HFSE, due to this low solubility in aqueous solution.

Sub-seafloor conditions and heat sources in the Logatchev hydrothermal system

The setting of the Logatchev hydrothermal system in ultramafic-dominated host rocks it is comparable to the Lost City and Rainbow hydrothermal fields (MAR, 30°N and 36°N respectively). The Rainbow hydrothermal field is located within ultramafic rocks on the western flank of a non-volcanic ridge at ~2600 m water-depth (Douville et al., 2002). The off-axis Lost City vent field is located on the top of a non-magmatic oceanic core complex, exposed by a major fault system (Boschi et al., 2006). The main lithologies of the Lost City vent field are very similar to the Logatchev hydrothermal field containing mainly serpentinized peridotites and gabbroic rocks (Boschi et al., 2006). Compared to the high vent-fluid temperatures of >350°C at Logatchev and Rainbow the fluid-temperatures reported from Lost City (30-75°C) are distinctly lower and are interpreted to be generated by active serpentinization at temperatures of >110°C (Früh-Green et al., 2003; Proskurowski et al., 2006). Based on geochemical constraints, Allen & Seyfried (2004) suggest higher sub surface fluid temperatures for the Lost City field in the range of 150-250°C. The high fluid temperatures of the Logatchev and Rainbow vents are related to a magmatic heat source. Geochemical data of serpentinites as well as the large amounts of basaltic and gabbroic rock found at Logatchev site indicate a high abundance of mafic intrusions (<20%) within the ultramafic host rocks. This is consistent with the results of ODP Leg 209 reported from Kelemen et al. (2007). In addition, at least one near-axis volcanic edifice is located 2 km west of the Logatchev field. This volcano may be linked to a possibly heat source in deeper parts of the crust. Fluids access to this heat source may be provided by deep, long-lived faults. A combination of vent fluid chemistry and heat balance models indicates that the Lost City hydrothermal system is most probably also fault controlled (Allen and Seyfried JR., 2003; Allen and Seyfried JR., 2004) and the fluids have also access to deeper crustal sections at higher temperatures or possibly to a magmatic source that could drive the hydrothermal system similar to Logatchev and Rainbow.

The main difference between the Logatchev site and Lost City as well as the Rainbow site is the topographical situation. Both, Lost City as well as Rainbow are localized at elevated positions were sedimentation is limited, whereas main parts of the Logatchev hydrothermal field are located in a depression filled with talus material and pelagic sediment (Fig. 2.10). This causes an increase in porosity and permeability in the subseafloor influencing fluid

pathways importantly and provide aquifers wherein fluids can spread out laterally in layers of mafic/ultramafic talus. Hence high amounts of seawater within these aquifers can be heated up conductively and being intermixed with the fluids in various proportions. These is supported by two TV-Grab stations (239GTV, 250GTV) that sampled such aquifers in a depth of about 50cm below the sediment covered surface. The aquifer at station 250 GTV, 50m SW of IRINA II revealed an on board temperature of about 50°C. Mineral formation temperatures of 170-200°C underneath a hydrothermal crust at IRINA II and Sr-isotopic data indicating that the intermixing of hot vent-type fluids with seawater is an important factor near the active smoking "hot spots" e.g., in porous aquifers and underneath hydrothermal crusts or cap rocks (TV-grab 35GTV >100°C on board temperature). Possibly the diffuse venting at sites "F" and ANYA is also related to a lateral fluid flow which is passing through the sediment cover in some places which is maybe supported from IRINA II.

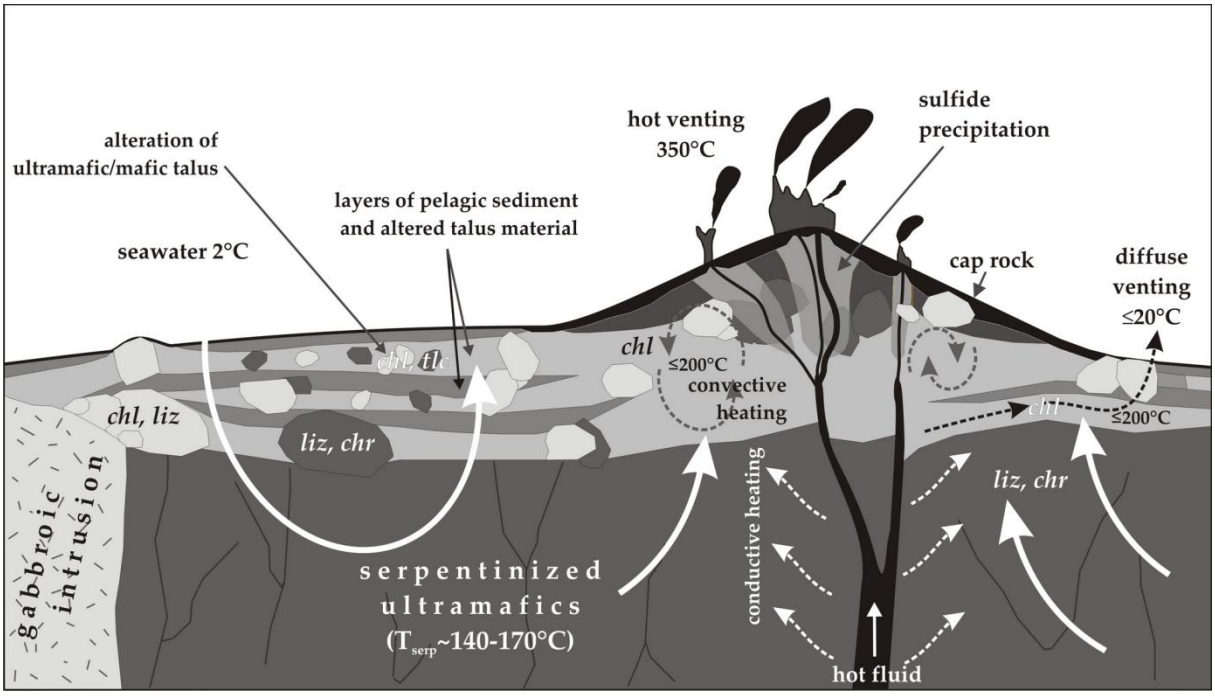

Fig. 2.10: Interpretative sketch of the subsurface processes at the Logatchev hydrothermal field to illustrate fluid upwelling, intermixing with seawater and the most important secondary mineral phases (chl = chlorite; chr = chrysotile; liz = lizardite; tlc = talc).

6. Conclusions

The samples from the Logatchev hydrothermal field reveal peridotite- and gabbro-fluid interactions that took place under a wide range of physico-chemical conditions involving fluids with variable silica activities and varying proportions of seawater. Studies of the mineralogy and trace element geochemistry of altered rocks from the Logatchev field area lead to the following conclusions:

- The high diversity of altered rocks in the area of the ultramafic-hosted Logatchev hydrothermal field yield a large variety in the geochemical composition depending on their mineralogy and geochemical environment (e.g., water/rock ratios, hydrothermal input, temperatures) which can show locally a high variability.
- Oxygen isotope data of lizardite concentrates suggest serpentinization temperatures of about 150-170°C. Chlorite formation took place underneath hydrothermal crusts as well as lateral hydrothermal aquifers at temperatures places of about 170-200°C.
- Sr isotopic data indicate locally high water/rock ratios up to 15.7. The fluid responsible for the secondary mineral formation was most probably seawater with variable amounts of intermixed hot, black smoker-type fluids.
- REE pattern of serpentinites and serpentine minerals show strong enrichments in LREE compared to fresh peridotites. In addition, several samples reveal significant positive Eu-anomalies which suggest an involvement of hydrothermal fluids during their alteration.
- Increases of HFSE e.g., Nb, Ta, Hf as well as LREE in the serpentinites can be interpreted by melt-rock interactions potentially associated with the emplacement of gabbroic intrusions. High amounts of gabbroic rocks as well as the presence of mafic/ultramafic contacts suggest that several mafic intrusions and dikes could have promoted hydrothermal circulation and serpentinization at LHF.
- The formation of talc occurs either in contact zones between mafic intrusions and serpentinized mantle peridotite as well as alteration product during fluid-rock interaction. Both processes require silica rich fluids that can be produced by mafic intrusions and/or the breakdown of pyroxenes in peridotite at elevated temperatures.
- Sr isotopic data of the vent fluids, high fluid temperatures, gabbroic samples as well as a volcano edifice near the Logatchev field indicate that a magmatic heat source drives the hydrothermal system at Logatchev. Fluids possibly have access to that heat source by deep, long lived faults.

7. **Acknowledgments**

The work was supported by grants from the Special Priority Program 1144 (SPP 1144) of the German Science Foundation. We thank all members of the shipboard parties during the cruises M60/3 and M64/2 as well as the R/V Meteor captain and crew. The authors gratefully acknowledge; Petra Fiedler (Kiel University) and Jutta Heinze (IFM-GEOMAR) for technical assistance with XRD analyses; Inge Dold (Kiel University) for sample preparation for oxygen isotope analyses; Peter Appelt and Barbara Mader (Kiel University) for help with microprobe analyses; Heike Anders (Bremen University) and Ulrike Westernströer, Heidi Blaschek (Kiel University) for ICP-MS analyses; Ana Kolevica (IFM-GEOMAR) for strontium isotope analyses; Edgars Rudzitis for help with sample preparation; and Wolfgang Bach, Frieder Klein and Sven Petersen for helpful discussions.

8. References

Albarède, F., Michard, A., Minster, J. F., and Michard, G., 1981. 87Sr/86Sr ratios in hydrothermal waters and deposits from the East Pacific Rise at 21°N. Earth and Planetary Science Letters 55, 229-236.

Allen, D. E. and Jr., W. E. S., 2005. REE controls in ultramafic hosted MOR hydrothermal system: An experimental study at elevated temperature and pressure. Geochimica et Cosmochimica Acta 69, 675-683.

Allen, D. E. and Seyfried JR., W. E., 2003. Compositional controls on vent fluids from ultramafic-hosted hydrothermal systems at midocean ridges: An experimental study at 400°C, 500 bars. Geochimica et Cosmochimica Acta 67, 1531-1542.

Allen, D. E. and Seyfried JR., W. E., 2004. Serpentinization and heat generation: Constraints from Lost City and Rainbow hydrothermal systems. Geochimica et Cosmochimica Acta 68, 1347-1356.

Alt, J. C. and Bach, W., 2003. Alteration of Oceanic Crust. In: Halbach, P. E., Tunnicliffe, V., and Hein, J. R. Eds.), Energy and Mass Transfer in Marine Hydrothermal Systems. Dahlem University Press, Berlin.

Alt, J. C., Teagle, D. A. H., Bach, W., Halliday, A. N., and Erzinger, J., 1996. Stable and strontium isotopic profiles through hydrothermally altered upper oceanic crut, Hole 504B. Proceedings of the Ocean Drilling Program, Scientific Results 148, 57-69.

Amini, M., 2007. The Role of High- and Low-Temperature Oceanic Crust Alteration for the Marine Calcium Budget. Ph.D dissertation Christian Albrechts Universität zu Kiel.

Atterberg, A., 1912. Die mechanische Bodenanalyse und die Klassifikation der Mineralböden Mittelschwedens. Intern. Mitt. f. Bodenkunde, 312-342.

Bach, W., Garrido, C. J., Paulick, H., Harvey, J., and Rosner, M., 2004. Seawater-peridotite interactions: First insights from ODP Leg 209, MAR 15. Goechemistry Geophysics Geosystems 5, 1-22.

Bach, W., Paulick, H., Garrido, C. J., Ildefonse, B., Meurer, W. P., and Humphris, S. E., 2006. Unraveling the sequence of serpentinization reactions: petrography, mineral chemistry, and petrophysics of serpentinites from MAR 15°N (ODP Leg 209, Site 1274). Geophysical Research Letters 33.

Batuyev, B. N., Kratov, A. G., Markov, V. F., Cherkashev, G. A., Krasnov, S. G., and Lisitsyn, Y. D., 1994. Massive sulfide deposits discovered at 14°45´N Mid-Atlantic Ridge. Bridge Newsletter 6, 6-10.

Bau, M., 1991. Rare-earth element mobility during hydrothermal and metamorphic fluid-rock interaction and the significance of the oxidation stage of europium. Chemical Geology 93, 219-230.

Bel´tenev, V., Shagin, A., Markov, V., Rozhdestvenskaya, I., Stepanova, T. V., Cherkashev, G. A., Fedorov, I., Rumyantsev, A., and Poroshina, I., 2004. A new hydrothermal field at 16°38.4´N, 46°28.5´W on the Mid-Atlantic Ridge. Inter Ridge News 13.

Bickle, M. J. and Teagle, D. A. H., 1992. Strontium alteration in the Troodos ophiolite: implications for fluid fluxes and geochemical transport in mid-ocean ridge hydrothermal systems. Earth and Planetary Science Letters 113, 219-237.

Bideaux, R. A., Bladh, K. W., and Nichols, M. C., 1995. Silica, silicates. Mineral Data Publishing, Tucson, AZ, United States.

Bogdanov, Y. A., Gurvich, E. G., Bogdanova, O. Y., Vikent´ev, I. V., Sivtsov, A. V., Isaeva, A. B., Gorshkov, A. I., and Sagalevich, A. M., 2004. Low-Temperature Deposits of the Logatchev Hydrothermal Field (Mid-Atlantic Ridge). Geology of Ore Deposits 46, 269-285.

Bosch, D., Jamais, M., Boudier, F., Nicolas, A., Dautria, J.-M., and Agrinier, P., 2004. Deep and High-temperature Hydrothermal Circulation in the Oman Ophiolite - Petrological and Isotopic Evidence. Journal of Petrology 45, 1181-1208.

Boschi, C., Früh-Green, G. L., Delacour, A., Karson, J. A., and Kelley, D. S., 2006. Mass transfer and fluid flow during detachment faulting and development of an oceanic core complex, Atlantis Massif (MAR 30°N). Geochemistry Geophysics Geosystems 7, 1-39.

Cannat, M., 1993. Emplacement of Mantle Rocks in the Seafloor at Mid-Ocean Ridges. Journal of Geophysical Research 98, 4163-4172.

Cannat, M., Bideau, D., and Bougault, H., 1992. Serpentinized peridotites and gabbros in the Mid-Atlantic Ridge axial valley at 15°37´N and 16°52´N. Earth and Planetary Science Letters 109, 87-106.

Cherkashev, G. A., Ashadze, A. M., and Gebruk, A. V., 2000. New Fields with manifestations of hydrothermal activity in the Logatchev area (14°N, Mid-Atlantic Ridge). InterRidge News 9, 26-27.

Decitre, S., Deloule, E., Reisberg, L., James, R., Agrinier, P., and Mével, C., 2002. Behavior of Li and its isotopes during serpentinization of oceanic peridotites. Geochemistry Geophysics Geosystems 3, 1-20.

Dosso, L., Bougault, H., and Joron, J. L., 1993. Geochemical morphology of the North Mid-Atlantic Ridge, 10°-24°N. Trace element-isotopes complementary. Earth and Planetary Science Letters 120, 443-462.

Douville, E., Charlou, J. L., Oelkers, E. H., Bienvenu, P., Jove Colon, C. F., Donval, J. P., Fouquet, Y., Prieur, D., and Appriou, P., 2002. The rainbow vent fluids (36°14′N, MAR): the influence of ultramafic rocks and phase separation on trace metal content in Mid-Atlantic Ridge hydrothermal fluids. Chemical Geology 184, 37-48.

Eberhardt, G. L., Rona, P. A., and Honnorez, J., 1988. Geologic Controls of Hydrothermal Activity in the Mid-Atlantic Ridge Rift valley: Tectonics and Volcanism. Marine Geophysical Research 10, 233-259.

Escartin, J. and Cannat, M., 1999. Ultramafic exposures and the gravity signature of the lithosphere near the Fifteen-Twenty Fracture Zone (Mid-Atlantic Ridge, 14°-16,5°N). Earth and Planetary Science Letters 171, 411-424.

Früh-Green, G. L., Kelley, D. S., Bernasconi, S. M., Karson, J. A., Ludwig, K. A., Butterfield, D. A., Boschi, C., and Proskurowski, G., 2003. 30,000 Years of Hydrothermal Activity at the Lost City Vent Field. Science 301, 495-498.

Früh-Green, G. L., Plas, A., and Lécuyer, C., 1996. Petrology and stable isotope constrains on hydrothermal alteration and serpentinization of the EPR shallow mantle at Hess Deep (Site 895). Proceedings of the Ocean Drilling Program, Scientific Results 147, 255-291.

Fujiwara, T., Lin, J., Matsumoto, T., Kelemen, P. B., Tucholke, B. E., and Casey, J. F., 2003. Crustal Evolution of the Mid-Atlantic Ridge near the Fifteen-Twenty Fracture Zone in the last 5 Ma. Geochemistry Geophysics Geosystems 4, 1-25.

Gablina, I. F., Mozgova, N. N., Borodaev, Y. S., Stepanova, T. V., Cherkashev, G. A., and Il′in, M. I., 2000. Copper Sulfide Associations in Recent Oceanic Ores of the Logatchev Hydrothermal Field (Mid-Atlantic Ridge, 14°45′N). Geology of Ore Deposits 42, 296-316.

Garbe-Schönberg, C.-D., 1993. Simultaneus determination of thirty-seven trace elements in twenty-eight international rock standards by ICP-MS. Geostandard Newsletters 17, 81-97.

Gebruk, A. V., Chevaldonné, P., Shank, T., Lutz, R. A., and Vrijenhoek, R. C., 2000. Deep-sea hydrothermal vent communities of the Logatchev area (14°45′N, Mid-Atlantic Ridge): diverse biotopes and high biomass. Journal of the Marine Biological Association of the United Kingdom 80, 383-393.

Govindaraju, K., 1994. Compilation of Working Values and Descriptions for 383 Geostandards. Geostandard Newsletters 18, 1-158.

Harper, G. D., J.R., B., and R.J., K., 1988. A field, chemical, and stable isotope study of subseafloor metamorphism of the Josephine Ophiolite, California-Oregon. Journal of Geophysical Research, B, Solid Earth and Planets 93, 4625-4656.

Hart, R. A., Erlank, A. J., and Kable, E. J. D., 1974. Sea floor basalt alteration: some chemical and Sr isotopic effects. Contributions to Mineralogy and Petrology 44.

Hémond, C., Hoffman, A. W., Vlastélic, I., and Nauret, F., 2006. Origin of MORB enrichment and relative trace element compatibilities along the Mid-Atlantic Ridge between 10 and 24°N. Geochemistry Geophysics Geosystems 7, 1-22.

Humphris, S. E., Halbach, M., and Juniper, K., 2003. Low-temperature Alteration - Fluxes and Mineralization. In: Halbach, P. E., Tunnicliffe, V., and Hein, J. R. Eds.), Dahlem Workshop Report 89 - Energie and Mass Transfer in Marine Hydrothermal Systems. Dahlem University Press.

Jochum, K. P., Nohl, U., Herwig, K., Lammel, E., Stoll, B., and Hofmann, A. W., 2005. GeoReM: A New Geochemical Database for Reference Materials and Isotopic Standards. Geostandards and Geoanalytical Research 29, 333-338.

Kelemen, P. B., Kikawa, E., Miller, D. J., and Shipboard Scientific Party, 2007. Leg 209 Summary: Processes in a 20-km-thick conductive boundary layer beneath the Mid-Atlantic Ridge, 14°-16° N. In: Kelemen, P. B.,

Kikawa, E., and Miller, D. J. Eds.), Proceedings of the Ocean Drilling Program, Scientific Results, 209: College Station, TX (Ocean Drilling Program).

Kimbal, K. L. and Gerlach, D. C., 1886. Sr isotopic constraints on hydrothermal alteration of ultramafic rocks in two oceanic fracture zones from the South Atlantic Ocean. Earth and Planetary Science Letters 78, 177-188.

Koschinsky, A., Billings, A., Devey, C. W., Dubilier, N., Duester, A., Edge, D., Garbe-Schönberg, C.-D., German, C. R., Giere, O., Keir, R., Lackschewitz, K. S., Mai, H. A., Marbler, H., Mawick, J., Melchert, B., Mertens, C., Peters, M., Sanders, S., Schmale, O., Schmidt, W., Seifert, R., Seiter, C., Stöber, U., Suck, I., Walter, M., Weber, S., Yoerger, D., Zarrouk, M., and Zielinski, F., 2006. Discovery of new hydrothermal vents on the southern Mid-Atlantic Ridge (4°S-10°S) during cruise M68/1. InterRidge News 15, 9-15.

Krasnov, S. G., Cherkashev, G. A., Stepanova, T. V., Batuyev, B. N., Krotov, A. G., Malin, B. V., Maslov, M. N., Markov, V., Poroshina, I., Samovarov, M., Ashadze, A. M., Lazareva, L. I., and Ermolayev, I. K., 1995. Detailed geological studies of hydrothermal fields in the north atlantic. Geological Society Special Publication 87, 43-64.

Kuhn, T., Alexander, B., Augustin, N., Birgel, D., Borowski, C., Carvalho, L. M. d., Engemann, G., S. Ertl, L. F., Grech, C., Hekinian, R., Imhoff, J. F., Jellinek, T., Klar, S., Koschinsky, A., Kuever, J., Kulescha, F., Lackschewitz, K. S., Petersen, S., Ratmeyer, V., Renken, J., Ruhland, G., Scholten, J., Schreiber, K., Seifert, R., Süling, J., Türkay, M., Westernströer, U., and Zielinski, F., 2004a. Mineralogical, geochemical, and biological investigations of hydrothermal systems on the Mid-Atlantic Ridge between 14°45'N and 15°05'N (HYDROMAR I). Meteor Berichte 03-04, 1-61.

Kuhn, T., Alexander, B., Augustin, N., Birgel, D., Borowski, C., de Carvalho, L. M., Engemann, G., Ertl, S., Franz, L., Grech, C., Herzig, P. M., Hekinian, R., Imhoff, J. F., Jellinek, T., Klar, S., Koschinsky, A., Kuever, J., Kulescha, F., Lackschewitz, K. S., Petersen, S., Ratmeyer, V., Renken, J., Ruhland, G., Scholten, J., Schreiber, K., Seifert, R., Süling, J., Türkay, M., Westernströer, U., and Zielinski, F., 2004b. The Logatchev hydrothermal field - revisited: preliminary results of the R/V METEOR Cruise HYDROMAR I (M60/3). Inter Ridge News 13, 1-4.

Kuhn, T., Petersen, S., Lackschewitz, K. S., Augustin, N., Franz, L., Brügmann, G., and Devey, C. W., 2005. Hydrothermal processes in the activ Logatchev-1 hydrothermal field: new insights from mineralogy and geochemestry of massive sulfides and alteration products Russian Ridge Workshop, VNIIOkeangeologia, St. Petersburg.

Lackschewitz, K. S., Armini, M., Augustin, N., Dubilier, N., Edge, D., Engemann, E., Fabian, M., Felden, J., Franke, P., Gärtner, A., Garbe-Schönberg, D., Gennerich, H.-H., Hüttig, D., Marbler, H., Meyerdierks, A., Pape, T., Perner, M., Reuter, M., Ruhland, G., Schmidt, K., Schott, T., Schroeder, M., Schroll, G., Seiter, C., Stecher, J., Strauss, H., Viehweger, M., Weber, S., Wenzhöfer, F., and Zielinski, F., 2005. Longterm study of hydrothermalism and biology at the Logatchev field, Mid-Atlantic Ridge at 14°45'N (revisit 2005) (HYDROMAR II)Meteor Berichte 05.

Lackschewitz, K. S., Armini, M., Augustin, N., Dubilier, N., Edge, D., Engemann, E., Fabian, M., Felden, J., Franke, P., Gärtner, A., Garbe-Schönberg, D., Gennerich, H.-H., Hüttig, D., Marbler, H., Meyerdierks, A., Pape, T., Perner, M., Reuter, M., Ruhland, G., Schmidt, K., Schott, T., Schroeder, M., Schroll, G., Seiter, C., Stecher, J., Strauss, H., Viehweger, M., Weber, S., Wenzhöfer, F., and Zielinski, F., in press. Longterm study of hydrothermalism and biology at the Logatchev field, Mid-Atlantic Ridge at 14°45'N (revisit 2005) (HYDROMAR II)Meteor Berichte 05.

Lackschewitz, K. S., Devey, C. W., Stoffers, P., Botz, R., Eisenhauer, A., Kummetz, M., Schmidt, M., and Singer, A., 2004. Mineralogical, geochemical and isotopic characteristics of hydrothermal alteration processes in the active, submarine, felsic-hosted PACMANUS field, Manus Basin, Papua New Guinea. Geochimica et Cosmochimica Acta 68, 4405-4427.

McDonough, W. F. and Sun, S.-s., 1995. The composition of the Earth. Chemical Geology 120, 223-253.

Mehra, O. P. and Jackson, M. L., 1960. Iron oxide removal from soils and clays by dithionite-citrate system buffered with sodium bicarbonate. Clays and Clay Minerals 7, 317-327.

Moore, D. M. and Reynolds, R. C., 1989. X-ray Diffraction and the Identification and Analysis of Clay Minerals. Oxford University Press.

Niu, Y., 2004. Bulk-rock Major and Trace Element Compositions of Abyssal Peridotites: Implications for Mantle Melting, Melt Extraction and Post-melting Processes Beneath Mid-Ocean Ridges. Journal of Petrology 45, 2423–2458.

O´Hanley, D. S., 1996. Serpentinites - Records of Tectonic and Petrological History. Oxford University Press, New York, Oxford.

Palandri, J. L. and Reed, M. H., 2004. Geochemical models of metasomatism in ultramafic systems: Serpentinization, rodingitization, and sea floor carbonate chimney precipitation. Geochemica et Cosmochimica Acta 65, 1115-1138.

Paulick, H., Bach, W., Godard, M., De Hoog, J. C. M., Suhr, G., and Harvey, J., 2006. Geochemistry of abyssal peridotites (Mid-Atlantic Ridge, 15°20´N, ODP Leg 209): Implications for fluid/rock interaction in slow spreading environments. Chemical Geology 234, 179-210.

Proskurowski, G., Lilley, M. D., Kelley, D. S., and Olson, E. J., 2006. Low temperature volatile production at the Lost City Hydrothermal Field, evidence from a hydrogene stable isotope geothermometer. Chemical Geology 229, 331-343.

Rona, P. A., Widenfalk, L., and Boström, K., 1987. Serpentinized ultramafics and hydrothermal activity at the Mid-Atlantic Ridge crest near 15°N. Journal of Geophysical Research 92, 1417-1427.

Salters, V. J. M. and Stracke, A., 2004. Composition of the depleted mantle. Geochemistry Geophysics Geosystems 5, 1-27.

Salvi, S., Fontan, F., Monchoux, P., Williams-Jones, A. E., and Moine, B., 2000. Hydrothermal Mobilization of High Field Strength Elements in Alkaline Igneous Systems: Evidence from the Tamazeght Complex (Morocco). Economic Geology 95, 559-576.

Salvi, S. and Williams-Jones, A. E., 1996. The role of hydrothermal processes in concentrating high-field strength elements in the Strage Lake peralkaline complex, northeastern Canada. Geochemica et Cosmochimica Acta 60, 1917-1932.

Savin, S. M. and Lee, M., 1988. Isotopic Sudies of Phyllosilicates. In: Bailey, S. W. (Ed.), Hydrous Phyllosilicates (exclusive of micas). Mineralogical Society of America.

Schmidt, K., Koschinsky, A., Garbe-Schönberg, D., De Carvalho, L. M., and Seifert, R., 2007. Geochemistry of hydrothermal fluids from the ultramafic-hosted Logatchev hydrothermal field, 15°N on the Mid-Atlantic Ridge: temporal and spartial investigation. Chemical Geology 242, 1-21.

Streckeisen, A., 1974. Classification and nomenclature of plutonic rocks recommendations of the IUGS subcommission on the systematics of Igneous Rocks. International Journal of Earth Sciences 63, 773-786.

Takazawa, E., Frey, F. A., Shimizu, N., and Obata, M., 2000. Whole rock compositional variations in an upper mantle peridotite (Horoman, Hokkaido, Japan): Are they consistent with a partial melting process? Geochemica et Cosmochimica Acta 64, 695-716.

Teagle, D. A. H., Alt, J. C., Chiba, H., and Halliday, A. N., 1998. Dissecting an active hydrothermal deposit: The strontium and oxigen isotopic anatomy of the TAG hydrothermal mound-anhydrite. Proceedings of the Ocean Drilling Program, Scientific Results 158, 129-141.

Wetzel, L. R. and Shock, E. L., 2000. Distinguishing ultramafic- from basalt-hosted submarine hydrothermal systems by comparing calculated vent fluid compositions. Journal of Geophysical Research 105, 8319-8340.

White, W. M. and Patchett, J., 1983. Hf-Nd-Sr isotopes and incompatible element abundance in island arcs - implications for magma origins and crust-mantle evolution. Earth and Planetary Science Letters 67, 167-185.

Wicks, F. J. and Whittaker, E. J. W., 1977. Serpentine Textures and Serpentinization. The Canadian Mineralogist 15, 459-488.

Wilson, S. A., 1997. Data compilation for USGS reference material BHVO-2, Hawaiian Basalt. U.S. Geological Survey Open-File Report.

9. Tables

Tab. 2.1: Overview to sample sites, positions and sampled lithologies for samples with relevance to this work.

Station	Lat (N)	Long (W)	Lithology	Abbreviations
32 GTV	14°45.11	44°58.71	Serp, MS, Mud	Atc = atacamite (copper-chlorite)
33 GTV	14°45.11	44°58.69	Serp, Gab, MC, Mud, Atc, OPX	Bas = basalts
35 GTV	14°45.19	44°58.75	Serp, FeO, MS,	FeO = Fe-oxides-hydroxides
49 GTV	14°55.48	44°54.29	Serp, Gab, Bas, Mud	Gab = gabbros with diff. degree of alteration
54 GTV	14°45.17	44°58.75	MS, FeO	HC = hydrothermal crust
53 ROV	14°45.108	44°58.698	MS, FeO	MC = manganese crusts
54 GTV	14°45.168	44°58.632	Serp, HC, Atc	MS = massive sulfides
57 GTV	14°42.30	44°53.87	Serp, MS, Gab, Bas	Mud = hydrothermal and/or pelagic sediments
62 GTV	14°45.23	44°58.83	Serp, HC, MS, SiS, Mud	OPX = orthopyroxene-rich cumulates (diff. alteration)
67 GTV	14°42.40	44°54.45	Serp, Gab, Bas, OPX	Qtz = quarz pieces
73 ROV	14°45.19	44°58.77	Serp, Gab, MS	Serp = serpentinized ultramafics with diff. degree of serpentinization
74 GTV	14°45.06	44°58.63	Serp, Gab, Mud	SiS = silicified Sediment
77 GTV	14°45.192	44°58.83	Mud	Tlc = talc pieces
78 GTV	14°45.19	44°58.88	Serp, Gab, MC	
79 GTV	14°45.20	44°58.71	MC, Mud	
82 GTV	14°45.34	44°58.88	Serp, Tlc, FeO, MC	
83 GTV	14°45.21	14°58.782	Serp, Gab, MS, HC	
239 GTV	14°45.078	44°58.722	Atc, FeO, MC, Tlc	
250 GTV	14°45.162	44°58.77	Serp, Gab, Qtz, MC, OPX	

Tab. 2.2: List of international reference standards, analyzed during the ICP-MS analytical runs, for controlling the accuracy of analytical results.

	AGV-1	AGV-1	BHVO-1	BHVO-1	BHVO-2	BHVO-2	BIR-1	BIR-1	JR-1	JR-1	UB-N	UB-N	62 GTV-1B	62 GTV-1B	49 GTV-3B	49 GTV-3B
	This work (n=2)	Reference values	This work (n=2)	Reference values	This work (n=6)	Reference values	This work (n=6)	Reference values	This work (n=1)	Reference values	This work (n=1)	Reference values	Repeated analyses (n=6)	Standard deviation	Duplicate analysis (n=2)	Standard deviation
	(ppm)	(ppm)	(ppm)	(ppm)	(ppm)	(ppm)	(ppm)	(ppm)	(ppm)	(ppm)	(ppm)	(ppm)	(ppm)	(%)	(ppm)	(%)
Li	10.5	12.0	4.9	4.6	4.4	*5.0*	3.0	3.4	68.4	*62.3**	32.0	*27.0**	3.2	16.8	2.9	11.4
Sc	12.1	12.2	32.1	31.8	32.5	32.0	46.4	44.0	6.0	*5.2**	12.2	*13.5**	9.4	10.4	5.9	10.1
V	129	121	315	317	330	317	332	313	9.8	*8.0**	62.7	*75.0**	37.0	9.1	44.7	0.62
Cr	*7.6*	10.0	273	*289*	292	280	380	382	1.47	*2.3**	1930	*2300**	698	8.1	1904	0.80
Co	15.0	15.3	42.0	45.0	45.0	45.0	54.6	51.4	0.60	*0.65**	99.1	*100**	126	7.4	110	0.43
Ni	14.9	16.0	110	*121*	121	119	175	166	0.63	*0.66**	1815	*2000**	1592	6.8	2550	0.51
Cu	57.3	60.0	129	*136*	131	127	118	126	2.7	*1.40**	22.3	*28.0**	1348	6.5	28.2	0.61
Zn	89.1	88.0	102	105	109	103	70.8	71.0	29.5	*30.0**	78.7	*85.0**	271	5.4	38.2	1.78
Ga	20.8	20.0	20.5	21.0	21.7	21.7	15.3	*16.0*	17.9	*17.6**	2.5	*2.7**	0.94	4.6	0.62	2.36
Rb	67.4	67.3	8.8	11.0	8.9	9.8	0.21	*0.21**	325	*257**	3.2	*3.5**	0.13	6.3	0.05	2.21
Sr	680	672	399	403	395	389	109	104	29.8	*30.0**	7.7	*7.6**	81.4	1.17	4.3	4.5
Y	18.6	20.0	23.8	27.6	25.1	26.0	15.0	16.0	42.8	*45.4**	2.3	*2.6**	1.58	1.69	0.44	4.8
Zr	243	227	167	179	183	172	15.5	14.0	89.1	*101**	3.6	*3.4**	17.2	3.5	0.55	13.2
Nb	13.5	15.0	16.8	*17.1*	17.7	*18.0*	0.54	*0.55*	15.1	*15.5**	0.05	*0.05**	0.05	8.2	0.13	0.71
Cs	1.26	1.28	0.10	0.13	0.10	*0.12**	0.01	*0.01**	20.2	*20.2**	11.0	*10.8**	0.01	1.61	0.001	9.9
Ba	1221	1203	136	139	131	130	6.793	*7.0*	38.6	*40.0**	27.1	*26.3**	52.2	2.4	0.92	10.6
La	37.6	37.6	15.0	15.8	15.2	15.0	0.63	0.62	19.3	*19.7**	0.30	*0.32**	0.37	1.85	0.18	3.9
Ce	69.2	67.0	36.8	39.0	37.9	38.0	1.97	1.95	47.0	*47.1**	0.74	*0.78**	1.00	2.8	0.52	2.8
Pr	8.7	*7.6*	5.4	*5.7*	5.4	*5.7**	0.39	*0.38**	6.2	*5.6**	0.11	*0.12**	0.14	3.1	0.07	4.4
Nd	32.2	33.0	24.6	25.2	25.1	25.0	2.5	2.5	23.6	*23.5**	0.58	*0.59**	0.67	4.4	0.32	3.0
Sm	5.9	5.9	6.1	6.2	6.3	*6.2*	1.17	*1.10*	5.8	*6.1**	0.21	*0.22**	0.18	2.7	0.07	3.1
Eu	1.22	1.60	2.1	2.1	2.2	*2.1**	0.57	0.54	0.25	*0.30**	0.08	*0.07**	0.25	4.6	0.05	3.5
Gd	5.0	5.0	6.2	*6.4*	6.4	*6.3*	1.98	1.85	5.6	*5.2**	0.31	*0.32**	0.23	3.2	0.07	3.9
Tb	0.67	0.70	0.946	*0.96*	0.95	*0.90*	0.38	*0.36**	0.97	*1.02**	0.06	*0.06**	0.03	4.2	0.01	3.9
Dy	3.6	3.6	5.4	5.2	5.4	*5.5**	2.8	2.5	6.2	*5.8**	0.41	*0.43**	0.22	4.6	0.07	3.2
Ho	0.67	0.70	0.98	*0.99*	1.01	*1.04*	0.61	*0.57**	1.28	*1.10**	0.09	*0.09**	0.05	5.1	0.01	4.1
Er	1.78	1.70	2.4	*2.4*	2.6	*2.6**	1.85	*1.70**	3.8	*3.8**	0.27	*0.28**	0.14	5.8	0.04	4.7
Tm	0.25	0.34	0.33	*0.33*	0.34	*0.35**	0.27	*0.26**	0.63	*0.67**	0.04	*0.04**	0.02	4.9	0.01	3.8
Yb	1.66	1.72	2.0	2.0	2.05	*2.0*	1.78	1.65	4.5	*4.5**	0.29	*0.30**	0.21	4.6	0.06	4.1
Lu	0.25	0.27	0.28	*0.29*	0.28	*0.28*	0.27	*0.26*	0.67	*0.71**	0.05	*0.05**	0.05	6.1	0.01	4.6
Hf	5.1	5.1	4.5	4.4	4.5	4.1	0.66	0.58	4.5	*4.7**	0.13	*0.12**	0.49	7.0	0.01	16.5
Ta	0.90	0.80	0.07	0.04	1.17	*1.4*	0.07	0.04	1.49	*1.9*	0.014	*0.015*	0.01	5.9	0.01	24.8
Pb	36.2	36.0	1.99	2.1	1.59	*1.7**	3.0	*3.1*	18.7	*19.1**	13.0	*12.4**	5.1	4.9	0.18	0.13
Th	6.1	6.5	1.25	1.08	1.20	*1.20*	0.03	*0.03**	23.4	*26.5**	0.07	*0.06**	0.04	4.9	0.03	9.1
U	1.94	1.92	0.43	*0.42*	0.44	*0.45**	0.01	*0.01**	8.488	*9.0**	0.06	*0.06**	0.71	5.9	0.81	1.32

Reference values font design: normal = recommended values (USGS); *italic* = information values (USGS); *italic** = GeoReM Database values

Tab. 2.3: Trace and rare earth element concentration in gabbroic rocks, sediments, serpentinites and mineral separates (values in ppm).

Sample ID	Sample Type	Li	Sc	V	Cr	Co	Ni	Cu	Zn	Ga	Rb	Sr	Y	Zr	Nb	Cs	Ba	La	Ce	Pr	Nd	Sm	Eu	Gd	Tb	Dy	Ho	Er	Tm	Yb	Lu	Hf	Ta	Tl	Pb	Th	U
33 GTV-1	bulk gabbro	1.43	41.4	140	180	33.9	155	82.4	30.8	11.8	0.39	180	5.2	5.1	0.18	0.01	14.0	0.72	1.72	0.29	1.48	0.54	0.37	0.71	0.13	0.88	0.19	0.52	0.08	0.52	0.08	0.18	0.02	0.10	0.17	0.02	0.02
49 GTV-4A	bulk gabbro	9.4	33.2	126	304	47.7	345	89.6	33.4	13.9	0.81	105	15.3	13.5	4.8	0.03	48.3	4.7	11.0	1.54	6.5	1.85	0.64	2.1	0.39	2.6	0.56	1.64	0.25	1.72	0.25	0.60	0.32	0.01	1.21	0.28	0.12
53 ROV-2	bulk gabbro	42.8	22.7	175	179	46.7	319	476	871	5.67	0.30	76.2	6.3	6.2	1.52	0.02	5.8	2.5	3.1	0.66	2.9	0.78	0.96	0.92	0.15	1.00	0.20	0.58	0.08	0.54	0.08	0.19	0.08	0.10	1.85	0.05	10.6
74 GTV-1A	bulk gabbro	5.1	43.8	167	43.0	40.5	74.0	93.9	53.6	12.9	0.83	166	7.7	11.1	0.97	0.02	21.0	1.30	3.01	0.47	2.4	0.82	0.51	1.08	0.20	1.35	0.28	0.81	0.12	0.81	0.12	0.36	0.06	0.00	0.25	0.09	0.05
78 GTV-3B	bulk gabbro	51.4	35.6	161	30.4	49.8	101	97.7	50.3	11.7	0.43	8.6	5.2	4.2	1.17	0.03	0.59	0.63	1.87	0.31	1.53	0.55	0.26	0.71	0.13	0.89	0.19	0.54	0.08	0.56	0.08	0.16	0.07	0.01	0.06	0.06	0.03
250 GTV-4	bulk gabbro	29.1	44.6	120	813	62.0	193	149	140	16.5	1.78	96.9	4.1	6.9	0.21	0.09	7.83	0.37	1.10	0.17	0.96	0.37	0.26	0.55	0.11	0.70	0.16	0.45	0.06	0.40	0.05	0.20	0.05	-	0.41	0.02	1.43
35 GTV-11A	bulk sediment	29.8	24.2	155	277	218	214	26169	1006	8.0	2.3	78.6	7.6	35.9	5.3	0.09	1231	9.7	18.7	2.2	8.7	1.35	0.35	1.08	0.17	1.11	0.26	0.87	0.14	0.97	0.15	1.02	0.39	-	93.8	3.1	8.9
74 GTV-3B	bulk sediment	15.1	3.6	328	55.0	37.0	60.5	14115	921	4.5	21.9	101	19.8	33.1	3.8	1.46	297	19.5	27.7	4.2	17.7	3.5	4.8	3.6	0.53	3.2	0.65	1.91	0.26	1.63	0.23	0.85	0.27	-	165	2.9	1.97
74 GTV-3C	bulk sediment	14.5	3.7	262	42.3	25.8	40.5	67368	555	4.5	21.9	63.3	18.5	32.6	3.71	1.77	268	21.2	31.3	4.0	16.7	3.3	4.2	3.2	0.44	2.6	0.52	1.42	0.20	1.36	0.19	0.82	0.26	-	55.3	2.8	93.8
77 GTV-2B	bulk sediment	16.0	17.5	468	1000	34.2	169	7661	500	9.7	4.0	3941	15.6	16.4	2.1	0.25	64.2	8.9	5.6	1.08	5.3	1.16	1.16	1.64	0.26	1.91	0.50	1.60	0.22	1.58	0.23	0.35	0.31	-	209	0.54	3.8
33 GTV-11	bulk serpentinite	7.8	20.1	77.2	3013	150.8	1326	4341	1583	1.82	0.44	7.0	0.49	1.15	0.16	0.004	3.3	0.09	0.90	0.08	0.38	0.17	0.06	0.14	0.03	0.22	0.04	0.11	0.02	0.16	0.02	0.02	0.01	0.02	1.53	0.01	1.75
33 GTV-17A	bulk serpentinite	27.6	33.1	142	41.1	29.1	60.7	193	180	12.1	6.8	177	4.9	6.4	0.35	0.72	23.1	0.87	2.1	0.33	1.70	0.57	0.43	0.76	0.14	0.95	0.20	0.55	0.08	0.56	0.08	0.23	0.03	0.01	0.25	0.03	0.23
35 GTV-4A	bulk serpentinite	17.2	11.3	75.5	438	219.4	312	26921	391	4.3	2.5	17.7	2.0	15.9	1.71	0.09	31.2	1.24	2.7	0.35	1.46	0.33	0.05	0.36	0.06	0.47	0.12	0.38	0.07	0.49	0.08	0.73	0.19	0.41	56.8	1.85	7.57
35 GTV-4B	bulk serpentinite	8.1	8.1	19.7	67.0	9.3	35.5	84.6	145	1.89	0.57	1631	1.71	1.91	0.10	0.03	136	0.24	0.54	0.08	0.42	0.16	0.26	0.25	0.05	0.32	0.07	0.19	0.03	0.18	0.03	0.07	0.03	0.26	3.1	0.03	6.1
35 GTV-9	bulk serpentinite	3.4	6.0	30.8	2407	92.3	1972	12.3	340	0.72	1.06	8.5	0.49	3.3	0.64	0.16	109	0.19	0.47	0.07	0.31	0.08	0.05	0.09	0.01	0.09	0.02	0.06	0.01	0.06	0.01	0.09	0.04	0.01	4.5	0.04	0.27
49 GTV-2	bulk serpentinite	0.30	6.85	28.2	1231	71.0	1683	21.8	41.9	0.47	0.02	22.3	0.32	0.44	0.01	0.001	0.46	0.01	0.02	0.01	0.03	0.01	0.01	0.02	0.004	0.03	0.01	0.03	0.01	0.04	0.01	0.005	0.003	0.05	0.10	0.001	0.59
49 GTV-5L	bulk serpentinite	11.3	7.6	35.9	1368	125.1	1873	27.3	45.0	2.2	0.62	12.2	8.3	1.81	2.1	0.02	6.1	1.92	5.7	0.89	4.02	1.11	0.25	1.20	0.22	1.40	0.29	0.81	0.12	0.82	0.12	0.12	0.11	0.05	0.40	0.22	0.33
57 GTV-2	bulk serpentinite	0.22	7.9	32.7	1298	70.5	1151	7.9	47.8	1.45	0.19	2.3	0.66	2.1	0.10	0.002	1.31	0.31	1.00	0.08	0.31	0.09	0.04	0.10	0.02	0.12	0.02	0.07	0.01	0.08	0.01	0.04	0.005	0.16	0.67	0.06	0.32
62 GTV-1A	bulk serpentinite	3.4	8.8	34.4	1502	98.5	1451	121.7	50.5	0.82	0.27	1.56	0.93	0.12	0.02	0.01	0.36	0.18	0.42	0.07	0.38	0.10	0.16	0.13	0.02	0.11	0.02	0.06	0.01	0.07	0.01	0.004	0.002	0.41	0.77	0.002	0.44
250 GTV-1A	bulk serpentinite	8.3	36.9	174	10033	142	1389	168	167	3.7	2.1	45.5	3.5	7.2	0.13	0.02	6.2	0.15	0.38	0.09	0.55	0.26	0.10	0.32	0.08	0.45	0.10	0.29	0.05	0.37	0.05	0.04	0.09	n.d.	3.4	0.01	4.3
33GTV-11	lizardite	2.8	11.6	52.6	586	107	1152	7020	2224	0.99	0.14	17.1	0.31	13.3	0.13	0.01	22.5	0.14	1.58	0.09	0.40	0.15	0.05	0.13	0.03	0.17	0.03	0.08	0.02	0.14	0.03	0.30	0.02	0.02	5.7	0.04	1.96
35GTV-4B	lizardite	5.9	21.2	32.9	177	14.8	57.4	520	546	2.9	0.14	1043	2.2	14.3	0.08	0.01	79.3	0.24	0.61	0.10	0.46	0.18	0.32	0.24	0.05	0.39	0.09	0.25	0.05	0.35	0.06	0.34	0.01	0.04	4.0	0.05	9.5
35GTV-9	lizardite	3.1	7.8	26.2	1144	92.2	1957	493	981	0.64	0.32	56.8	1.06	48.8	0.32	0.09	283	0.38	1.73	0.15	0.63	0.16	0.03	0.17	0.03	0.17	0.04	0.10	0.02	0.19	0.05	1.23	0.03	0.01	10.3	0.12	0.32
49GTV-2	lizardite	0.96	5.5	14.1	606	61.1	1000	228	117	0.24	0.10	335	0.78	85.7	0.10	0.01	94.0	0.28	0.67	0.06	0.23	0.05	0.02	0.08	0.01	0.10	0.03	0.09	0.02	0.22	0.06	2.5	0.03	0.06	3.1	0.09	0.65
49GTV-3B	lizardite	2.5	4.4	24.3	440	65.2	2108	252	128	0.33	0.12	8.4	0.49	27.7	0.16	0.01	116	0.41	1.06	0.11	0.44	0.09	0.06	0.08	0.01	0.09	0.02	0.06	0.01	0.11	0.02	0.75	0.02	0.05	4.0	0.09	0.70
49GTV-3E	lizardite	5.3	4.1	21.1	415	64.3	1203	403	114	0.30	0.17	93.0	0.82	54.2	0.19	0.01	96.6	0.51	1.15	0.12	0.48	0.10	0.18	0.10	0.02	0.13	0.03	0.10	0.02	0.21	0.05	1.39	0.04	0.06	3.4	0.11	0.49
49GTV-5C	lizardite	1.85	7.2	34.5	1102	74.9	1498	1662	1181	0.72	0.36	45.4	2.2	31.2	0.95	0.02	46.3	1.24	4.6	0.42	1.91	0.44	0.05	0.49	0.08	0.50	0.10	0.30	0.05	0.34	0.06	0.97	0.10	0.06	15.9	0.38	0.79

Sample ID	Sample Type	Li	Sc	V	Cr	Co	Ni	Cu	Zn	Ga	Rb	Sr	Y	Zr	Nb	Cs	Ba	La	Ce	Pr	Nd	Sm	Eu	Gd	Tb	Dy	Ho	Er	Tm	Yb	Lu	Hf	Ta	Tl	Pb	Th	U
49GTV-6B	lizardite	2.0	6.5	24.0	886	77.8	1657	753	2797	0.46	0.11	193	2.1	28.3	0.42	0.01	124	0.63	1.82	0.21	0.98	0.25	0.05	0.32	0.06	0.42	0.09	0.28	0.05	0.35	0.07	0.88	0.07	0.04	11.3	0.13	0.82
57GTV-1A-1	lizardite	4.2	12.8	59.0	3116	78.8	1652	263	112	1.89	0.29	22.9	0.89	17.9	0.11	0.02	37.2	1.29	1.64	0.16	0.56	0.08	0.10	0.08	0.01	0.10	0.03	0.08	0.01	0.13	0.03	0.45	0.03	0.12	2.6	0.07	1.06
62GTV-1B	lizardite	3.4	9.4	41.3	809	129	1710	1454	284	0.92	0.15	89.0	1.58	19.3	0.07	0.01	55.6	0.39	0.96	0.16	0.75	0.21	0.22	0.25	0.04	0.24	0.05	0.14	0.02	0.22	0.05	0.52	0.01	0.18	5.0	0.05	0.78
67GTV-2A	lizardite	0.23	4.8	32.5	329	74.5	1686	242	201	0.47	0.14	17.7	0.53	31.8	0.06	0.01	31.0	0.33	0.58	0.07	0.28	0.08	0.02	0.08	0.01	0.07	0.02	0.05	0.01	0.15	0.04	0.90	0.01	0.05	9.0	0.09	1.05
67GTV-2B	lizardite	0.30	5.2	31.1	499	113	1847	191	269	0.38	0.31	167	0.75	190	0.17	0.02	101	0.57	0.86	0.11	0.45	0.12	0.03	0.12	0.02	0.10	0.02	0.07	0.02	0.28	0.08	3.5	0.02	0.13	6.5	0.14	0.95
67GTV-2C	lizardite	0.31	7.3	27.1	821	97.4	1704	502	828	0.56	0.18	105	1.13	265	0.22	0.01	190	0.98	2.6	0.22	0.75	0.18	0.03	0.17	0.02	0.15	0.03	0.11	0.03	0.45	0.14	4.2	0.02	0.05	17.9	0.22	0.96
74GTV-2C	lizardite	5.2	9.5	67.0	1475	145	2417	2088	362	0.82	0.27	135	1.53	31.7	0.13	0.02	76.1	0.53	0.71	0.28	1.22	0.35	0.05	0.36	0.06	0.34	0.06	0.17	0.03	0.25	0.05	0.72	0.01	0.01	4.4	0.07	1.15
78GTV-2B	lizardite	0.17	6.3	21.5	925	81.5	1229	364	296	0.41	0.06	171	1.40	38.0	0.08	0.00	73.2	0.86	1.17	0.21	0.67	0.12	-	0.15	0.02	0.14	0.03	0.10	0.02	0.26	0.07	0.83	0.01	0.14	5.0	0.08	1.04
35GTV-4A	chlorite	10.7	29.7	179	1331	311	433	14323	510	6.4	0.29	81.6	4.3	46.0	2.3	0.03	20.2	1.62	3.3	0.42	1.87	0.44	0.07	0.52	0.09	0.75	0.18	0.64	0.11	0.80	0.13	1.30	0.20	0.04	25.8	2.7	6.3
35GTV-11A	chlorite	158	44.8	391	501	59.4	66.2	9761	721	14.5	0.25	9.4	19.9	92.6	7.1	0.02	14.1	41.1	94.2	9.7	34.4	5.0	0.78	3.7	0.53	3.2	0.70	2.2	0.35	2.5	0.39	2.3	0.53	0.08	111	11.5	24.6
250 GTV-4	chlorite	41.5	80.8	159	1028	56.9	205	289	256	20.2	6.4	19.4	3.3	17.5	0.88	0.41	10.8	1.75	6.3	0.45	2.1	0.62	0.25	0.68	0.12	0.78	0.17	0.47	0.07	0.50	0.07	0.51	0.09	-	30.5	0.45	8.9
239 GTV-4B	talc	71.0	0.23	207	33.0	20.0	150	8118	1023	4.7	0.36	21.9	8.4	7.4	0.17	0.02	19.1	3.6	1.27	0.73	3.3	0.71	1.95	0.91	0.14	0.91	0.22	0.69	0.09	0.62	0.10	0.11	0.03	-	100	0.04	13.1
239 GTV-4A	talc	20.6	0.44	1.84	2.5	3.6	20.1	392	279	2.6	0.14	11.7	1.17	4.2	0.08	0.005	1.13	0.01	0.02	0.002	0.01	0.00	0.05	0.001	-	0.001	0.001	0.002	0.001	0.002	-	0.04	0.04	-	0.12	0.01	4.7

Tab. 2.4: Isotopic compositions, calculated water/rock ratios and formation temperatures of mineral concentrates and selected bulk rock samples.

Sample ID	Sample Type	^{87}Sr / ^{86}Sr clay	calc. Water/Rock (Sr) *	$\delta^{18}O$ (‰) clay	calc. formation Temp. (°C) **
33GTV-1	gabbronorite	0.70290			
33GTV-11	lizardite separate	0.70951	2.1	5.4	152-183
33GTV-12	serpentinite	0.70874	1.0		
35GTV-9	lizardite separate	0.70898	2.0	6.3	133-159
49GTV-2	serpentinite	0.70915	6.2		
49GTV-2	lizardite separate	0.70939	3.6	4.5	175-210
49GTV-3B	lizardite separate	0.70908	3.4		
49GTV-4A	gabbronorite	0.70371			
49GTV-3E	lizardite separate	0.70939	3.7		
49GTV-5A	serpentinite	0.70892	1.6		
49GTV-5C	lizardite separate	0.70927	15.7		
49GTV-6B	lizardite separate	0.70935	4.9	5.6	148-177
57GTV-1A-1	lizardite separate	0.70947	2.4	5.6	148-177
57GTV-2	serpentinite	0.70855	0.7		
62GTV-1B	lizardite separate	0.70943	2.9	5.4	152-183
67GTV-2A	lizardite separate	0.70915	6.7		
67GTV-2B	serpentinite	0.70916	7.5		
67GTV-2B	lizardite separate			6.3	133-159
67GTV-2C	lizardite separate	0.70928	11.7		
74GTV - 1A	gabbronorite	0.70291			
74GTV-2C	lizardite separate	0.70961	1.52	6.9	122-146
77GTV 1	serpentinite	0.70907	3.20		
78GTV-2B	lizardite separate	0.70959	1.6	6.5	129-155
35GTV-4A	chlorite separate	0.70833		5.6	170-200
250GTV-4	chlorite separate	0.70924			
239GTV-4A	talc	0.70911			
239GTV-4B	talc	0.70922			

* calculated water/rock ratio with average Sr=0.58 ppm and $^{87}Sr/^{86}Sr$=0.7022 for a possible precursor rock (average W/R = 4.3)

** calculated range of formation temperatures is from 0-100% hydrothermal influence (calculation after O´Hanley, 1996)

Chapter 3:
Mineralogical and chemical mass changes in mafic and ultramafic rocks

Abstract

We have analyzed serpentinites and gabbros from the area of the ultramafic hosted Logatchev Hydrothermal Field (MAR, 15°N) for their mineralogy and chemical composition. The degree of serpentinization of harzburgites and dunites is 90-95%, whereas gabbros are mostly rather fresh. Our calculations of relative gains and losses of major and trace elements as well as mineralogical observations reveal that a large variety of alteration styles take place at the Logatchev hydrothermal field. A combination of serpentinization, hydrothermal fluids, melt-rock interaction and low-temperature seafloor weathering lead to significant gains and losses of major and trace elements. We found that serpentinization at Logatchev was isochemical for the most major elements (excepting a loss of TiO_2 and CaO). However, the concentration of trace elements e.g., Cu, Nb, Ba, La, Sm, Eu, Th or U increases strongly in the serpentinites. In addition, gabbroic intrusions are a sink for MgO during the formation of chlorite and serpentine after clinopyroxene and play a major role as distributors of SiO_2, TiO_2, CaO, and Na_2O as well as numerous trace elements in the circulating fluids. The differentiation of alteration styles and the correlation with associated elemental fluxes reveals that the influence of hot, hydrothermal fluids is significant for the whole Logatchev field. Only samples very close to active black smoker-type vent-sites display distinct uptakes in Cu, Ba, La, Sm and Eu as the results of strong hydrothermal influence. Serpentinization, melt/rock interaction of serpentinites and mafic intrusions, and low-temperature seafloor weathering are the dominating alteration processes in this area.

1. Introduction

The ultramafic hosted Logatchev hydrothermal field (named after the Russian research vessel Professor Logatchev which discovered the field in 1993) at the Mid-Atlantic Ridge (14°45´N) was intensively sampled during the R/V Meteor cruises M60/3 and M64/2 in 2004 and 2005.

Studies of serpentinites and gabbroic rocks from this area have shown that serpentinization, hydrothermal activity, as well as the interaction of ultramafic host-rocks with mafic intrusions are major processes at the MAR at 15°N (Augustin et al., submitt.; Bach et al., 2004a; Paulick et al., 2006). Additionally, many recent studies have described the effects of different alteration styles for diverse geological settings: Melt/rock interaction

mobilize elements with high field strength (HFSE) and light rare-earth elements (LREE) in about equal proportions (Niu, 2004; Paulick et al., 2006). Alteration under high fluid/rock ratios at low, as well as high temperatures influence significantly the budgets of major and trace elements, as well as the formation of secondary minerals in different manners (Bach et al., 2003; Hart et al., 1974; Jochum and Verma, 1996; Lackschewitz et al., 2000a; Macdougall et al., 1979; Talbi et al., 1999; Verma, 1992).

This work is part of the German Priority Program SPP-1144: "From Mantle to Ocean", funded by the Deutsche Forschungsgemeinschaft (DFG). A major scientific objective of this priority program is to investigate the interrelationship of geological, geochemical, and biological processes in the active Logatchev hydrothermal field at 14°45´N, MAR (Kuhn et al., 2004b; Lackschewitz et al., in press)

This paper uses a combination of mineralogical and geochemistry analyses and to examine and differentiate the alteration styles. The aim of this work is to examine the proportions and significances of the different alteration processes and their associated element fluxes to mafic and ultramafic rocks in the area of the Logatchev hydrothermal field.

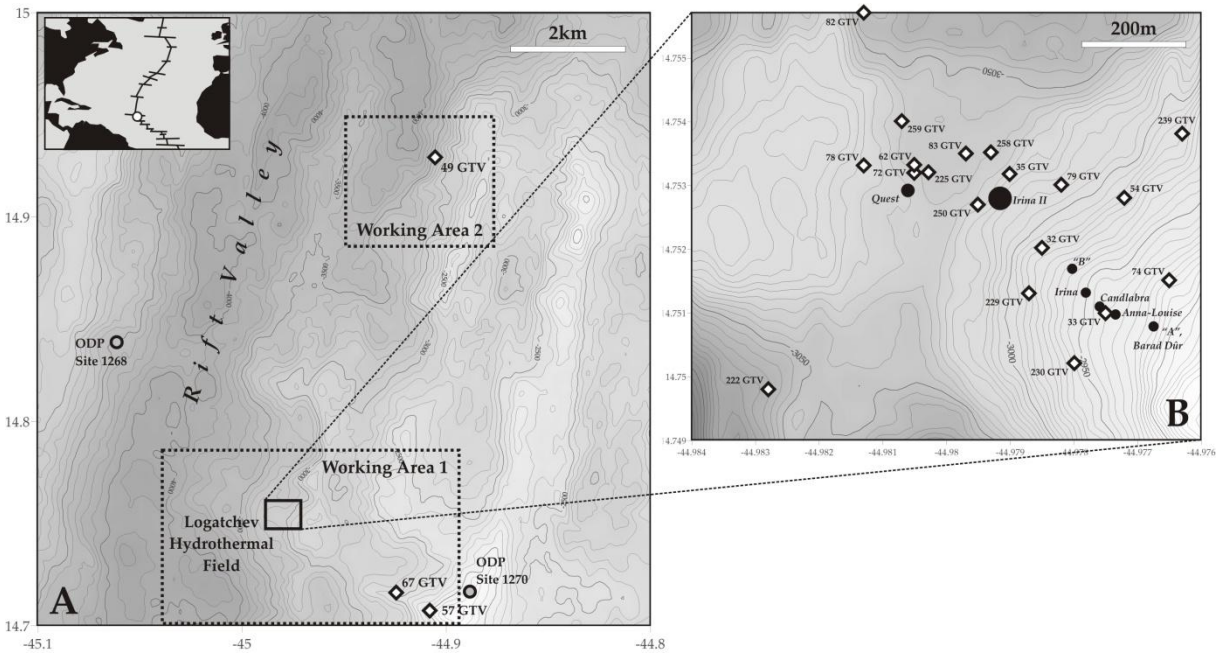

Fig. 3.1: (A) Overview map is showing the working areas 1 (Logatchev hydrothermal field) and 2 at the Mid-Atlantic ridge at 14°45´N (diamonds indicate TV-Grab sample stations during Meteor cruise M60/3. (B) Detailed Map with sampling stations during Meteor cruises M60/3 and M64/2 (black circles: positions of known active vent sites)

2. Regional Setting

The Logatchev Hydrothermal Field was first discovered in 1993 by Russian scientists (Batuyev et al., 1994; Cherkashev et al., 2000) and is part of a ultramafic-hosted hydrothermal system situated at 14°45′N, 44°59′W. It is located at the lower, eastern ridge-flank between two terrace-like structures at about 3000 m water depth close to the axial valley (Fig. 3.1). The Logatchev Hydrothermal Field extends at least 800 m in a NW-SE direction and 200 m in the SW-NE direction. The field was the central part of Working Area 1 of the 2004 cruise M60/3 (Kuhn et al., 2004a). The main parts of the Logatchev hydrothermal field are located in a depression, which is filled with talus debris and pelagic sediment. This causes an increase in porosity and permeability in the subseafloor, which in turn influences fluid pathways (Augustin et al., submitt.). Host rocks of the Logatchev Hydrothermal Field are mainly serpentinized harzburgites and lherzolites with significant amounts of more than 20% of gabbroic rocks (Augustin et al., submitt.; Kuhn et al., 2004b).

The sampled harzburgites and dunites are extensively serpentinized (>90-95%). Only serpentinized harzburgites occasionally show relicts of pyroxene and/or olivine. The sampled gabbroic rocks are mostly rather fresh to moderately altered.

Working Area 2 is situated about 20 km north of the active Logatchev field around 14°54′N, 44°54′W (Fig. 3.1a) and is hosted by ultramafic rocks and subordinate outcrops of gabbros and basalts (Krasnov et al., 1995; Kuhn et al., 2004b). Bathymetric and photographic mapping of the seafloor has shown that rather fresh basalts and pillow mounds are characteristic for the rift valley and the lower part of the rift flank (Kuhn et al., 2004b). The upper parts of the eastern rift flank are mainly characterized by serpentinized peridotites (Kuhn et al., 2004b)

3. Methods

During this study, we analyzed 31 rock samples from the active Logatchev hydrothermal field (Working area I) and 8 rock samples from Working Area 2 for mineralogical and chemical composition.

After drying, the samples were divided into fine (<63 μm) and coarse fractions (>63 μm) by wet sieving. The rock samples were crushed gently before separating the fine fraction. Grain size separation into silt (2-63 μm) and clay fraction (<2 μm) was performed according to Stokes′ law by settling the particles in, water filled cylinders (Atterberg, 1912; Moore and Reynolds, 1989).

The Bulk rock and clay mineralogy were determined by X-ray diffractometry (XRD) at the IFM-Geomar, Kiel and the Institute for Geosciences, University of Kiel, Germany, by using a Philips X-ray diffractometer PW 1710 with automatic divergence slit and monochromatic CoKα or CuKα radiation. Bulk rock samples were powdered and pressed to tablets for measurements. Oriented clay samples were produced by vacuum filtration

through a 0.15-µm filter. Measurements on the clay samples were carried out on air-dried as well as on glycol-saturated samples. Raw Data processing were performed by using the freeware MacDiff (Petschick, 2001) which was designed for the analysis and display of X-ray powder diffractogrammes.

Major element concentrations of 39 bulk rock samples (24 serpentinites, 15 gabbroic rocks) were determined by X-ray fluorescence spectrometry (XRF) at the BGR in Hanover.

For preparation, samples were crushed and subsequently ground down to grain sizes <60 µm. One gram of sample powder is ignited for 15 minutes in a ceramic crucible at 1030°C in order to expel volatile phases. Reweighting of the samples yielded the loss on ignition (LOI). In general, the LOI primary comprises H_2O and CO_2. Subsequently, the sample material is mixed with a flux, depending on the measured LOI. Then the sample-flux mixtures were fused at 1200°C in Pt-crucibles. The resulting glass-chips are spectrometrically analyzed (XRF) with a Philips PW 1480 spectrometer equipped with a Cr X-ray tube and a Philips PW 2400 spectrometer with an Rh tube.

The major element compositions of clay minerals were analyzed in thin sections with a CamScan CS24 microprobe at the Institute for Geosciences, University of Kiel.

4. **Results**

Petrology and Mineralogy

Mineral assemblages were determined by X-ray diffraction (XRD) and petrographically by microscope analyses as well as by scanning electron microscope (SEM) investigations. The Logatchev hydrothermal field and Working Area 2 are characterized by serpentinites and gabbros of different compositions. An overview about mineral assemblages of samples from the Logatchev Hydrothermal field is given in Table 1.

Mainly harzburgites and dunites are the precursor rocks of the serpentinites. The degree of serpentinization varies from 80-90% in the harzburgites to nearly complete serpentinization (90-100%) of the dunites. In harzburgites relicts of partial serpentinized, coarse orthopyroxene can be found. Relicts of olivine are rare (Fig. 3.2a).

X-ray diffraction studies show that lizardite is the most dominate serpentine mineral, (Fig. 3.2a+b) often found together with magnetite. Lizardite is characterized by distinct reflections at 7.33 Å, 4.6 Å, and 3.6 Å, 2.50 Å, 2.15 Å, 1.79 Å (Fig. 3.3a). In contrast to lizardite, chrysotile exhibits distinct reflections at 7.33 Å, 4.61 Å, 3.6 Å, 2.66 Å, 2.45 Å, 1.83 Å and 1.74 Å. Chrysotile is a minor serpentine phase in some samples and occurs mainly in fractures and fissures (Fig. 3.2c+d). Mostly the serpentinized dunites (e.g., 49GTV-2) contain slightly higher amounts of chrysotile-asbestos in small mm-sized veins. Lizardite occurs mainly in three textural associations:

(1) mesh-textured lizardite (associated with magnetite) was commonly formed by replacing olivine along grain boundaries and microfractures (Wicks and Whittaker, 1977;

Wicks et al., 1977). In general, the whole groundmass of the serpentinites is composed by mesh-cell structured lizardite (Fig 3.2b).

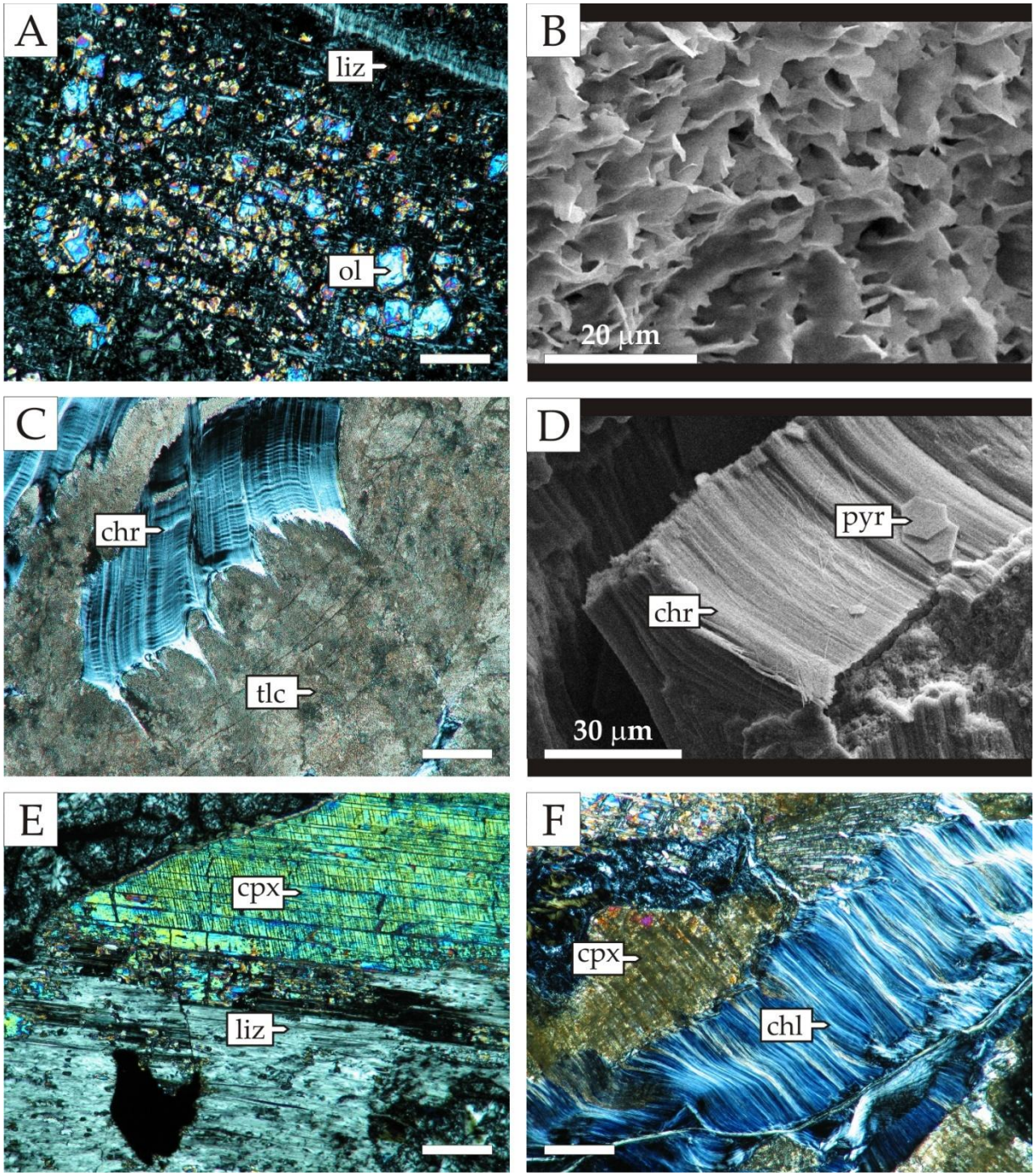

Fig. 3.2: Thin section photomicrographs and SEM pictures of samples from the Logatchev hydrothermal field: (A) Area of lizardite (liz) formed after olivine (ol; 49GTV-5A). (B) SEM picture of lizardite mesh cells (222GTV-2A). (C) Massive talc (tlc) formation after chrysotile (chr; 49GTV-1A3). (D) SEM picture of vein filling chrysotile (chr) with little sulfide crystals (covellite (cov); 62GTV-1B). (E) Bastite (lizardite (liz)) formation after clinopyroxenes (cpx) in a gabbro (78GTV-3A). (F) Chlorite (chl) formation after clinopyroxene (cpx; 78GTV-3A). Note figures A, C, E and F with crossed nikols; scale is 200µm if no other indication.

(2) serpentinization of orthopyroxenes (Fig. 3.2e) often forms pseudomorphs after pyroxene which are generally called bastites (Wicks and Whittaker, 1977). Serpentinization of pyroxenes begins at the grain boundaries and fractures, follows the cleavages and commonly forms lizardite-fibers parallel to the original pyroxene cleavage (Wicks and Whittaker, 1977).

(3) Lizardite-filled veins and fractures were observed in all serpentinite samples. These veins typically consist of fibrous or pillar-like to platy lizardite.

Talc is only significant in some samples (Fig. 3.2c) but more or less a minor phase in most of the studied serpentinites. Only two samples consist of nearly pure Talc (239GTV-4A and -4B). Talc could be identified by XRD from significant reflections at 9.34 Å, 4.66 Å, 4.55 Å and 3.116 Å (Fig. 3.3b). In thin sections talc mostly occur as very small grains with characteristic second order interference colors.

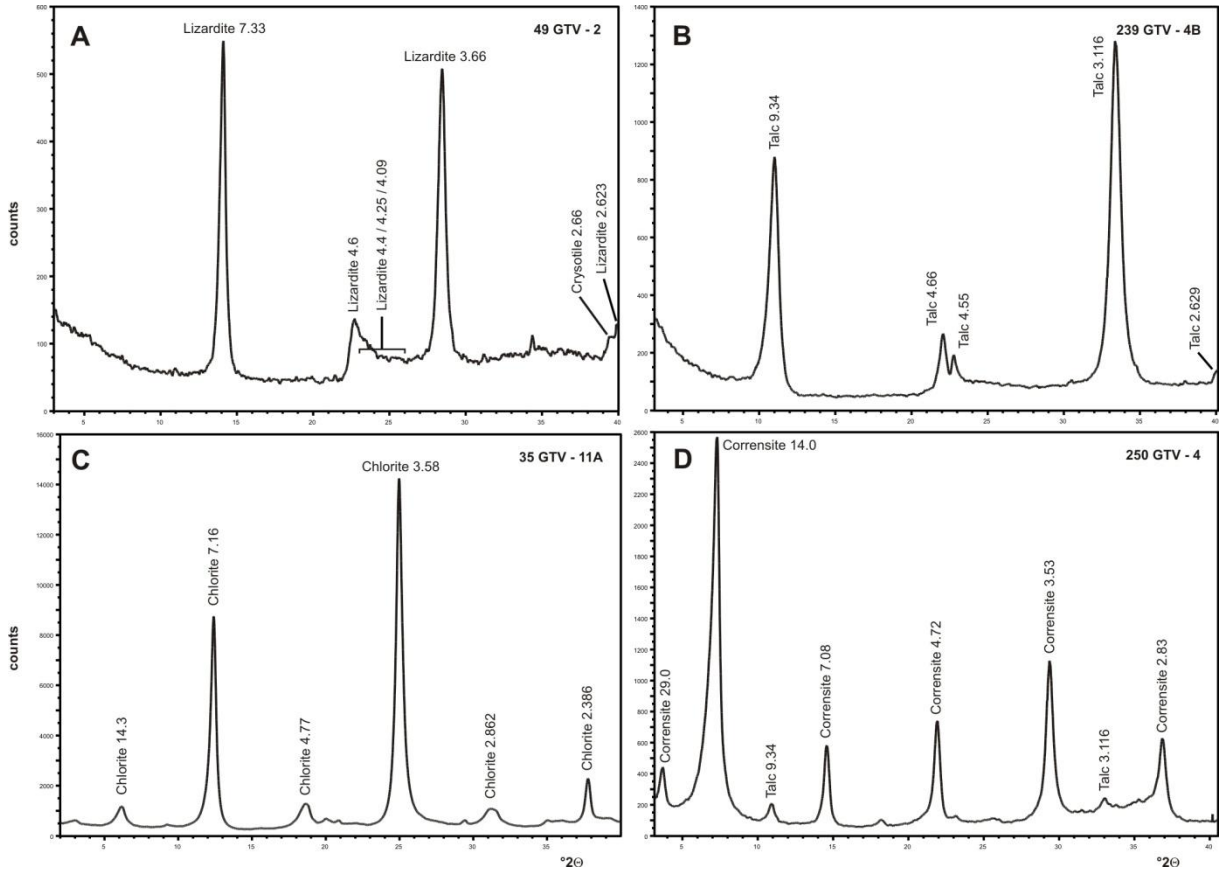

Fig. 3.3: Samples of nearly monomineralic X-ray diffraction patterns of dry, clay-sized fraction: (A) lizardite, (B) talc, (C) chlorite and (D) corrensite.

The coarse to medium-grained gabbronorites are mostly rather fresh and are little affected by hydrothermal and/or seawater alteration. Fresh gabbros show mostly coarse-grained

textures, with hypidiomorphic clinopyroxenes and xenomorph, granular plagioclase. XRD analyses of some more strongly altered gabbros from porous aquifers (250GTV) reveal nearly monomineralic chlorites in the clay-size fraction (<2◎ m). The chlorites were identified by XRD from clay-sized fraction by the (001) spacing at 14.3Å which remains unaffected by glycol saturation (Fig. 3.3c). The most common phases are clinochlore-type chlorites, which are often related to serpentine minerals and are typical for hydrothermal alteration of clinopyroxenes (Bideaux et al., 1995). Microscopically the chlorites showing bluish interference colors mostly occur on grain boundaries and alteration rims of clinopyroxenes (Fig. 3.2f). Some altered samples comprise corrensite, a regularly ordered mixed-layer mineral composed of 50% chlorite and 50% smectite (Bideaux et al., 1995; Meunier, 2005; Shau et al., 1990) often formed at high temperatures >200°C (Lackschewitz et al., 2000b). Corrensite produces characteristic reflexions at 29.0 Å, 14.0 Å, 7.08 Å, 4.72 Å as well as 3.53 Å and 2.83 Å (Fig. 3.3d).

In addition to the chlorite group minerals, we found lizardites in the gabbros (Fig. 3.2e). The lizardite shows a mesh cell texture that suggests the lizardite is formed mainly after olivine (Wicks and Whittaker, 1977) as well as bastite textures that suggest formation after clinopyroxenes (Wicks and Whittaker, 1977).

Chemical Composition

An overview to the chemical bulk composition of serpentinites and gabbros is given in Table 2.

The analytical totals of 24 XRF analyses of bulk serpentinites range from 98 to 101% with LOIs from 11.5 to 15.5 wt%. SiO_2 as well as MgO represent the dominant major element oxides in serpentinites. The SiO_2 values of the serpentinites range between 36.4 and 41.8 wt% with an average value of 39.4 wt%. The SiO_2/MgO ratio of about 1.05 due to MgO concentrations of 32.2 – 39.1 wt% (37.1 wt% in average) is typically for serpentinites. The concentrations of Fe_2O_3 vary between 6.2 and 11.5 wt% (7.5 wt% average). Other major element oxides e.g., TiO_2, Al_2O_3, MnO, CaO as well as Na_2O and K_2O are less important and generally exhibit very low concentrations below 1-2 wt%.

We have analyzed 12 less altered gabbro samples as well as 1 moderately altered gabbro samples. The analytical totals of all analyzed gabbros are >99% in average. Less altered gabbros reveal SiO_2 concentrations of 39.5 – 57.9 wt% (50.4 wt% average). The Mg concentration show an average of about 10.0 wt% (8.6-29.2 wt%). Fe_2O_3 and Al_2O_3 reveal average concentrations of 7.7wt% and 15wt% respectively. However, two samples (73GTV-1B2, 74GTV-2D) show unusually low Al_2O_3 concentrations of 0.19 and 1.13wt% (Tab. 1). The total alkali value (Na_2O + K_2O) vary from 0.14 to 3.2wt%. TiO_2 and MnO show only minor concentrations in all analyzed gabbros below 1.0wt%. The major element concentration of single minerals was determined by microprobe analyses on three serpentinites, one less

altered gabbro and one strongly altered reddish serpentinite which are representative for the characteristic lithologies of the Logatchev hydrothermal field as well as Working Area 2.

The mean concentration values as well as calculated structural formulas of 24 plagioclase, 43 olivine as well as 88 pyroxene analyses are shown in Table 3. The calculated structural formula of plagioclase reveals an anorthite component of 0.68 (albite 0.31) and lead to an labradorite-type plagioclase (Spear, 1995). The total of tetrahedral cations is 4.0 with proportions of 2.3 for Si and 1.67 for Al^{IV}. The calculated total of octahedral cations in olivine is 2.0 containing 1.8 Mg and 0.18 Fe (Tab. 3). This suggests a forsterite component of 90% which is typical for rock forming olivine (Matthes, 1996).

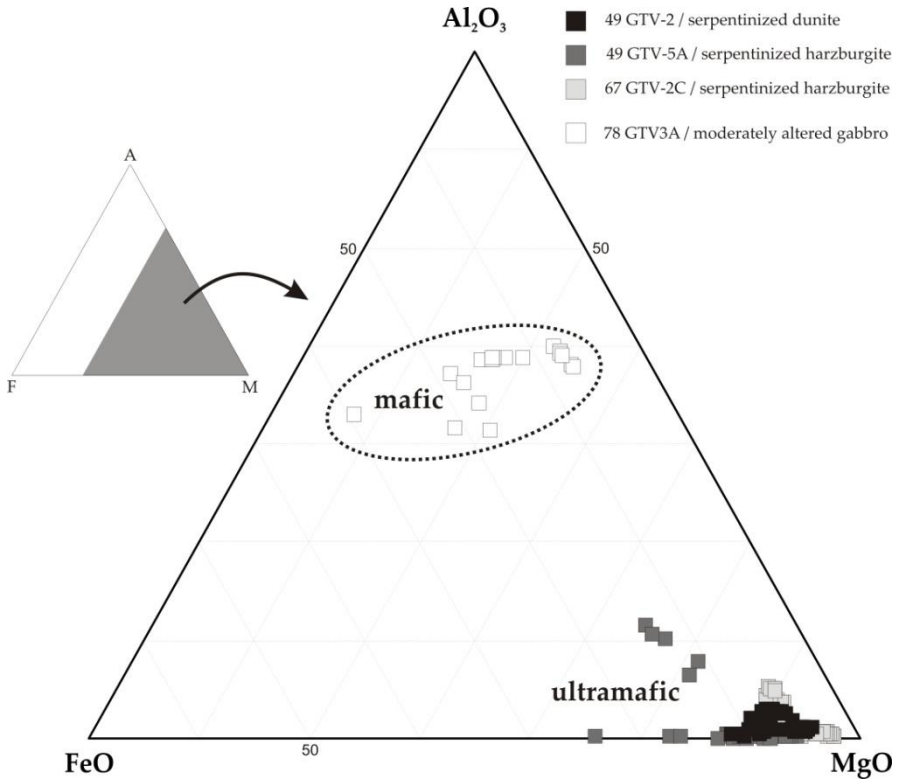

Fig. 3.4: AFM-Diagram of lizardites in serpentinized peridotites as well as in altered gabbro. The enrichment of Al2O3 in lizardites of mafic origin is readily apparent.

The structural formulae of pyroxenes from gabbro as well as serpentinites reveal a total of octahedral cations of 1.9 and 2.3, respectively. The total of tetrahedral cations is 1.81 for relict pyroxene in serpentinite and 2.1 for pyroxene in gabbro. The structural formula of pyroxene from serpentine reveals a total Mg of 2.0 and Fe of 0.19 which indicates a near enstatite end member of the enstatite-ferrosilite series (Matthes, 1996; Spear, 1995). Gabbroic pyroxenes have 0.87 Mg, 0.74 Ca as well as 0.26 Fe, which suggests an augite with strong affinity to diopside (Matthes, 1996).

A summary of microprobe analyses and calculated structural formulas of phyllosilicates as lizardite and chlorite is given in Table 3. The totals of lizardite analyses range between

78.0 and 86.6%. These relatively low totals are most likely caused by an essential loss of H_2O during the measurements.

Lizardites were analyzed in serpentinites as well as in altered gabbros. Lizardites that were formed as secondary phase after clinopyroxenes in gabbroic rocks show a clear difference in their Al_2O_3-FeO concentration and a bigger amesite component than lizardites from ultramafics (Fig. 3.4). Structural formulas of ultramafic lizardites give a total of 2.0 of tetrahedral cations, which is completely containing Si. Octahedral cations reveal a mean total of 2.9 with 2.8 Mg and 0.13 Fe. Therefore, the structural formulae of ultramafic lizardites indicate that Mg-lizardites with a cation-total of 5.0 and the empirical formula $Si_2Mg_3O_5(OH)_4$ replace olivine as well as orthopyroxene in ultramafic rocks (Anthony et al., 1995).

Lizardites in gabbros show a mean cation-total of 4.9, which is close to the ultramafic lizardites. Less altered gabbros reveal lizardites with Si and Al as tetrahedral cations (1.49 and 1.16 respectively) indicating a significant deviation from the Mg end-member composition towards amesite ($Mg_4(Si,Al)_3O_5(OH)_4$; O´Hanley (1996)). In addition, gabbroic lizardites show a higher Fe content in the octahedral cations (~0.3) and significantly lower Mg of 1.9.

The chlorites from the less altered gabbros (78GTV-3A) are characterized by a SiO2 concentration of 33.3 wt% and an MgO concentration of 29.3 wt%. The concentration of Al_2O_3 and Fe_2O_3 is about 15.5wt% and 7.5wt% respectively. Based on the high MgO and Al_2O_3 values these chlorites are classified as aluminan to ferroan chlinochlores (Deer et al., 1992; Newman, 1987). The number of cations in the octahedral site of the chlorites is 11.8 which is typical for trioctahedral chlorites (Newman, 1987).

5. **Discussion**

Compositional effects of alteration

The Logatchev hydrothermal field (LHF) and the surrounding area are characterized by many different physico-chemical conditions leading to different alteration styles with distinctive behaviors of elements. Based on the mineralogy the LHF is characterized by three main alteration types:

Serpentinization under seawater conditions is the most dominant alteration-type occurring to the ultramafic host-rocks at the Logatchev field and Working Area 2 (Augustin et al., submitt.; Bach et al., 2004; Kuhn et al., 2004b; Paulick et al., 2006). Serpentinization is characterized by the formation of serpentine minerals and magnetite from olivine and orthopyroxene (Fig. 3.2a+b). Undiluted high-temperature hydrothermal alteration only occurs very close to the active vent sites and fluid pathways. Due to a mixing of seawater and hydrothermal fluid a combination of both hydrothermal and seawater-alteration at elevated temperatures takes place in closer areas to active vents. Therefore, gabbroic samples

show chlorite and serpentine formation after clinopyroxene. Serpentinites can reveal the formation of chrysotile after lizardite and additionally the formation of talc (Fig. 3.2c-f). Alteration at low-temperature seawater conditions is ubiquitous in the LHF. The seafloor-weathering reveals no significant changes in the mineralogy of the sampled rocks, excepting some samples that show hematite formation after magnetite and the oxidation of sulphides (e.g., formation of goethite; Tab. 3.1). In addition, melt/rock interaction occurs often in serpentinites of the LHF and the area around 15°N. This is supported by gabbroic intrusions which represent more than 20% of the host rocks (Bach et al., 2004; Kuhn et al., 2004a).

To calculate alteration-related chemical mass changes, we compared major and trace element concentrations of mafic and ultramafic rocks from the LHF with fresh peridotites and gabbros. For the calculation of gains and losses of major element composition in serpentinites we used reconstructed precursor major element concentrations from Paulick et al. (2006). For calculations of trace element variations in serpentinites we used the analyzed trace element data of Augustin et al. (submitt.) and compared them to the concentrations in least altered harzburgites from Leg 209 (Paulick et al., 2006). To calculate major element fluxes in moderately altered gabbros we used comparative data of calculated protolith from Talbi et al. (1999) as well as trace element data from mostly fresh gabbros from Augustin et al. (submitt.). The element concentrations of fresh rocks and calculated precursors are listed in Table 3.4. The calculation of chemical changes is based on the method of Gresens (1967), which has been modified by Grant (1986):

$$C_i^A = [M^0/M^A][C_i^0 + \Delta C_i]$$

in which C_i^A = concentration of component *i* in the altered rock; M^0 = mass of the fresh, unaltered rock; M^A = mass of the altered rock; C_i^0 = concentration of component *i* in the precursor rock and ΔC_i = change in concentration of component *i*. To calculate the mass change term (M^0/M^A) for serpentinization processes we used experimental data from Shervais et al. (2005) which reported an overall mass gain of ~25 g/100 g, comparable with the reported mass addition from Paulick et al. (2006) of 20-30 g/100 g. For one moderately altered gabbro sample we calculated elemental gains and losses with a mass change of 2g/100 g (Talbi et al., 1999). The comparison of the magnitudes of major element oxide and trace element fluxes for the serpentinization/alteration processes at the LHF as well as in Working Area 2 allows us to infer relative elemental gains and losses (Tab. 3.4).

Paulick et al. (2006) reported that rock-dominated serpentinization reveal only little geochemical deviations from the precursor except the addition of H_2O. In contrast, fluid dominated serpentinization often shows talc alteration of serpentinites due to the circulation of silica-rich fluids an addition of SiO_2 to the serpentinites (Bach et al., 2004; Paulick et al., 2006). Serpentinization at the LHF results in only a small gain of FeO and MgO (Fig. 3.5a). The concentration of FeO could be elevated due to the incorporation of FeO into lizardite and magnetite from a fluid during the serpentinization. A gain of MgO during hydrothermal

alteration of peridotites can be excluded because of the absence of MgO in hydrothermal fluids (Douville et al., 2002; Schmidt et al., 2007). However, a high portion of seawater in the hydrothermal fluids can provide an increase in MgO. The small increase of SiO_2 could be related to an absorption of SiO_2 from the fluid and the formation of talc (Bach et al., 2004; Paulick et al., 2006).

The concentration of Al is not significantly changed (enrichment factor (EF) <0.5). The very little uptake in Al_2O_3 possibly depends on a little higher Al concentration in spinell or orthopyroxenes of the Logatchev serpentinites than in the calculated precursors (Anthony et al., 1995; Paulick et al., 2006). The loss of Ti from gabbroic intrusions during hydrothermal alteration and absorption of TiO_2 to lizardite and magnetite during serpentinization can explain the increase of the concentration of TiO_2 in serpentinite samples from Working Area 2 (Fig. 3.5a). In serpentinites from the Logatchev field Ti is significantly decreased. Talbi et al. (1999) reported that Ti is released from gabbros to the fluid during hydrothermal alteration. Possibly hydrothermal alteration also leads to the depletion of TiO_2 in serpentinites from the Logatchev field. CaO shows significant losses in the serpentinites because of the release of CaO into the circulating fluid (Hart et al., 1974; Talbi et al., 1999). This enables late stage carbonate veining, which has been already reported from the 15°N area (Bach et al., 2004; Kuhn et al., 2004a). Due to the very low concentrations of Na_2O in fresh peridotites (0.01 wt%; Paulick et al., 2006) the very high gain of Na_2O (EF>1000) is most

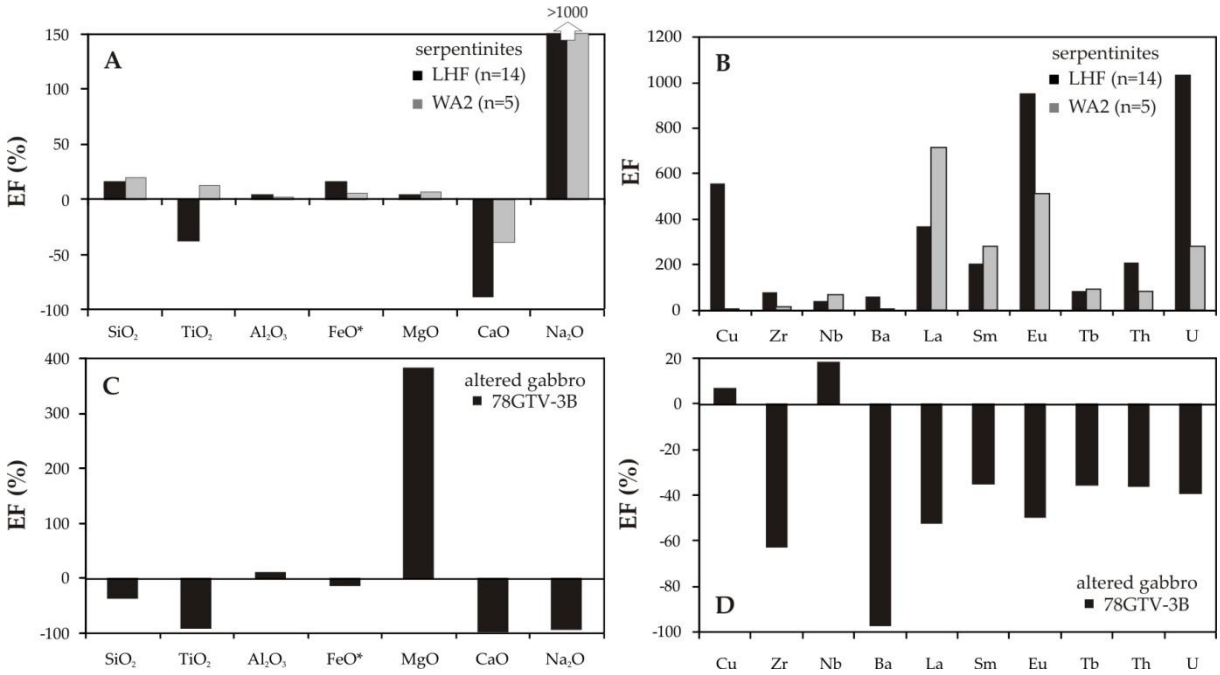

Fig. 3.5: Illustrated gains and losses of selected major and trace elements of (A+B) serpentinized peridotites from the Logatchev hydrothermal field and Working Area 2 and (B+C) one altered gabbro sample from the Logatchev field. The gains and losses are given as enrichment factors (EF) in percentage of the precursor value (A, C, D) or as pure enrichment factors (EF) to the precursor value (B).

likely related to seawater-alteration because high-temperature hydrothermal alteration of the rocks should result in a loss of Na_2O. The concentration of Na_2O in serpentinites from ODP Leg 209 is comparable to the concentration in serpentinites from Logatchev and Working Area 2 (Paulick et al., 2006).

For trace element in serpentinites, we calculated gains and losses of Cu, Zr, Nb, Ba, Tb, Th and U as well as the REE La, Sm and Eu because these elements are representative tracers for the described different alteration styles above (Fig. 3.5b, c).

Bogdanov et al., (1997) and Kuhn et al., (2004b) have shown that Cu-sulfides represents one of the most abundant sulphides in the Logatchev field. While Cu is relatively low in samples from Working Area 2, Cu is highly increased in serpentinite samples from the LHF (Fig. 3.5b) which is most probably related to finely dispersed Cu-sulfides in the area of the active Logatchev field (Augustin et al., submitt.).

During melt-rock interaction relatively immobile, incompatible elements Zr, Nb and Tb as well as the LREE become mobile in about equal proportions (Augustin et al., submitt.; Niu, 2004; Paulick et al., 2006). All analyzed samples from Logatchev and Working Area 2 are enriched in Zr, Nb and Tb (Fig. 3.5b). This suggests that melt-rock interaction plays an important role to the serpentinites at Logatchev as well as Working Area 2.

The elemental gain of Ba is significantly lower at Working Area 2 (EF~3) than in the Logatchev field (EF~60). Possibly the distinctly high concentrations of Ba in the hydrothermal fluids (Douville et al., 2002) lead to a more significant enrichment of Ba in the LHF serpentinites during hydrothermal alteration. In addition, the increase of Ba is also reported by Hart et al. (1974) from low-temperature sea-floor altered basalts. Possibly, the combination of both hydrothermal and seawater alteration, lead to the significantly increased Ba concentration at the LHF.

The distinct increase of U in all serpentinite samples (Fig. 3.5b) most likely is connected to low-temperature alteration. Increased U concentrations are also reported from oxidatively-altered rocks of ODP Leg 504B (Bach et al., 2003) and seawater-altered basalts (Verma, 1992). In addition, Valsami-Jones and Ragnarsdóttir (1997) reported from hydrothermally altered basaltic rocks that U as well as Th reveal a significantly higher mobility during high-temperature hydrothermal alteration. Therefore, we suggest that the very strong gain of U and the significantly increased Th concentration in serpentinites from the LHF is caused by hydrothermal alteration.

Figure 3.5b shows that serpentinites from the LHF reveal significant higher enrichment factors for Eu than serpentinites from Working Area 2 (49GTV). La and Sm also reveal high enrichment factors. La reveals a stronger gain in Working Area 2 than in the LHF. Augustin et al. (submitt.) reported that vent-type fluids which are enriched in light rare earth elements (LREE) as well as interaction with mafic melts can explain the enrichment of LREE in the host rocks of the LHF. This is supported by works of Niu, (2004) and Paulick, (2006). The strength of Eu-anomalies plays an important role in determining the strength of the hydrothermal component (Augustin et al., submitt.). We suggest that the strong increase of Eu in samples from the LHF reflects alteration under hydrothermal conditions.

The increase of La, Sm and Eu in samples from Working Area 2 is most probably related to melt/rock interaction because in contrast the LHF serpentinites are additionally strong enriched in Cu, Ba, Eu, Th, and U. These elements are most likely good indicators for hydrothermal alteration. The relatively low gain of these elements in samples from Working Area 2 compared to the LHF suggests that hydrothermal activity at Working Area 2 is much lower. Therefore, the enrichment of U, LREE as well as Zr and Nb in samples from Working Area 2 reflects melt-rock interaction and low-temperature seafloor alteration.

Figure 3.5c illustrates the extreme loss of TiO_2, CaO and Na_2O in an altered gabbro (78GTV-3B), whereas the concentration of MgO increases to more than 350% (Tab. 3.4). The high loss of SiO_2, TiO_2, CaO and Na_2O is most likely related to hydrothermal alteration by circulating fluid and the breakdown of Ti-oxides as well as clinopyroxenes and plagioclase. The low gains and losses of Al_2O_3 and FeO indicate a relative immobility of these elements during alteration. The formation of Mg-rich clay minerals after clinopyroxenes can explain the strong uptake of MgO in the altered gabbro. The Mg-concentration in the clinopyroxene (15.8 wt %) is much too low to form chlorites and lizardites with Mg-concentrations of >29.0 wt% (Tab. 3.3). Therefore, the Mg must have been supplied by Mg-rich fluids, e.g. seawater or seawater-mixed hydrothermal fluids.

To calculate relative elemental variations for trace elements in one altered gabbro sample (78GTV-3B) we used the average gabbro composition from relatively fresh gabbros from the LHF(Augustin et al., submitt.). The calculated losses of all selected trace elements except Cu and Nb suggest that gabbroic intrusions are a major source for trace elements in the geochemical system (Fig. 3.5d) at the Logatchev field. Cu reveals a little gain in the altered, which again indicates the presence of finely dispersed Cu-sulphides as described for the serpentinite samples from the LHF. The general loss of Zr and Tb could be related to melt/rock interaction processes and the associated higher mobility of these elements (Niu, 2004), which leads to an enrichment of these elements in the ultramafic rocks. However, the increase of Nb in the gabbro sample also could be related to melt/rock interaction processes (Niu, 2004). Ba and the LREE are enriched fluids from the Logatchev field (Douville et al., 2002; Schmidt et al., 2007). The loss of Ba and the REE from the gabbro suggests that fluid/rock interactions under hydrothermal conditions lead to a release of these elements to the fluid. In addition, the loss of U is most likely an exchange of U with seawater during low-temperature seafloor alteration (Macdougall et al., 1979; Verma, 1992). However, the loss of U together with Th could also be related to hydrothermal alteration and a resulting higher mobility of Th and U at high temperatures (Valsami-Jones and Ragnarsdóttir, 1997).

6. **Conclusions**

The mineralogical and geochemical investigations of mafic and ultramafic samples to differentiate the alteration styles and associated element fluxes that have affected the sampled rocks lead to the following conclusions:

- The serpentinization of ultramafic rocks in the area of the Logatchev hydrothermal field was isochemical concerning the major elements, excepting TiO_2 and CaO. Due to the formation of lizardite and magnetite, the concentration of TiO_2 increases significantly in samples from Working Area 2. A loss of CaO is common for all ultramafic as well as mafic samples from this area and most likely related to the release of CaO to the circulating fluids during both hydrothermal and low-temperature seafloor alteration.
- The physicochemical environment mainly controls the increase of trace elements in ultramafic rocks. Strong hydrothermal input leads to a significant enrichment of Ba, LREE, and Eu. In addition, the Th, U mobility increases distinctly during high-temperature hydrothermal alteration.
- Hydrothermal alteration of mafic intrusions play a major role in providing SiO_2, TiO_2, Na_2O as well as numerous trace elements to the circulating fluids. MgO is the only element oxide that shows distinct increases in gabbroic rocks, which is related to the formation of Mg-rich silicates like chlorites and lizardites from clinopyroxenes. In addition, the massive loss of major and trace elements from gabbroic rocks compared with the local fluid chemistry indicates that gabbroic intrusions represent potentially heat sources to drive the hydrothermal system at Logatchev.
- Effects of strong hydrothermal alteration at high or elevated temperatures are only observed in samples from the LHF. Therefore, hydrothermal influence is strongly limited to small areas around the vent sites and the hydrothermal pathways and aquifers.
- Significant indications for recent or previous hydrothermal activities were not observed in major and trace element chemistry of sampled rocks from Working Area 2. We suggest that serpentinization, melt/rock interaction and low-temperature seafloor weathering caused the elemental variations in the samples. Therefore, hydrothermal activity at Working Area 2 is very low or inexistent.

7. **Acknowledgements**

This work was supported by grants from the Special Priority Program 1144 (SPP 1144) of the German Science Foundation (DFG). We thank all members of the shipboard parties during the cruises M60/3 and M64/2 as well as the R/V Meteor captain and crew. The authors gratefully acknowledge Petra Fiedler (Kiel University) and Jutta Heinze (IFM-GEOMAR) for technical assistance with XRD analyses; Peter Appelt and Barbara Mader (Kiel University) for help with microprobe analyses; Edgars Rudzitis for his help with sample preparation; and Sven Petersen for always helpful discussions.

8. References:

Anthony, J.W., Bideaux, R.A., Bladh, K.W. and Nichols, M.C., 1995. Handbook of Mineralogy - Volume II - Silicates. Mineral Data Publishing.

Atterberg, A., 1912. Die mechanische Bodenanalyse und die Klassifikation der Mineralböden Mittelschwedens. Intern. Mitt. f. Bodenkunde: 312-342.

Augustin, N. et al., submitt. Alteration Processes at the Ultramafic-Hosted Logatchev Hydrothermal Field, MAR 14°45´ N: Trace Elements and Isotope Signatures as Tracers for Water/Rock and Melt/Rock interaction. Submitted to Chemical Geology.

Bach, W., Garrido, C.J., Paulick, H., Harvey, J. and Rosner, M., 2004. Seawater-peridotite interactions: First insights from ODP Leg 209, MAR 15. Goechemistry Geophysics Geosystems, 5(No. 9): 1-22.

Bach, W., Peucker-Ehrenbrink, B., Hart, S.R. and Blusztajn, J.S., 2003. Geochemistry of hydrothermally altered oceanic crust: DSDP/ODP Hole 504B - Implications for seawater-crust exchange budgets and Sr- and Pb-isotopic evolution of the mantle. Geochemistry Geophysics Geosystems, 4(3): 29.

Batuyev, B.N. et al., 1994. Massive sulfide deposits discovered at 14°45´N Mid-Atlantic Ridge. Bridge Newsletter, 6: 6-10.

Bideaux, R.A., Bladh, K.W. and Nichols, M.C., 1995. Silica, silicates. Handbook of Mineralogy, 2. Mineral Data Publishing, Tucson, AZ, United States, 904 pp.

Bogdanov, Y.A., Bortnikov, N.S., Vikent´ev, I.V., Gurvich, E.G. and Sagalevich, A.M., 1997. A New Type of Modern Mineral-forming System: Black Smokers of the Hydrothermal Field at 14°45´N Latitude, Mid-Atlantic Ridge. Geology of Ore Deposits, 39(1): 58-78.

Cherkashev, G.A., Ashadze, A.M. and Gebruk, A.V., 2000. New Fields with manifestations of hydrothermal activity in the Logatchev area (14°N, Mid-Atlantic Ridge). InterRidge News, 9(2): 26-27.

Deer, W.A., Howie, R.A. and Zussman, J., 1992. An Introduction to the Rock-Forming Minerals (2nd Edition). Longman, Essex, 712 pp.

Douville, E. et al., 2002. The rainbow vent fluids (36°14´N, MAR): the influence of ultramafic rocks and phase separation on trace metal content in Mid-Atlantic Ridge hydrothermal fluids. Chemical Geology, 184: 37-48.

Grant, J.A., 1986. The isocon diagram - A simple solution to Gresen´s equation of metasomatic alteration. Economic Geology, 81: 1976-1982.

Gresens, R.L., 1967. Composition-volume relationships of metasomatism. Chemical Geology, 2: 47-65.

Hart, R.A., Erlank, A.J. and Kable, E.J.D., 1974. Sea floor basalt alteration: some chemical and Sr isotopic effects. Contributions to Mineralogy and Petrology, 44(219-230).

Jochum, K.P. and Verma, S.P., 1996. Extreme enrichment of Sb, Tl and other trace elemnts in altered MORB. Chemical Geology, 130: 289-299.

Krasnov, S.G. et al., 1995. Detailed geological studies of hydrothermal fields in the north atlantic. Geological Society Special Publication, 87: 43-64.

Kuhn, T. et al., 2004a. Mineralogical, geochemical, and biological investigations of hydrothermal systems on the Mid-Atlantic Ridge between 14°45'N and 15°05'N (HYDROMAR I). Meteor Berichte 03-04: 1-61.

Kuhn, T. et al., 2004b. The Logatchev hydrothermal field - revisited: preliminary results of the R/V METEOR Cruise HYDROMAR I (M60/3). Inter Ridge News, 13: 1-4.

Lackschewitz, K.S. et al., in press. Longterm study of hydrothermalism and biology at the Logatchev field, Mid-Atlantic Ridge at 14°45'N (revisit 2005) (HYDROMAR II), Meteor Berichte 05.

Lackschewitz, K.S. et al., 2000a. Formation and Transformation of Clay Minerals in the Hydrothermal Deposits of Middle Valley, Juan de Fuca Ridge, ODP Leg 169. Economic Geology, 95: 361-390.

Lackschewitz, K.S., Singer, A., Botz, R., Garbe-Schönberg, D. and Stoffers, P., 2000b. Mineralogy and Geochimistry of Clay Minerals Near a Hydrothermal Site in the Escanaba Trough, Gorda Ridge, Northeast Pacific Ocean. Proceedings of the Ocean Drilling Program, Scientific Results, 169.

Macdougall, J.D., Finkel, R.C., Carlson, J. and Krishnaswami, S., 1979. Isotopic evidence for uranium exchange during low-temperature alteration of oceanic basalt. Earth and Planetary Science Letters, 42: 27-34.

Matthes, S., 1996. Mineralogie. Springer, Berlin-Heidelberg, 499 pp.

Meunier, A., 2005. Clays. Springer, Berlin-Heidelberg, 472 pp.

Moore, D.M. and Reynolds, R.C., 1989. X-ray Diffraction and the Identification and Analysis of Clay Minerals. Oxford University Press.

Newman, A.C.D., 1987. Chemistry of Clays and Clay Minerals. Mineralogical Society Monograph, No 6. John Wiley & Sons Inc, 480 pp.

Niu, Y., 2004. Bulk-rock Major and Trace Element Compositions of Abyssal Peridotites: Implications for Mantle Melting, Melt Extraction and Post-melting Processes Beneath Mid-Ocean Ridges. Journal of Petrology, 45(12): 2423–2458.

O´Hanley, D.S., 1996. Serpentinites - Records of Tectonic and Petrological History. Oxford University Press, New York, Oxford, 277 pp.

Paulick, H. et al., 2006. Geochemistry of abyssal peridotites (Mid-Atlantic Ridge, 15°20´N, ODP Leg 209): Implications for fluid/rock interaction in slow spreading environments. Chemical Geology, 234: 179-210.

Petschick, R., 2001. MacDiff 4, Frankfurt (Main), pp. Mac Diff is a programme for analysis and display of X-ray powder diffractogrammes on Apple Macintosh platforms.

Schmidt, K., Koschinsky, A., Garbe-Schönberg, D., De Carvalho, L.M. and Seifert, R., 2007. Geochemistry of hydrothermal fluids from the ultramafic-hosted Logatchev hydrothermal field, 15°N on the Mid-Atlantic Ridge: temporal and spartial investigation. Chemical Geology, 242: 1-21.

Shau, Y.-H., Peacor, D.R. and Essene, E.J., 1990. Corrensite and mixed-layer chlorite/corrensite in metabasalt from northern Taiwan: TEM/AEM, EMPA, XRD, and optical studies. Contributions to Mineralogy and Petrology, 105: 123-142.

Shervais, J.W., Kolesar, P. and Andreasen, K., 2005. A Field and Chemical Study of Serpentinization - Stonyford, California: Chemical Flux and Mass Balance. International Geology Review, 47: 1-23.

Spear, F.S., 1995. Metamorphic Phase Equilibria and Pressure-Temperature-Time Paths. Mineralogical Society of America, Washington, D.C., 799 pp.

Talbi, E.H., Honnorez, J., Clauer, N., Gauthier-Lafaye, F. and Stille, P., 1999. Petrology, isotope geochemistry and chemical budgets of oceanic gabbro-seawater interactions in the Equatorial Atlantic. Contributions to Mineralogy and Petrology, 137: 246-266.

Valsami-Jones, E. and Ragnarsdóttir, K.V., 1997. Controls on uranium and thorium behavior in ocean floor hydrothermal systems: examples from the Pindos ophiolite, Greece. Chemical Geology, 135: 263-274.

Verma, S.P., 1992. Seawater alteration effects on REE, K, Rb, Cs, Sr, U, Th, Pb and Sr-Nd-Pb isotope systematics of Mid-Ocean Ridge Basalt. Geochemical Journal, 26: 159-177.

Wicks, F.J. and Whittaker, E.J.W., 1977. Serpentine Textures and Serpentinization. The Canadian Mineralogist, 15: 459-488.

Wicks, F.J., Whittaker, E.J.W. and Zussman, J., 1977. An idealized model for serpentine textures after olivine. Canadian Mineralogist, 15: 446-458.

9. **Tables**

Tab. 3.1: Mineralogical assemblages of representative samples of the Logatchev hydrothermal field and Working Area 2 as determined by X-ray diffraction analyses (clay size fraction and bulk rock are combined for this overview).

	plg	px	hbl	qz	liz	chr	mgt	tlc	hem	goe	chl	cor	sm	ill	crm	cpy	py	anh	gyp	bar	cc
32 GTV-3f					+++	++	+														
33 GTV-5	+++	++						+			+		+								
33 GTV-9	+++	++						o			+		+								
33 GTV-10	+++	+						+													
33 GTV-11					+++	++	+														
33 GTV-17 A	+++												+								
35 GTV-1f	+	+									+						++			+++	
35 GTV-4a						o					++					+++	o				
35 GTV-4b																		+++	++		
35 GTV-9					+++	++	+														
35 GTV-11A											+++					++					
49 GTV-2					+++	+	++														
49 GTV-3B					+++	+	++														
49 GTV-3E					+++	++	++														
49 GTV-4A	+++		+++								+										
49 GTV-5A					+++	++	+	++			+										
49 GTV-5C					+++		++														
49 GTV-5L					+++		+	+			o										
49 GTV-6B					+++	+	++														
54 GTV-5b-2					+++	++	+	++	+												
54 GTV-5c-3					+++	++		+	++								+				
57 GTV-1a-1					+++	+	++														
62 GTV-1b					+++	++	+						o				+				
62 GTV-8b				+	o	+							+								+++
67 GTV-2a		+			+++	++	+										o				
67 GTV-2b		+			+++	++	+														
67 GTV-2c					+++	++	+										o				
67 GTV-2e					+++	+	++														
74 GTV-2c					+++	++	+														
74 GTV-2d					+++	++		++													
74 GTV-4				+++									++								
78 GTV-2b					+++	++	+														
82 GTV-3											+++										
82 GTV-4d				+++						++	+			+							
239 GTV-4a								+++													
239 GTV-4b								+++													
239 GTV-4c								+++			+++	o									
250 GTV-1a									+++		+				++						
250 GTV-4	++										+++	+									
250 GTV-7								+			+++	+									

Abbreviations: plg - plagioclase; px - pyroxene; hbl - hornblende; qz - quarz; liz - lizardite; chr - chrysotile; mgt - magnetite; tlc - t
hem - hematite; goe - goethite; chl - chlorite; cor - corrensite; sm - smectite; ill - illite; crm - chromite, cpy - chalcopyrite; py - py
anh - anhydrite, gyp - gypsum; bar - barite, cc - calcite, agt - aragonite

Symbols: (+++) - abundand; (++) - common; (+) - minor; (o) - traces

Tab. 3.2: X-Ray fluorescence analyses of major element concentrations of serpentinites and gabbros from the Logatchev Hydrothermal field as well as Working Area 2 (values in wt%).

	Sample ID	SiO_2	TiO_2	Al_2O_3	Fe_2O_3	MnO	MgO	CaO	Na_2O	K_2O	P_2O_5	*LOI*	*Total*	*FeO calc.*
serpentinites	**33 GTV-11**	38.5	0.02	1.55	11.5	0.14	32.2	0.16	0.6	0.1	0.01	*13.2*	*98.0*	*10.3*
	35 GTV-5	39.7	0.02	1.0	9.2	0.09	37.4	0.05	0.2	0.02	0.02	*13.1*	*101*	*8.3*
	35 GTV-9	39.4	0.08	1.48	8.6	0.12	37.1	0.06	0.04	0.02	0.02	*13.5*	*100*	*7.7*
	49 GTV-1A3	40.2	0.02	1.48	6.2	0.22	35.9	0.98	0.1	0.1	0.02	*13.8*	*99.1*	*5.6*
	49 GTV-2	38.7	0.007	0.61	6.8	0.10	38.3	0.76	0.1	0.02	0.01	*13.6*	*99.2*	*6.2*
	49 GTV-3A	39.5	0.02	0.69	7.3	0.07	38.8	0.24	0.02	0.01	0.02	*13.6*	*100*	*6.6*
	49 GTV-3E	40.5	0.007	0.59	6.5	0.09	37.9	0.21	0.1	0.03	0.02	*13.3*	*99.3*	*5.8*
	49 GTV-5A	41.8	0.03	1.05	8.3	0.15	35.6	0.38	0.1	0.03	0.01	*11.5*	*99.1*	*7.5*
	49 GTV-5C	38.8	0.02	0.89	7.4	0.09	38.4	0.27	0.03	0.02	0.02	*13.2*	*99.3*	*6.7*
	49 GTV-6A	41.3	0.02	0.62	7.0	0.06	38.0	0.69	0.2	0.03	0.01	*12.6*	*100*	*6.3*
	57 GTV-1A1	39.4	0.02	0.94	7.3	0.21	38.9	0.11	-	0.01	0.03	*13.5*	*100*	*6.6*
	57 GTV-2	36.9	0.05	1.95	10.9	0.11	37.7	0.07	0.01	0.01	0.03	*12.3*	*100*	*9.8*
	62 GTV-1A	40.3	0.01	0.7	8.8	0.11	37.1	0.05	0.1	0.01	0.01	*13.0*	*100*	*7.9*
	62 GTV-1B	39.1	0.004	0.68	8.8	0.11	36.0	0.03	0.2	0.02	0.01	*13.8*	*99.3*	*7.9*
	62 GTV-3A	39.7	0.01	0.29	8.6	0.10	37.0	0.05	0.2	0.01	-	*14.5*	*100*	*7.7*
	62 GTV-3B	39.9	0.04	1.95	7.6	0.13	35.7	0.05	0.1	0.02	0.01	*13.2*	*99.2*	*6.9*
	67 GTV-2A	37.8	0.005	0.39	7.5	0.06	37.6	1.85	0.1	0.03	0.02	*14.0*	*99.4*	*6.8*
	67 GTV-2B	37.6	0.01	0.39	7.0	0.08	37.8	2.74	0.1	-	0.02	*15.2*	*101*	*6.3*
	67 GTV-2C	37.6	0.005	0.64	6.8	0.08	37.3	2.07	0.1	0.03	0.02	*14.6*	*99.3*	*6.1*
	67 GTV-2E	36.4	0.009	0.44	6.8	0.10	35.9	3.71	0.1	0.04	0.04	*15.5*	*99.3*	*6.1*
	67 GTV-3A1	37.5	0.04	0.79	8.5	0.17	37.2	2.15	0.01	0.01	0.03	*14.2*	*101*	*7.6*
	73 ROV-1B1	40.9	0.01	0.8	7.0	0.09	36.7	0.06	0.1	0.1	0.02	*13.1*	*99.1*	*6.3*
	77 GTV-1	40.4	0.01	0.64	6.9	0.08	38.8	0.07	0.1	0.01	0.02	*13.1*	*100*	*6.2*
	78 GTV-2B	38.8	0.004	0.38	7.5	0.12	39.1	0.03	0.1	0.03	0.01	*13.3*	*99.4*	*6.7*
gabbroics	**33 GTV-1**	50.3	0.24	17.4	5.3	0.11	10.0	13.7	1.63	0.05	0.01	*1.06*	*99.8*	*4.8*
	33 GTV-10	50.9	0.39	15.0	7.5	0.14	9.7	12.7	1.88	0.10	0.02	*1.57*	*99.9*	*6.8*
	33 GTV-16	51.2	0.26	18.1	7.1	0.12	8.6	11.2	2.3	0.10	0.02	*1.15*	*100*	*6.4*
	33 GTV-4	51.3	0.29	16.3	8.1	0.15	8.9	11.4	2.4	0.07	0.01	*0.78*	*99.7*	*7.3*
	33 GTV-9	50.4	0.57	15.0	7.7	0.19	8.6	13.2	2.4	0.11	0.02	*1.56*	*99.7*	*6.9*
	49 GTV-4A	49.2	0.38	14.2	7.9	0.21	12.4	9.3	2.9	0.17	0.03	*2.91*	*99.7*	*7.1*
	67 GTV-1A	46.8	0.18	10.7	10.5	0.19	19.5	4.2	1.60	0.12	0.03	*6.72*	*101*	*9.4*
	73 ROV-1A1	39.5	0.22	10.1	9.5	0.32	16.3	8.3	1.97	0.30	0.08	*11.3*	*99.1*	*8.5*
	73 ROV-1B2	57.9	0.002	0.19	6.3	0.09	29.2	0.03	0.12	0.02	0.03	*5.68*	*99.7*	*5.7*
	74 GTV-1A	51.2	0.35	15.9	7.9	0.15	9.6	11.6	2.0	0.09	0.01	*0.84*	*99.6*	*7.1*
	74 GTV-2D	52.0	0.01	1.13	8.1	0.14	27.9	0.37	0.33	0.07	0.01	*8.66*	*98.9*	*7.3*
	78 GTV-4B	49.3	0.23	17.3	5.8	0.15	10.3	11.6	2.2	0.07	0.01	*2.96*	*99.8*	*5.3*
	83 GTV-4B	48.2	0.22	18.6	5.7	1.03	9.1	10.2	2.5	0.10	0.01	*3.91*	*99.6*	*5.1*

Tab. 3.3: Microprobe analyses and calculated mineral formulas of primary and secondary minerals in serpentinites and gabbroic rocks from the Logatchev hydrothermal field as well as from Working Area 2 (concentrations are given in wt%).

Sample ID	78 GTV-3A	49 GTV-2	49 GTV-5A	67GTV-2C	78 GTV-3A	78 GTV-3A	49 GTV-5A	49 GTV-5A	78 GTV-3A
host rock	gabbro	serpentinite	serpentinite	serpentinite	gabbro	gabbro	serpentinite	serpentinite	gabbro
analyses	n=46	n=95	n=49	n=61	n=18	n=24	n=43	n=54	n=34
mineral	chlorite	lizardite	lizardite	lizardite	lizardite	plagioclase	olivine	pyroxene	pyroxene
Element (wt%)									
SiO_2	33.3	41.4	41.4	41.0	31.0	51.1	41.1	49.2	52.5
TiO_2	-	0.03	0.03	-	0.08	-	-	0.04	0.56
Al_2O_3	15.5	0.56	0.52	0.60	20.5	31.3	-	1.81	2.8
FeO	7.5	3.1	4.6	1.69	7.6	0.43	9.1	6.3	8.4
MnO	0.38	-	-	-	0.77	-	0.14	0.14	0.24
MgO	29.3	39.0	37.7	39.1	26.8	-	49.2	36.44	15.75
CaO	-	-	-	-	-	13.9	-	0.51	18.7
Na_2O	-	-	-	-	-	3.5	-	0.13	0.32
K_2O	-	-	-	-	-	0.06	-	-	-
Cr_2O_3	-	0.22	0.27	0.44	-	-	-	0.71	0.04
Sum	*85.9*	*84.3*	*84.5*	*82.8*	*86.7*	*100.3*	*99.5*	*95.3*	*99.2*
Cations	28-oxygens	7-oxygens	7-oxygens	7-oxygens	7-oxygens	8-oxygens	4-oxygens	6-oxgenes	6-oxgenes
Si	6.5	2.0	2.0	2.0	1.49	2.3	1.00	1.81	1.95
Al (IV)	1.54	0.03	0.03	0.03	1.16	1.67	-	0.08	0.12
Sum tet.	*8.0*	*2.0*	*2.0*	*2.0*	*2.6*	*4.0*	*1.0*	*1.9*	*2.1*
Ti	-	-	-	-	-	-	-	0.001	0.02
Al (VI)	2.01	-	-	-	-	-	-	-	-
Fe	1.21	0.13	0.18	0.07	0.30	0.02	0.18	0.19	0.26
Mn	0.06	-	-	-	0.03	-	0.003	0.004	0.008
Mg	8.5	2.8	2.7	2.8	1.9	-	1.8	2.00	0.87
Ca	-	-	-	-	-	0.68	-	0.02	0.74
Na	-	-	-	-	-	0.31	-	0.01	0.02
Cr	-	0.01	0.01	0.02	-	-	-	0.02	0.001
Sum oct.	*11.8*	*2.9*	*2.9*	*2.9*	*2.3*	*1.0*	*2.0*	*2.3*	*1.9*
Sum of Cations	*19.8*	*5.0*	*5.0*	*5.0*	*4.9*	*5.0*	*3.0*	*4.1*	*4.0*

Tab. 3.4: Calculated gains and losses of major and trace elements in serpentinites and gabbro from the Logatchev hydrothermal field (LHF) and Working Area 2 (49GTV). In Addition, the element concentrations of precursor rocks is listed.

major elements	calc. EF (%) LHF-Serp. (n=15)	calc. EF (%) 49GTV (n=5)	calc. EF (%) 78GTV-3B	*calc. concentration in fresh gabbro (Talbi et al., 1999; n=4) in wt%*	*calc. concentration in fresh peridotite (Paulick et al., 2006; n=13) in wt%*
	bulk serpentinites		gabbro		
	mass addition: 25 g/100 g		*ass addition: 2 g/100 g*		
SiO_2	16.5	19.9	-36.3	*49.2*	*43.6*
TiO_2	-37.5	12.6	-90.3	*3.5*	*0.02*
Al_2O_3	4.0	2.5	9.2	*15.4*	*0.87*
FeO*	16.3	6.2	-12.6	*8.9*	*7.67*
MgO	4.5	6.8	382.3	*5.9*	*46.2*
CaO	-88.7	-38.7	-97.2	*14.1*	*0.8*
Na_2O	1329	1199	-92.5	*2.9*	*0.01*
trace elements	**calc. EF LHF-Serp. (n=14)**	**calc. EF 49GTV (n=5)**	**calc. EF (%) 78GTV-3B**	***average fresh gabbro (LHF; n=3) ppm***	***concentration in fresh harzburgite (Paulick et al., 2006; n=2) in ppm***
	bulk serpentinites		gabbro		
Cu	554.9	2.5	31.3	*89.6*	*7.0*
Zr	77.9	16.2	-96.0	*11.1*	*0.06*
Nb	41.6	67.6	-66.7	*0.97*	*0.01*
Ba	61.7	3.1	-95.8	*21.0*	*0.69*
La	369.5	713.9	-83.7	*1.30*	*0.001*
Sm	206.6	278.6	-85.4	*0.82*	*0.001*
Eu	952.8	510.1	-80.4	*0.51*	*0.0003*
Tb	84.3	93.6	-85.2	*0.20*	*0.0008*
Th	207.5	80.5	-67.8	*0.09*	*0.001*
U	1033	278.5	-58.0	*0.05*	*0.003*

List of Figures

List of Tables

Publications related to this thesis

Papers

Kuhn, T., Alexander, B., **Augustin, N.**, Birgel, D., Borowski, C., de Carvalho, L. M., Engemann, G., Ertl, S., Franz, L., Grech, C., Herzig, P. M., Hekinian, R., Imhoff, J. F., Jellinek, T., Klar, S., Koschinsky, A., Kuever, J., Kulescha, F., Lackschewitz, K. S., Petersen, S., Ratmeyer, V., Renken, J., Ruhland, G., Scholten, J., Schreiber, K., Seifert, R., Süling, J., Türkay, M., Westernströer, U., and Zielinski, F., 2004. The Logatchev hydrothermal field - revisited: preliminary results of the R/V METEOR Cruise HYDROMAR I (M60/3). *Inter Ridge News* **13**, pp. 1-4.

Augustin, N., Lackschewitz, K. S., Botz, R., Eisenhauer, A., Garbe-Schönberg, D., Kuhn, T., and Schmidt, M. (in review) Alteration Processes at the Ultramafic-Hosted Logatchev Hydrothermal Field, MAR 14°45´ N: Trace Elements and Isotope Signatures as Tracers for Water/Rock and Melt/Rock interaction. Submitted to *Chemical Geology*.

Augustin, N., Lackschewitz, K.S., Kuhn, T. (submitted) Mineralogical and Chemical Mass Changes in Mafic and Ultramafic Rocks from the Logatchev Hydrothermal Field (MAR, 15°N). Submitted to *Marine Geology*

Kuhn, K., **Augustin, N.**, Kuhn, T., Borowski, C., Hekinian, R., Petersen, S. (submitted): The influence of the overall geology on the formation and structure of the Logatchev hydrothermal field (15° N MAR), submittet to *Lithos*

Conference Abstracts

Augustin N., Lackschewitz, K.S., Devey, C.W., and Eisenhauer, A. (2005): Hydrothermal alteration in the high-temperature Logatchev vent field: implications for seawater-ultramafic rock interaction. DMG Aachen, *Berichte der deutschen Mineralogischen Gesellschaft, Beiheft zum European Journal of Mineralogy*, **v.17**, p. 7.

Lackschewitz, K.-S, **Augustin, N.**, Devey, C.W., Eisenhauer, A., Garbe-Schönberg, D., James, R. (2005): Hydrothermal Alteration in the Logatchev Hydrothermal Field: Implications From Secondary Mineral Assemblages and Mineral Chemistry. Eos Trans. AGU, **86(52)**, Fall Meet. Suppl. abstract OS22A-02.

Augustin, N., Lackschewitz, K. S., Devey, C. W., Eisenhauer, A., Garbe-Schönberg, D., and James, R. H. (2006): The history of water-rock interaction at Logatchev hydrothermal field as stored in the secondary mineral paragenesis. *Geophysical Research Abstracts* **8**, SRef-ID: 1607-7962/gra/EGU06-A-02195.

Augustin, N., Lackschewitz, K.S., Garbe-Schoenberg D., Paulick H., Kuhn T., Schmidt K. (2006): Geochemistry of fluids and least altered to altered ultramafic and mafic rocks/minerals as Tracer for Water-Rock Interaction at the Logatchev Hydrothermal Field, *Abstracts of talks and posters presented at the 3. SPP 1144-Workshop*, 4.-6. July 2006, Etelsen

Franz L.; Kuhn, T.; Petersen, S.; **Augustin, N.**; Fretzdorff, S. & Hékinian,R. (2007): Syn- and post-magmatic evolution of the oceanic lithosphere underneath the Logatchev hydrothermal field (MAR 14°45`N). 5th Swiss Geoscience Meeting Bern, Abstract Volume, 89-91.

Augustin, N., Lackschewitz, K. S., Botz, R., Eisenhauer, A., Garbe-Schönberg, D., Kuhn, T., Paulick, H., Schmidt, M., and Devey, C., 2007. Alteration processes at the Logatchev Hydrothermal Field: REE, HFSE and Isotope Signatures as Tracers for Water/Rock and Melt/Rock interaction. *Terra Nostra* **2007/1-2**, p. 37.

Danksagung

In erster Linie gebührt mein Dank meinen „Doktorvätern“ Dr. Klas Lackschewitz und Prof. Colin Devey ohne die diese Arbeit im Rahmen des Schwerpunktprogrammes (SPP) 1144 „Vom Mantel zum Ozean: Energie-, Stoff- und Lebenszyklen an Spreizungsachsen“ nicht möglich gewesen wäre.

Ganz besonderer Dank gilt dabei aber Dr. Klas Lackschewitz. In jeder Hinsicht stand er mir während der letzten Jahre mit Rat und Tat zur Seite, sei es bei der Finanzierung des Forschungsprojekts, bei der Arbeit an Bord der Forschungsschiffe, der Auswertung und Interpretation der Labordaten oder das Lesen und Korrigieren der Veröffentlichungen. Somit hat er einen großen Anteil daran, dass die hier vorliegende Arbeit zustande gekommen ist.

Ganz besonders großer Dank gilt meiner Frau Jeannette, welche stets für mich da war und mir während der letzten Jahre immer die größte Stütze war. Ich danke ihr herzlichst für die vielen verständnisvollen als auch verständnislosen Blicke.

Auch danke ich Dr. Sven Petersen herzlichst als unersetzlichen Diskussionspartner für konstruktive Kritik und den erbaulichen Austausch von Ideen. Ebenso danke ich ihm sehr für die Finanzierung des letzten Jahres!

Dr. Thomas Kuhn war immer ein guter Gesprächspartner und eine große Hilfe bei der Erstellung der ersten bathymetrischen Karten.

Inge Dold, Dr. Mark Schmidt und Dr. Reiner Botz waren unermüdlich bei der Reparatur der Sauerstoffisotopenanlage und der Vorbereitung der Proben. Lange hat es gedauert aber es hat sich gelohnt. Vielen Dank!

Bei der Vorbereitung und Durchführung der Korngrößentrennung sowie der Röntgendiffraktometrie waren mir Petra Fiedler und Jutta Heinze eine große Hilfe und führten die Röntgendiffraktometriemessungen durch. An der Mikrosonde halfen mir Barbara Mader und Dr. Peter Appelt. Ana Kolevica führte die Strontiumisotopenanalysen durch. Auch danke ich Heike Anders, Heidi Blaschek, Petra Fiedler, Ulrike Westernströer sowie Dr. Dieter Garbe-Schönberg für die Unterstützung bei der Laborarbeit und die Durchführung der ICP-MS Analysen.

Meine Bedienungsanleitung für das Elektronenmikroskop war Mario Thöner – hat doch gut geklappt…

Edgars „Eddi“ Rudzitis hat sehr viel bei der Probenaufbereitung und Analyse geholfen. Vielen Dank!

Dr. „Macho“ Amini und Andrea Gärtner waren mir stets gute Freunde und Kolleginnen. Ich danke beiden herzlich für die vielen Gespräche und Diskussionen an Bord sowie an Land.

Auch danke ich den vielen Teilnehmern des SPP 1144 für die vielen Diskussionen und Gespräche. Ganz besonders zu erwähnen ist dabei Dr. Holger Paulick von dem ich viel über Serpentinisierung und Alteration gelernt habe.

Bei all der Hilfe und Unterstützung, die mir in den letzten Jahren von so vielen Menschen wiederfahren ist bleibt mir nur zu sagen, dass ich hier noch lange nicht alle aufgezählt habe und diese bitte nachsichtig seien mögen.

Für alle eventuell übrig gebliebenen Unzulänglichkeiten bin ich am Ende selbst verantwortlich.

Vielen Dank!
Nico